Phase transition and Spin transport in Complex Systems : Frustrated spin systems, Molecular and Liquid Crystals

Danh Tai Hoang

UNIVERSITY OF CERGY – PONTOISE
Laboratory for Theoretical Physics and Modelling
CNRS - UMR 8089
---------oOo---------

THESIS

presented for the award of the degree of
DOCTOR OF SCIENCES
in **Theoretical Physics**

by:

HOANG Danh Tai

TITLE:

PHASE TRANSITION AND SPIN TRANSPORT IN COMPLEX SYSTEMS: FRUSTRATED SPIN SYSTEMS, MOLECULAR AND LIQUID CRYSTALS

Date of Defense: 15 November 2012

Composition of jury

Dr. Philippe Depondt	Université Pierre et Marie Curie (Paris 6) (President)
Prof. Hung The Diep	Université de Cergy-Pontoise (Advisor)
Prof. Hamid Kachkachi	Université de Perpignan (Member of jury)
Prof. Miron Kaufman	Cleveland State University, USA (Referee)
Dr. Martial Mazars	Université de Paris-Sud (Paris 11) (Referee)

Acknowledgments

"If we knew what it was we were doing, it would not be called research, would it?"

Albert Einstein (1879−1955)

Many people have helped me during the development of this thesis. First and foremost, I would like to thank my advisor Prof. H. T. DIEP for his invaluable guidance and encouragement. He provided a motivating, enthusiastic, and critical atmosphere during the many discussions for the completion of this research.

I am very grateful to Government of Vietnam for financing these studies. I extend my sincere thanks to the French Embassy in Hanoi who has given me a scholarship to cover social charges.

My sincere thanks go to other members of the LPTM: S. Villemin, C. Gerard, A. Jollived, F. Koukiou, ... In particular, I would also like to thank Prof. T. T. TRUONG who has helped me to solve a lot of daily problems. To get a quick adaptation to life in France, I've been getting a lot of help from PhD students in the laboratory: Y. Magnin, H. Nonne, V. Boccetti, G. Filali, F. Piguet. You are great! I have learned so much from all of you. I thank you.

I wish to thank my vietnamese friends: Son, Hoan, Hanh, Nam, Vinh + Thu, Kien + Thu, Tung + Diep, "Team members MEF2-2008". We share wonderful memories as the foreign students in France. I am glad to count you as my good friends.

I am very grateful to Dr. P. Depondt, Prof. H. Kachkachi, Prof. M. Kaufman, and Dr. M. Mazars for examining my work and for numerous suggestions to improve the present dissertation.

Last, but certainly not least, I would like to thank my family who helped me get where I am today. The expectations of my parents, the constant love of my wife and my daughter, ... have given me energy. I dedicalte the achievements obtained in this thesis to my daugter whom I have missed have the opportunity to witness her birth. Her love and agility are great motivation for me.

List of Abbreviations

MC	:	Monte Carlo
GS	:	ground state
NN	:	nearest neighbor
NNN	:	next-nearest neighbor
SC	:	simple cubic
FCC	:	face-centered cubic
HCP	:	hexagonal-close-packed
Fig.	:	figure
Eq.	:	equation
2D	:	two dimensions
3D	:	three dimensions

Contents

List of Figures

List of Tables

Introduction

The strong development of statistical physics in the last four decades has helped us to understand more deeply the nature of phase transition phenomena in many systems [9, 10, 11].

There exist two main methods to study phase transitions with more precision than early theories such as mean-field theory, spin-wave theory, low- and high-temperature expansions: the first one is the renormalization group method which has been formalized in the 1970s with new concepts based on the system symmetry and scale [12, 13]. The second one are numerical simulation methods, in particular Monte Carlo (MC) methods, which form the largest and most important class of numerical methods used for solving problems in statistical physics [14, 15, 16].

However, there are complicated systems where one encounters many difficulties, for instance systems with competing interactions, or frustrated spins systems. In any event, systems with competitive interactions are excellent candidates to test approximations and to improve theories. Many properties of these systems are still not well understood at present [17]. Some of the controversial subjects have been only recently solved. An example is the nature of the phase transition in stacked triangular antiferromagnets with XY and Heisenberg spins [18, 19].

In **spin frustrated systems**, one cannot find a configuration of spins to fully satisfy the interaction (bond) between every pair of spins. A well-known example is the stacked triangular antiferromagnet with interaction between nearest neighbor (NN) as show in Fig. 0.1. Three Ising spins reside on the corners of a triangle with

antiferromagnetic interactions between them; their total energy is minimized when each spin is aligned opposite to its neighbors. Once the first two spins align in an antiparallel configuration, the third one cannot simultaneously minimize its interactions with the other two. Its two possible orientations, up and down, give the same energy. The ground state (GS) is thus twofold degenerate, and the third spin is frustrated.

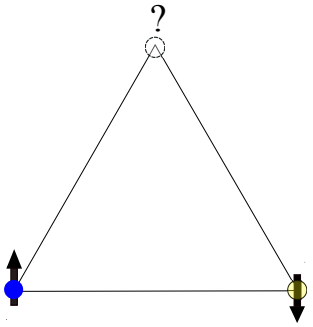

Figure 0.1: Example of frustration in two dimensions (2D): stacked triangular antiferromagnet with interaction between NN.

In this thesis, we are interested in two frustrated systems: The first one is a simple cubic (SC) lattice, with nearest and next-nearest neighbor (NNN) antiferromagnetic interactions, J_1 and J_2 (namely, the $J_1 - J_2$ model). The second one is a hexagonal-close-packed (HCP) lattice where we suppose the in-plane interaction J_1 and inter-plane interaction J_2, both antiferromagnetic. This part of the thesis was motivated by the fact that to date, many frustrated spin systems in three dimensions (3D) are known to undergo a first-order transition to the paramagnetic phase [18, 19]. We wish to test if all 3D frustrated systems have to have a first-order transition. This clarification is our opinion very important predictions in other systems.

We will also study another case where the interaction is **dipolar interaction** which contains two terms in competition with each other. Here, we consider a SC lattice where each site is occupied by an axial molecule. The molecular axis can be along the x, y or z direction. Let us denote the orientation of the molecule at the lattice site i by a unit segment, not a vector, which can lie in the x, y or z direction. We attribute it a Potts variable σ=1, 2, 3 when it respectively lies along the x, y and

z axes. The Hamiltonian is given by:

$$\mathcal{H} = -\sum_{(i,j)} J_{i,j}\delta(\sigma_i,\sigma_j) + D\sum_{(i,j)}\{\frac{\mathbf{S}(\sigma_i)\cdot\mathbf{S}(\sigma_j)}{r_{i,j}^3} - 3\frac{[\mathbf{S}(\sigma_i)\cdot\mathbf{r}_{i,j}][\mathbf{S}(\sigma_j)\cdot\mathbf{r}_{i,j}]}{r_{i,j}^5}\}\delta(\sigma_i,\sigma_j) \tag{0.1}$$

where σ_i is the 3-state Potts variable at the lattice site i; $\mathbf{S}(\sigma_i)$ is defined as the unit vector lying on the axis corresponding to the value of σ_i; $\mathbf{r}_{i,j}$ is the vector of modulus $r_{i,j}$ connecting the site i to the site j; D is the magnitude of the dipolar coupling which depends on the material. The first sum is performed over the nearest sites σ_i and σ_j while the second one is limited at some cutoff distance r_c.

We are interested in the case $J_{i,j} > 0$. Let us discuss about the GS ordering. When $D = 0$, the GS is uniform with one orientation value. When $D > 0$, the first term in the dipolar sum favors perpendicular configuration, while the second one favors parallel molecules on the same axis. The GS thus depends on D and r_c. A phase transition could be of complicated nature due to this competition.

On the other hand, **thin films and quasi-two-dimensional materials** are one of the most important domains studied during the last 30 years, not only in fundamental sciences such as statistical physics but also in materials science and many interdisciplinary areas such as biophysics and biochemistry. They have many technological applications in electronics, data storage, and catalysis in the case of metalon-metal films, and in biotechnology and pharmacology in the case of molecular films. An abundance of important experimental data on physics of surfaces and ultrathin magnetic structures obtained by various techniques have been reviewed in the references [20] and [21]. In parallel to these experimental developments, much theoretical effort has also been devoted to the understanding of physical mechanisms lying behind new properties found in nanoscale objects such as ultrathin films, ultrafine particles, quantum dots, spintronic devices, etc. This effort is aimed not only at providing explanations for experimental observations but also at predicting new effects for future experiments [22, 23, 24, 25, 26].

This has motivated us to consider a thin film with the Potts model described above.

We add to the Hamiltonian an anisotropy term:

$$\mathcal{H}_a = -A \sum_i s_z(i)^2 \tag{0.2}$$

For simplicity, we discuss here in the pure 2D case. When $A = 0$, the dipolar interaction causes an in-plane ordering as expected: the absolute value of the second term for axial molecules is larger than the first term by a factor 3, making the in-plane parallel state more favorable. When the dipolar interaction energy is small compared to the anisotropy term, the GS is perpendicular. The nature of the GS, perpendicular or parallel, thus depends on the ratio D/A.

The behavior is also interesting in a system composed of **dimers** interacting with each other via a NN exchange and a dipolar coupling. Each dimer occupies a link between two nearest sites of a SC lattice. Without the dipolar interaction, the interaction between neighboring molecules will give rise to an orientational order of molecular axes at low temperature. This situation is similar to a 3-state Potts model in 3D, but the difference resides in the fact that dimers are moving from one bond to another while in the Potts model, the particle stays at its lattice site. The dynamics which leads to excited states is not the same: dimers have self-avoiding constraints.

The main part of this thesis is devoted to the use of various MC methods including standard MC method and histogram method [27, 28, 29]. The GS of the systems can be determined by the steepest descent method as well as by analysis.

Simultaneously with the study of the nature of phase transition mentioned above, we also study the **spin resistivity** which is an important subject in condensed-matter physics. It has been extensively studied in magnetic thin films and multi-layers. The so-called giant magneto-resistance used in data storage devices, magnetic sensors, etc., was experimentally discovered 20 years ago [30, 31, 32]. Since then, intensive investigations, both experimentally and theoretically, have been carried out [32, 33]. The so-called spintronics was born with spectacular rapid developments in relation to industrial applications. Experiments have shown that the resistivity indeed depends on the itinerant spin orientation and the lattice spin ordering [34, 35, 36, 37, 38, 39].

At low temperature, the main magnetic scattering is due to spin-wave excitations [40], the resistivity is proportional to the square of the temperature. However at higher temperature the spin-wave theory is not valid, so that calculation of the resistivity is not possible, in particular in the critical region around the Curie temperature in simple ferromagnets, let alone other complicated magnetic orderings. The theory of De Gennes-Friedel predicts that resistivity should show a divergent peak. However, experiments in various magnetic materials ranging from semiconductors to superconductors [4, 41, 2, 3, 1, 5, 37, 38, 42, 43, 44] show indeed an anomaly at the transition temperature, but the peak is more or less rounded, not as sharp as expected from the divergence of the correlation length. It has been shown in fact that [45, 46] the form of the peak depends on the length of the correlation included in the calculation of resistivity: if only short-range correlations are taken into account, then the peak is very rounded. In the case of antiferromagnets, Haas has shown the absence of a resistivity peak [47]. The dependence of the spin transport on the magnetic ordering in particular in the phase transition region of the frustrated systems is studied in this work.

The thesis is organized as follows:

Chapter 1 is devoted to the introduction to MC simulations to study phase transitions, including the principles of MC simulations, the general structure of a standard MC program, the critical exponents, finite-size scaling theory, and histogram methods. We also present in this chapter the models and methods to study spin resistivity in magnetic materials by MC simulations.

Chapter 2 treats mainly phase transitions and spin transport in frustrated systems. We introduce in this chapter the basic notions on frustrated systems. Then we present the GS and the phase transition of the $J_1 - J_2$ model with Ising spins and the HCP lattice with both Ising and XY spin. The spin resistivity is calculated for the Ising case in the two systems.

Chapter 3 shows the effect of dipolar interactions in molecular crystals. The model

considered in this chapter is a Potts model which takes into account the exchange interaction between NN molecules and a dipolar interaction between molecular axes in three dimensions. We investigate the GS and the nature of the phase transition in this model for the different values of magnitude of dipolar coupling and cutoff distance.

Chapter 4 describes the GS and the phase transition in a system composed of dimers interacting with each other via a NN exchange and a dipolar coupling. The results are shown in the two cases of polarized and non-polarized dimers.

A general conclusion and future developments are given in the end of this thesis.

Chapter 1

Monte Carlo simulations for the study of Phase Transitions and Spin Transport

We start this chapter by reviewing some basic knowledge of statistical physics. The principle of the MC method is also presented. For the study of phase transition phenomena, we give the general structure of a standard MC program. We introduce critical exponents which describe the behavior of the thermodynamical properties near the transition point in second-order phase transitions, as well as finite size scaling theory to describe the bulk properties of a finite system of linear dimension with periodic boundary conditions. Histogram methods including single- and multi-histograms are also introduced in this chapter.

The second issue mentioned in this chapter is the study of spin resistivity in magnetic materials. This is a very important issue in electronic devices and their applications. After summarizing the theoretical and experimental results, we give the structure of a MC program for the study of the spin transport, and we describe in details the interactions that appear in our model, including interactions between lattice spins, interactions between lattice spins and itinerant spins, etc.

1.1 Basics of statistical physics

Equilibrium statistical physics provides methods for the study of systems at equilibrium by using different statistical ensembles of states. The average of a quantity A is defined as:

$$\langle A \rangle = \sum_{i=1}^{N} A_i . P_i, \tag{1.1}$$

where A_i is the value of A in the microscopic state i and P_i is the probability of this state.

For a system in thermal equilibrium with a reservoir at temperature T, the equilibrium occupation probability, called "canonical probability", is:

$$P_i = \frac{1}{Z} \cdot e^{-\frac{E_i}{k_B . T}}, \tag{1.2}$$

where E_i is the energy of state i, k_B is Boltzmann's constant and Z is the partition function:

$$Z = \sum_{i=1}^{N} e^{-\frac{E_i}{k_B . T}} = \sum_{i=1}^{N} e^{-\beta E_i}, \tag{1.3}$$

with $\beta = \frac{1}{k_B . T}$.
Eq. (1.1) is rewritten as follows:

$$\langle A \rangle = \frac{1}{Z} \sum_{i=1}^{N} A_i e^{-\beta E_i}. \tag{1.4}$$

The expectation value of the energy $\langle E \rangle$, which is also the quantity we know from thermodynamics as the internal energy E, is thus given by

$$\langle E \rangle = \frac{1}{Z} \sum_{i=1}^{N} E_i e^{-\beta E_i}. \tag{1.5}$$

Using Eq. (1.3) we can rewrite this equation as

$$\langle E \rangle = -\frac{1}{Z} \frac{\partial Z}{\partial \beta} = -\frac{\partial ln Z}{\partial \beta}. \tag{1.6}$$

The specific heat is given as the derivative of the internal energy with respect to the temperature:

$$C_V = \frac{\partial \langle E \rangle}{\partial T} = k_B \beta^2 \frac{\partial^2 lnZ}{\partial \beta^2}. \tag{1.7}$$

In statistical physics, averaged values of physical quantities as well as their relations are very important

$$\langle (E - \langle E \rangle)^2 \rangle = \langle E^2 \rangle - \langle E \rangle^2 \tag{1.8}$$

$$\langle E^2 \rangle = \frac{1}{Z} \sum_{i=1}^{N} E_i^2 e^{-\beta E_i} = \frac{1}{Z} \frac{\partial^2 Z}{\partial \beta^2}, \tag{1.9}$$

we have

$$\langle E^2 \rangle - \langle E \rangle^2 = \frac{1}{Z} \frac{\partial^2 Z}{\partial \beta^2} - \left[\frac{1}{Z} \frac{\partial Z}{\partial \beta} \right]^2 = \frac{\partial^2 lnZ}{\partial \beta^2}. \tag{1.10}$$

From Eq. (1.7) and Eq. (1.10) the specific heat then reads:

$$C_V = k_B \beta^2 \left(\langle E^2 \rangle - \langle E \rangle^2 \right) \tag{1.11}$$

Similarly, the susceptibility χ is related to the fluctuations of the magnetization M and is given by

$$\chi = \frac{\partial \langle M \rangle}{\partial B} = \beta \left(\langle M^2 \rangle - \langle M \rangle^2 \right) \tag{1.12}$$

where B is the applied magnetic field.

1.2 Introduction to Monte Carlo simulations

Simulation methods in general and in particular MC method are very popular in wide areas of science and engineering. Since the first implementation using "modern computing machines" was introduced by Metropolis and Ulam in 1949 [48], a number of improved methods have been proposed. These are presented in many books devoted to MC simulations [14, 16, 15].

1.2.1 Principles of Monte Carlo simulation

To simplify the illustration, and without loss of generality, we consider a system of spins. Using Eq. 1.1 we can calculate the average values of the physical quantities such as energy, magnetization, specific heat, susceptibility, etc. In principle, one has to use the totality of all micro-states. This is not realizable for systems with a large number of spins. To overcome this problem, in numerical simulations, one chooses the microscopic state probability, then compute the value of the physical quantity we are interested in and then take the average value to understand the system. But how to choose the most probable states? This will be done by the following procedure: Instead of choosing any micro-state, one could create a set of states (also called Markov chain) in which a state M is created from the previous state N by just changing the value of the i^{th} spin from S_{i1} to S_{i2} (the values of the other spins remain unchanged) with a probability of moving $w(N \to M)$. A sufficient condition to achiete this is to impose the principle of detailed balance [14, 15]:

$$P(N)w(N \to M) = P(M)w(M \to N), \tag{1.13}$$

where

$$P(N) = \frac{1}{Z(T)}e^{-\beta E(N)} \quad \text{and} \quad P(M) = \frac{1}{Z(T)}e^{-\beta E(M)} \tag{1.14}$$

are the equilibrium probabilities of state N and M respectively.

The condition of detailed balance given by Eq. 1.13 implies that, at equilibrium, the average number of moves $N \to M$ is the same as the average number of inverse moves $M \to N$. As this is true for any two arbitrary states it follows that if the system in equilibrium is submitted to moves that obey the detailed balance condition there will be no change in the probability of any state and the system will remain in equilibrium.

One deduces:

$$\frac{w(N \to M)}{w(M \to N)} = \frac{e^{-\beta E(M)}}{e^{-\beta E(N)}} = e^{-\beta \Delta E}, \tag{1.15}$$

with $\Delta E = E(M) - E(N)$.

Note the relation $w(N \to M) = 1 - w(M \to N)$, one thus has

$$w(N \to M) = \frac{e^{-\beta \Delta E}}{1 + e^{-\beta \Delta E}}. \tag{1.16}$$

The solution proposed by Metropolis et al [48, 49] is

$$w(N \to M) = \begin{cases} 1 & \text{if} \quad \Delta E < 0 \\ e^{-\beta \Delta E} & \text{if} \quad \Delta E \geq 0. \end{cases} \tag{1.17}$$

The state M can be different from the state N by the value of the i^{th} spin. So the difference in energy ΔE between these two states is the energy difference of the i^{th} spin in the two states.

Thus the i^{th} spin will change its value from S_{i1} to S_{i2} if the energy of the i^{th} spin when its value equals S_{i1} is less than its energy when its value equals S_{i2}. Otherwise, the probability of this change is $e^{-\beta \Delta E}$. This procedure is the Metropolis algorithm.

1.2.2 Structure of a standard Monte Carlo simulation program

The structure of standard Monte Carlo simulation program can be summarized by 3 main steps as in Fig. 1.1.

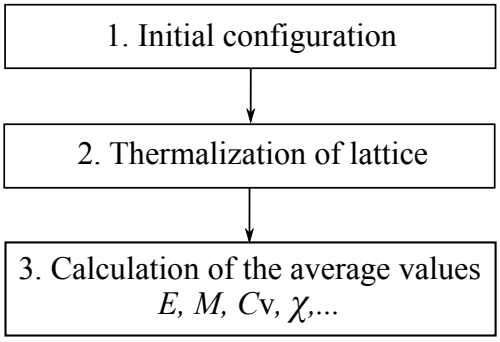

Figure 1.1: Scheme of algorithm standard MC method.

- **Step 1:** Choose an initial state of lattice: assign a value to each spin S_i. We often choose the initial state as the ground state, this allows optimization of calculation time.

- **Step 2:** Thermalization of lattice:

  (i) For each spin i^{th}, we update its value using the following procedure (see Fig. 1.2):

  - Calculation of its energy E^i_{old}.

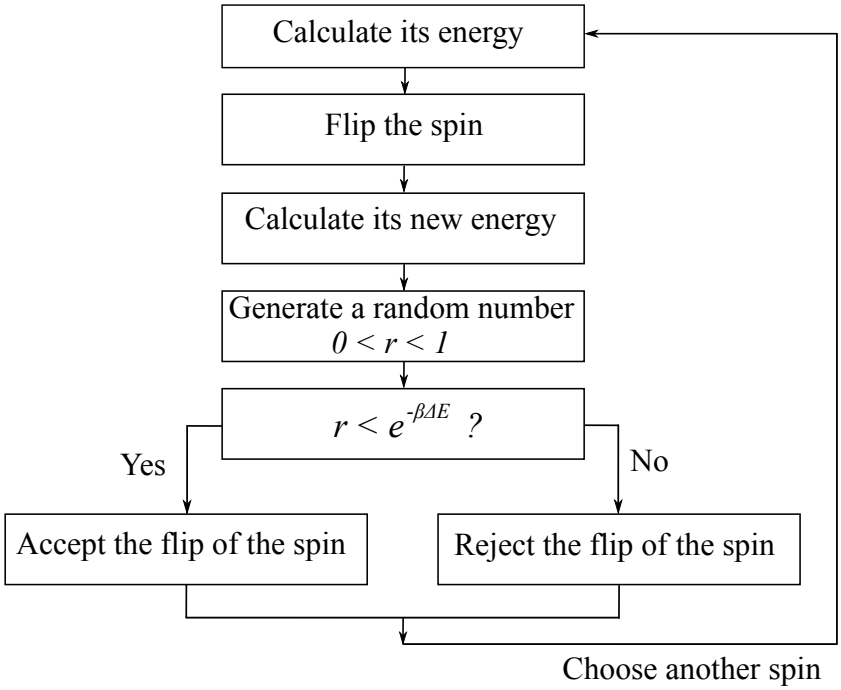

Figure 1.2: Scheme of step "update value of spin" in standard MC method.

  - Change the value of this spin (flip the spin) and calculation its new energy E^i_{new}.

  - Generate a random number r such that $0 < r < 1$. If $r < e^{-\beta\Delta E}$ (where $\Delta E = E^i_{\text{new}} - E^i_{\text{old}}$), the transition is accepted, the spin will be flipped.

  (ii) Proceed to step (i) for all the spins. When all spins are considered, we say that we have made a MC step.

(iii) Perform N_1 MC steps to obtain a system at equilibrium.

- **Step 3:** Perform N_2 MC steps, during this stage one calculates the value A_i of the considered quantity A. After that, calculate the average value of the quantity A with the formula:

$$\langle A \rangle = \frac{1}{N_2} \sum_{i=1}^{N_2} A_i \tag{1.18}$$

It should be noted that the value of N_1 and N_2 have to be large enough to ensure accurate results.

1.3 Monte Carlo simulations in the study of phase transitions

The anomalies in physical behavior which occur when a system undergoes a phase transition have been a major focus for physicists for many years [11]. The nature of the transition from one phase to another is one of the most important problems in statistical physics and in various areas of materials science, this is not limited to physics. Since the introduction of the renormalization group [12, 13] with new concepts based on the system symmetry and scales, the understanding of the nature of the phase transition in many systems has become clearer.

There exists two main types of phase transition: first- and second-order phase transition. In the first-order transition, when the system size is large enough, the energy and order parameter have a discontinuity at the phase transition, the values of heat capacity and the susceptibility are not defined (see Fig. 1.3). In the second-order phase transition, the treatment is much more subtle, the plots of energy and magnetization versus temperature show an inflection point at the phase transition, corresponding to the maximum of heat capacity and susceptibility (see Fig. 1.4). We can also define them as follows: The first-order phase transition is a type of phase transition in which one (or more) of the first partial derivatives of the bulk free energy per site is

discontinuous. In contrast, the second-order phase transition is one in which all first derivatives of the bulk free energy per site are continuous.

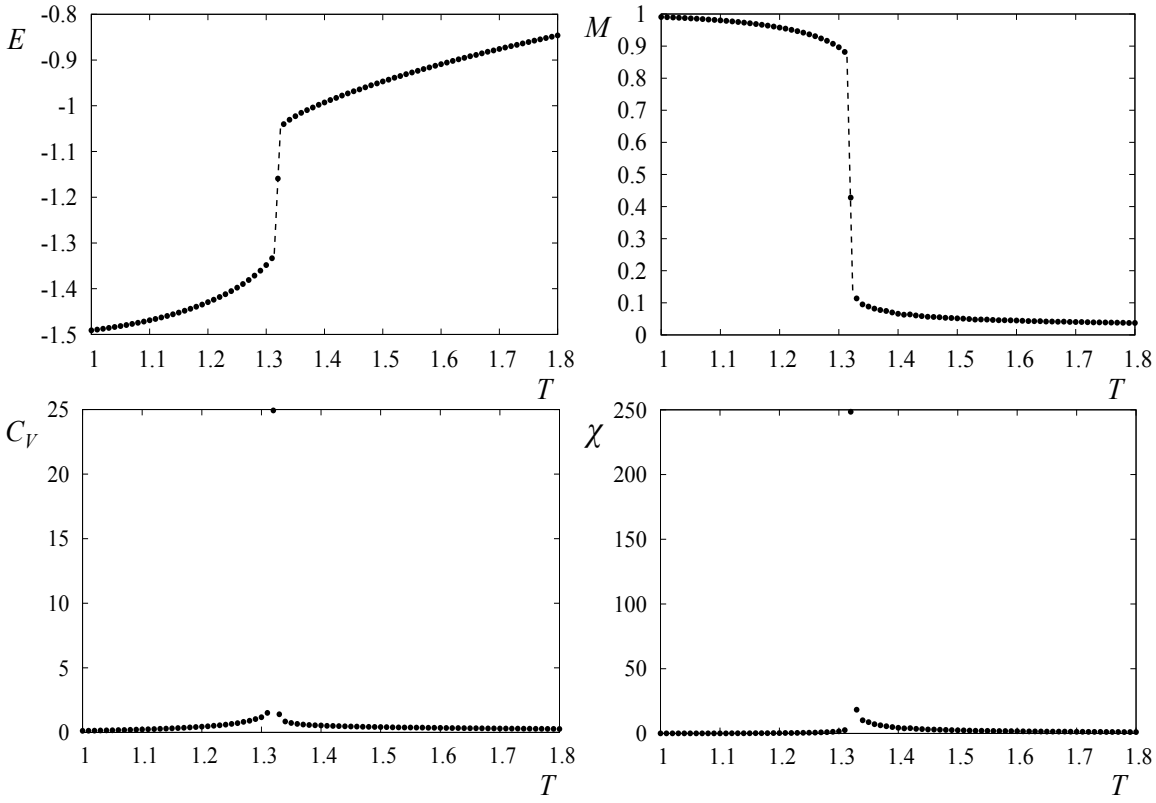

Figure 1.3: Energy per spin E, order parameter M, specific heat C_V and susceptibility χ versus temperature T in the first-order phase transition.

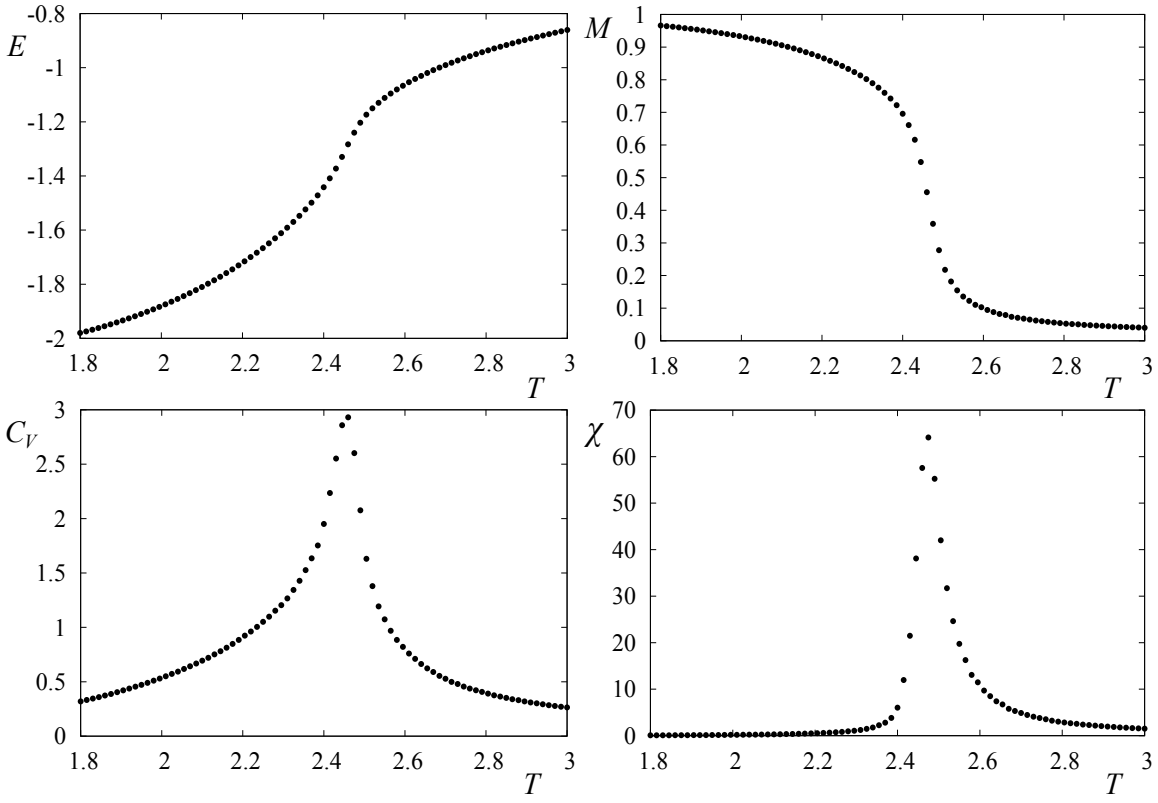

Figure 1.4: Energy per spin E, order parameter M, specific heat C_V and susceptibility χ versus temperature T in the second-order phase transition.

1.3.1 Critical exponents

For a second-order phase transition we can introduce the critical exponents which describe the behavior of the thermodynamical properties near the phase transition. These exponents are:

- the specific heat exponent α:

$$C_V(T) \propto |1 - \frac{T}{T_c}|^{-\alpha} \qquad (\text{for } T < T_c \text{ or } T > T_c), \tag{1.19}$$

- the susceptibility exponent γ:

$$\chi(T) \propto |1 - \frac{T}{T_c}|^{-\gamma} \qquad (\text{for } T < T_c \text{ or } T > T_c), \tag{1.20}$$

-the correlation length exponent ν:

$$\xi(T) \propto |1 - \frac{T}{T_c}|^{-\nu} \qquad (\text{for } T < T_c \text{ or } T > T_c), \tag{1.21}$$

- the magnetization exponents β and δ:

$$M(T) \propto |1 - \frac{T}{T_c}|^{\beta} \qquad (\text{for } T < T_c), \tag{1.22}$$

$$M(T) \propto H^{\frac{1}{\delta}} \qquad (\text{at } T = T_c), \tag{1.23}$$

- the correlation function exponent η:

$$G(r) \propto \frac{1}{r^{d-2+\eta}} \qquad (\text{at } T = T_c). \tag{1.24}$$

1.3.2 Finite-size scaling

Finite size scaling theory describes the bulk properties of a finite system of linear dimension with periodic boundaries. The approach was first developed by Fisher [50, 51, 52]. According to this theory, the free energy of a system of linear dimension L is given by

$$F(L, T, H) = L^{-(2-\alpha)/\nu} \mathcal{F}^0(tL^{1/\nu}, HL^{(\gamma+\beta)/\nu}). \tag{1.25}$$

where the reduced temperature is $t = \frac{T-T_c(L)}{T_c(L)}$; $T_c(L)$ is the critical temperature for a system of size L; H is the magnetic field; and $\alpha, \beta, \gamma, \nu$ are the critical exponents defined above.
In the case of zero-field $H = 0$, Eq. (1.25) is rewritten as:

$$F(L,T) = L^{-(2-\alpha)/\nu}\mathcal{F}^0(tL^{1/\nu}). \tag{1.26}$$

Setting $x = tL^{1/\nu}$ one has:

$$F(L,T) = L^{-(2-\alpha)/\nu}\mathcal{F}^0(x). \tag{1.27}$$

One can determine various physical quantities such the as order parameter, the susceptibility and the divergent part of the specific heat:

$$M(L,T) = L^{-\beta/\nu}\mathcal{X}^0(x), \tag{1.28}$$

$$\chi(L,T) = L^{\gamma/\nu}\mathcal{Y}^0(x), \tag{1.29}$$

$$C_V(L,T) = L^{\alpha/\nu}\mathcal{Z}^0(x), \tag{1.30}$$

At the phase transition $T = T_c(L), x = 0$, and one has:

$$M_{T_c}(L) \propto L^{-\beta/\nu}, \tag{1.31}$$

$$\chi_{\max}(L) \propto L^{\gamma/\nu}, \tag{1.32}$$

$$C_{V\max}(L) \propto L^{\alpha/\nu}. \tag{1.33}$$

Other scalings relevant to a continuous transition are:

$$V_{1\max}(L),\ V_{2\max}(L) \propto L^{1/\nu}, \tag{1.34}$$

where V_1 and V_2 are the moments of order 1 and 2 respectively.

$$V_1 = \langle\frac{\partial lnM}{\partial\beta}\rangle \tag{1.35}$$

$$V_2 = \langle\frac{\partial lnM^2}{\partial\beta}\rangle \tag{1.36}$$

We also can rewrite them as:

$$V_1 = \frac{\langle ME \rangle}{\langle M \rangle} - \langle E \rangle, \tag{1.37}$$

$$V_2 = \frac{\langle M^2 E \rangle}{\langle M^2 \rangle} - \langle E \rangle. \tag{1.38}$$

The critical temperature is given by

$$T_c(L) = T_c(\infty) + AL^{-1/\nu}. \tag{1.39}$$

Note that, these results are valid only for large L. For small lattices, corrections to finite-size scaling must be taken into account in the form of a term $L^{-\theta/\nu}$ due to the effect of irrelevant scaling fields and nonlinearities in the scaling variables:

$$T_c(L) = T_c(\infty) + AL^{-1/\nu} + BL^{\theta/\nu}. \tag{1.40}$$

In the case of a first-order transition, the maxima of the susceptibility and the divergent part of the specific heat are proportional to the volume of the system:

$$\chi_{\max} \propto L^d, \tag{1.41}$$

$$C_{\max} \propto L^d. \tag{1.42}$$

And the critical temperature is determined by

$$T_c(L) = T_c(\infty) + AL^{-1/d}. \tag{1.43}$$

In this thesis, the determination of critical exponents for second-order phase transition in particular by the method of finite-size scaling shall not be treated. The calculation of critical exponents for Potts model with defects is under way. This topic is not included in this thesis.

1.3.3 Histogram Methods

To accurately determine the transition temperature as well as the critical exponents, one has to estimate the heights of the maxima of the specific heat C_V and the susceptibility χ. But the results obtained from standard MC simulations are a set of individual points corresponding to different temperatures, and the interpolation between two successive temperatures is not exact in the transition region. The histogram methods have been proposed to overcome this difficulty [27, 28, 29]. There exist two histogram methods: the single-histogram method and the multi-histogram method.

A. Single-histogram Method

This method is based on the following relation: the probability distribution functions at temperature T and T_0 are written respectively as:

$$P(T, E) = Ce^{-\beta E}, \tag{1.44}$$

$$P(T_0, E) = C_0 e^{-\beta_0 E}, \tag{1.45}$$

where C and C_0 are the coefficients determined by the normalization.

So one has:

$$P(T, E) = \frac{C}{C_0} P(T_0, E) e^{-(\beta-\beta_0)E}. \tag{1.46}$$

After normalization, we find that:

$$\frac{C}{C_0} = \frac{1}{\sum_E P(T_0, E) e^{-(\beta-\beta_0)E}}. \tag{1.47}$$

Replacing Eq. (1.47) into (1.46), we get:

$$P(T, E) = \frac{P(T_0, E) e^{-(\beta-\beta_0)E}}{\sum_E P(T_0, E) e^{-(\beta-\beta_0)E}}. \tag{1.48}$$

If we denote the histogram of energy E at temperature T_0 by $H(T_0, E)$ and the number of MC steps used to determine this histogram by N, we have:

$$P(T_0, E) = \frac{H(T_0, E)}{N}. \tag{1.49}$$

So Eq. (1.48) can be rewritten as:

$$P(T,E) = \frac{H(T_0,E)e^{-(\beta-\beta_0)E}}{\sum_E H(T_0,E)e^{-(\beta-\beta_0)E}}. \tag{1.50}$$

Using Eq. (1.50) we can calculate the probability at another temperature T from $H(T_0, E)$ at temperature T_0, and we can estimate the average value of the quantity A by:

$$\langle A(T)\rangle = \sum_E AP(T,E) \tag{1.51}$$

Because of the finite number of MC steps performed to obtain the histogram $H(T_0, E)$, the probability $P(T, E)$ obtained by using Eq. (1.50) is not accurate for values T far from the value of T_0. It is very important to check each $P(T, E)$ before using it. As a function of T, the form of the probability $P(T, E)$ is Gaussian (for second-order transitions). When T differs too much from T_0, its form is irregular [29, 53, 15]. The reliable range of T values decreases as the system size increases. Anyway, we have to choose T_0 in the critical region and use as large as possible number of MC steps .

We show in Fig. 1.5 the probability distribution in the dimensionless energy in the model $J_1 - J_2$ defined in the Introduction for $J_2/J_1 = 0.2$. The data from the MC simulation (black circles) were obtained at $T_0 = 1.884$. The other probabilities are calculated by using Eq. (1.50) at $T_1 = 1.850$ (blue void circles) and $T_2 = 1.805$ (red diamonds).

We show as an example in Fig 1.6 the result obtained by the single-histogram method as compared to the result by standard MC method.

B. Multi-histogram Method

As discussed above, the single-histogram method provides reliable results only for a relatively narrow range of the temperatures T around T_0. To overcome this problem, we can use the multi-histogram method, which was first discovered by Ferrenberg and Swendsen [27, 28]. In this method, data taken at different temperatures are combined

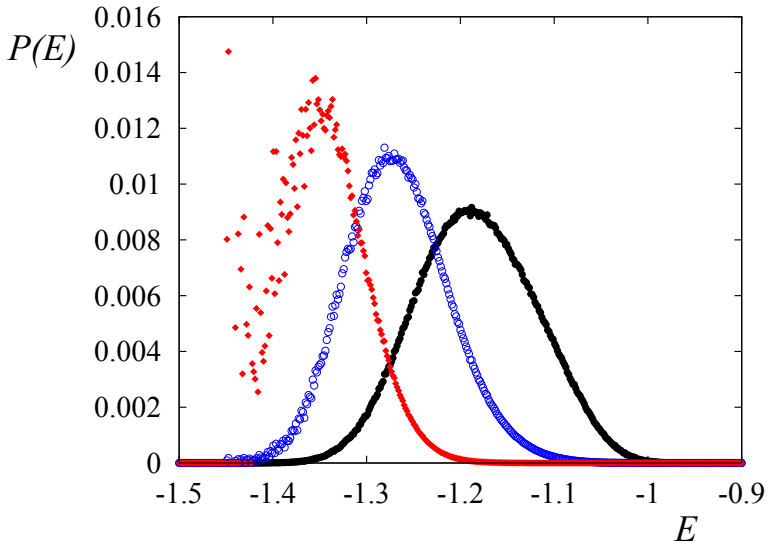

Figure 1.5: Energy histogram $P(E)$ versus E for model $J_1 - J_2$ with $J_2/J_1 = 0.2$. The data from the simulation (black circles) were obtained at $T_0 = 1.884$. The other values where obtained using the single-histogram method at $T_1 = 1.850$ (blue open circles) and $T_2 = 1.805$ (red diamonds). See text for comments.

so as to produce a more accurate estimate of the relevant distribution over a relatively wide range of temperature. It can be applied to an arbitrary number of simulations. The basic ideas of this method was discribed quite clearly by Newman and Barkema [14].

As we have discussed above, the histograms are Gaussian in second-order transitions. In first-order transitions, the histograms shows a double-peak structure at the transition temperature, it indicates the coexistence of the ordered and disordered phase at this point (see Fig. 1.7).

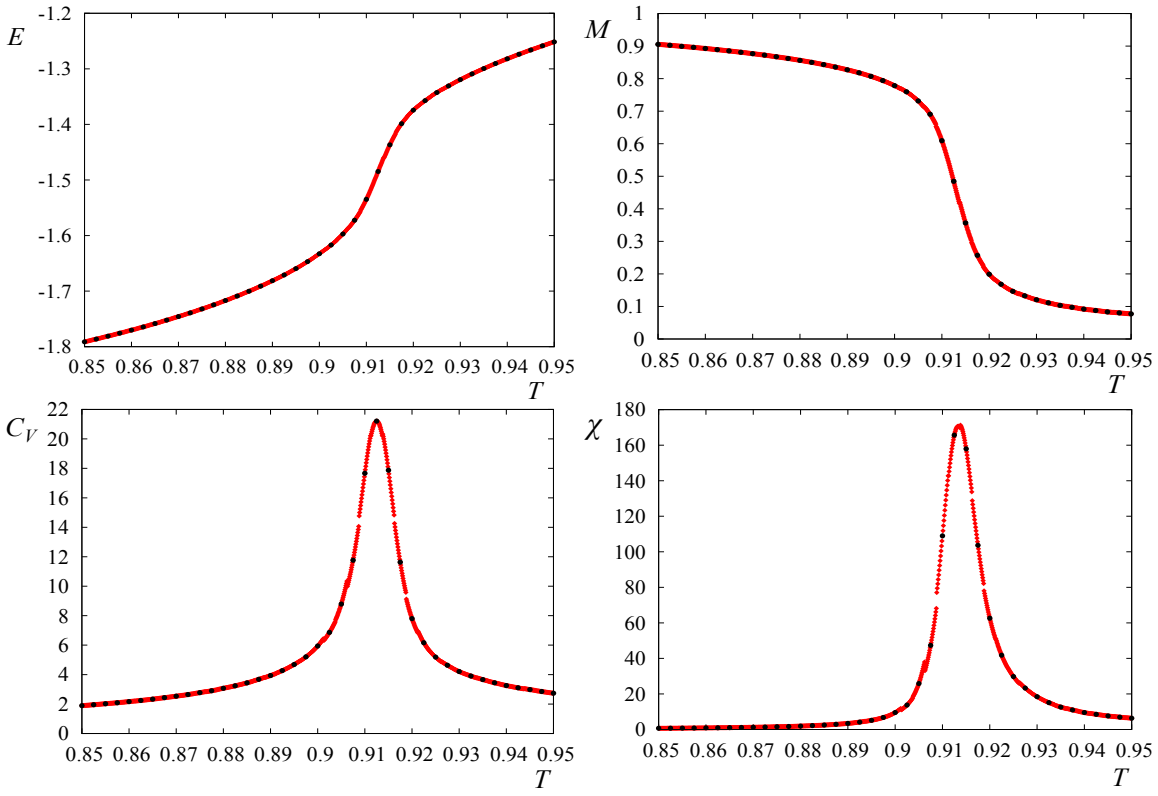

Figure 1.6: Results, obtained by standard MC method (black circles) and single-histogram method (red diamond), are presented together for comparison.

1.4 Monte Carlo simulations in the study of spin transport

1.4.1 Introduction

The study of the behavior of the resistivity is one of the fundamental tasks in material science. This is because the transport properties occupy the first place in electronic devices and their applications. The resistivity has been studied since the discovery of the electron a century ago [40, 54, 32], first with the simple Drude theory using the classical free particle model with collisions due to atoms in the crystal [55, 32]. The following relation is established between the conductivity σ and the electronic

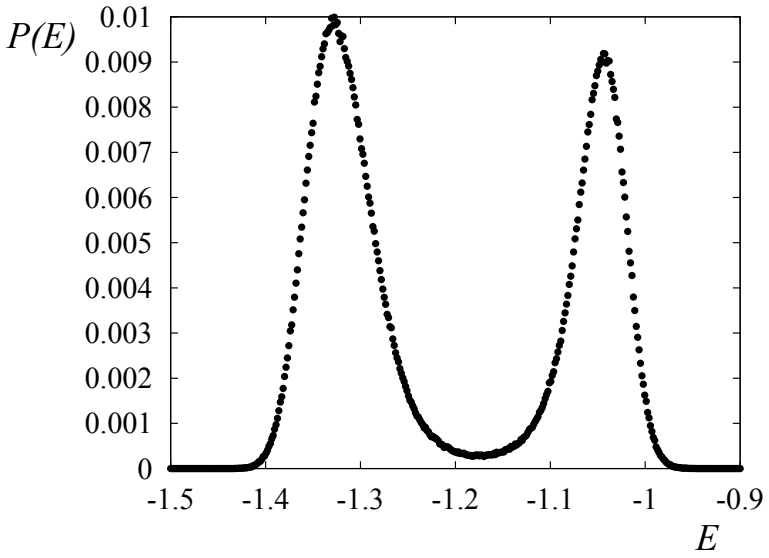

Figure 1.7: The probability distribution in the model $J_1 - J_2$ for $\eta = 0.26$ at the transition temperature $T_c = 1.3195$.

parameters e (charge) and m (mass):

$$\sigma = \frac{ne^2\tau}{m} \tag{1.52}$$

where τ is the electron relaxation time, namely the average time between two successive collisions. In more sophisticated treatments of the resistivity where various interactions are taken into account, this relation is still valid with two modifications:
(i) the electron mass is replaced by its effective mass which includes various effects due to interactions with its environment,
(ii) the relaxation time τ is not a constant but depends on collision mechanisms.

The first modification is very important, the electron can have a "heavy" or "light" effective mass which modifies its mobility in crystals. The second modification has a strong impact on the temperature dependence of the resistivity: τ depends on some power of the electron energy, this power depends on the diffusion mechanisms such as collisions with charged impurities, neutral impurities, magnetic impurities, phonons, magnons, etc. As a consequence, the relaxation time averaged over energy, $< \tau >$, depends differently on T according to the nature of the collision source.

The properties of the total resistivity thus stem from different kinds of diffusion processes. Each contribution has in general a different temperature dependence. Let us summarize the most important contributions to the total resistivity $\rho_t(T)$ at low temperature (T) in the following expression

$$\rho_t(T) = \rho_0 + A_1 T^2 + A_2 T^5 + A_3 \ln \frac{\mu}{T}, \tag{1.53}$$

where A_1, A_2 and A_3 are constants. The first term is T-independent, the second term proportional to T^2 represents the scattering of itinerant electrons at low temperature by lattice spin-waves. Note that the resistivity caused by a Fermi liquid is also proportional to T^2. The T^5 term corresponds to low temperature resistivity in metals. This is due to the scattering of itinerant electrons by phonons. Note that at high temperature, metals show a linear-T dependence. The ln term is the resistivity due to the quantum Kondo effect caused by a magnetic impurity at very low temperature.

We are interested in this thesis in the spin resistivity ρ of magnetic materials. This subject has been investigated intensively both experimentally and theoretically for more than five decades. The rapid development of the field is due mainly to many applications in particular in spintronics.

Experiments have been performed in many magnetic materials including metals, semiconductors and superconductors. One interesting aspect of magnetic materials is the existence of a magnetic phase transition from a magnetically ordered phase to the paramagnetic (disordered) state. Very recent experiments such as those performed on the following compounds show different forms of anomaly of the magnetic resistivity at the magnetic phase transition temperature: ferromagnetic $SrRuO_3$ thin films [42], Ru-doped induced ferromagnetic $La_{0.4}Ca_{0.6}MnO_3$ [1], antiferromagnetic ϵ-$(Mn_{1-x}Fe_x)_{3.25}$ Ge [2], semiconducting $Pr_{0.7}Ca_{0.3}MnO_3$ thin films [44], superconducting $BaFe_2As_2$ single crystals [43], and $La_{1-x}Sr_xMnO_3$ [5]. Depending on the material, ρ can show a sharp peak at the magnetic transition temperature T_C [39] or only a change of its slope, or an inflexion point. The latter case gives rise to a peak of the differential resistivity $d\rho/dT$ [37, 36].

As for theories, the T^2 magnetic contribution in Eq. (1.53) has been obtained from the magnon scattering by Kasuya [40]. However, at high T in particular in the region of the phase transition, much less has been known. De Gennes and Friedel [56] proposed the idea that the magnetic resistivity results from the spin-spin correlation so it should behave as the magnetic susceptibility, thus it should diverge at T_C. Fisher and Langer [45], and Kataoka [46] have suggested that the range of spin-spin correlation changes the shape of ρ near the phase transition. The resistivity due to magnetic impurities has been calculated by Zarand et al. [57] as a function of the Anderson's localization length. This parameter expresses in fact a kind of correlation sphere induced around each impurity. Their result shows that the resistivity peak depends on this parameter, in agreement with the spin-spin correlation idea.

1.4.2 Model and Method

Although many theoretical investigations have been carried out, to our knowledge, to date, very few MC simulations have been performed regarding the temperature dependence of the dynamics of spins participating in the current. In paper [58] published in 2003, G. Alvarez and E. Dagotto have presented a single-band model to study the dynamical and transport properties in diluted magnetic semiconductor. Another model is the one and two-orbital double-exchange models to study colossal magnetoresistance behavior in manganites which was presented in 2006 by C. Sen et al. [59].

The model we use here to study spin transport takes into account the following interactions:

- Interactions between lattice spins, given by the Hamiltonian of the lattice.
- Interactions between itinerant spins and lattice spins given by

$$\mathcal{H}_l = -\sum_{i,j} I_{i,j} \vec{\sigma}_i . \vec{S}_j, \tag{1.54}$$

where $\vec{\sigma}_i$ is the spin of the itinerant electron i, and $I_{i,j}$ denotes the interaction that depends on the distance between the electron i and the spin $\vec{S}_j$ at the lattice site j. We use the following interaction expression:

$$I_{i,j} = I_0 e^{-C_1 r_{ij}} \quad \text{with} \quad r_{ij} = |\vec{r}_i - \vec{r}_j|, \tag{1.55}$$

where I_0 and C_1 are constants. The interaction range is limited to a sphere of radius D_1.

- Interactions between itinerant spins: In the same way, interactions between itinerant electrons are modelled by:

$$\mathcal{H}_m = -\sum_{i,j} K_{i,j} \vec{\sigma}_i . \vec{\sigma}_j, \tag{1.56}$$

$$K_{i,j} = K_0 e^{-C_2 r_{ij}}, \tag{1.57}$$

with $\vec{\sigma}_i$ the spin of the itinerant electron i and $K_{i,j}$ the interaction strength depending on the distance between the electrons i and j. The choice of the constants K_0 and C_2 is discussed in the chapter 2. The interaction range is limited to a sphere of radius D_2.

- Chemical potential term: Since the interactions between itinerant electrons are attractive, we need to add a chemical potential in order to avoid a possible collapse of electrons at some points in the crystal and to ensure an homogeneous distribution of electrons during the simulation. The chemical potential term is given by

$$\mathcal{H}_c = D[n(\vec{r}) - n_0], \tag{1.58}$$

where D is a constant parameter appropriately chosen, $n(\vec{r})$ the concentration of itinerant spins in the sphere of cutoff radius D_2 centered at the position $\vec{r}$ of the itinerant spin under consideration, and n_0 the averaged concentration.

- Electric field term:

$$\mathcal{H}_E = -e\vec{\epsilon}.\vec{\ell} \tag{1.59}$$

where e is the charge of electron, $\vec{\epsilon}$ the applied electrical field and $\vec{\ell}$ the displacement vector of an electron.

Note that in Eq. (1.58) the chemical potential is proportional to density, as it is for perfect gases, and leads to a density gradient term in the Boltzmann's equation. This electrochemical potential contains a term proportional to electron density times the electric potential as written in Eq. (1.59) in the case of a uniform electric field. Of course the difference between Eq. (1.58) and Eq. (1.59) is due to the fact that the electric field in Eq. (1.58) is due to internal charges while in Eq. (1.59) it is due to an external potential.

1.4.3 Structure of a Monte Carlo program to the study of spin transport

We can summarize here the structure of our MC program to study of spin transport by our model as in Fig. 1.8.

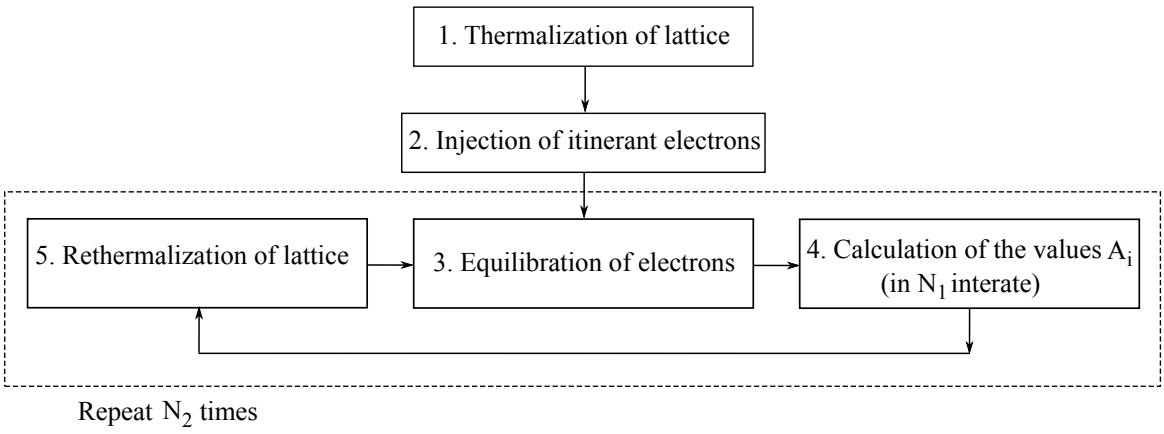

Figure 1.8: Scheme of algorithm MC method to study spin transport.

- **Step 1:** Thermalization of the system without itinerant electrons to obtain an

equilibrium lattice at a given temperature T.

- **Step 2:** Random injection of N_0 itinerant electrons into the system.

- **Step 3:** Equilibrating the itinerant electrons using the following updating:

  (i) For each itinerant electron:
  - Calculation of the energy of this electron E_{old}.
  - Move the electron under consideration to a new position with a step of length l in an arbitrary direction. Note that the move is rejected if the electron falls in a sphere of radius r_0 centered at a lattice spin or at another itinerant electron. This excluded space comes from the Pauli exclusion principle. Then calculation of the new energy E_{new}.
  - Use the Metropolis algorithm to accept or reject the electrons displacement.

  (ii) Choose another itinerant electron and start again this procedure. When all itinerant electrons have been considered, we say that we have made a MC step per electron.

  (iii) Perform a large number of MC steps to obtain an equilibrium electron state.

- **Step 4:** Continue to perform N_1 MC steps; at each stage, calculate the value A_i of the considered quantity A.

- **Step 5:** Rethermalization of the lattice to take another disconnected lattice configuration. Then we equilibrate the itinerant electrons corresponding to the new lattice configuration. After that, we also perform N_1 MC steps to estimate the value of the considered quantity A.

Repeat the above cycle N_2 times and calculate the average value of the quantity A by the formula:

$$\langle A \rangle = \frac{1}{N_1.N_2} \sum_{i=1}^{N_1.N_2} A_i, \tag{1.60}$$

where $N_1.N_2$ is the totals number of MC steps used to determine A.

For example, the resistivity ρ is defined as

$$\rho = \frac{1}{n}, \tag{1.61}$$

where n is the number of itinerant electrons crossing a unit area perpendicular to the x direction per unit of MC time. To know this number, we count them at three "detector" surfaces perpendicular to the x direction: the first at $N_x/4$, the second at $N_x/2$ and the third at $3N_x/4$. Averaging the resistivity over these three positions helps to further improve the results (in the previous works [60, 61, 62] they were counted only at the end of the sample).

In order to choose an optimal value for N_1, we consider the following temperature dependence of the relaxation time τ_L in non frustrated spin systems. The relaxation time is expressed in this case [63, 64, 65] as

$$\tau_L = \frac{A}{|1 - T/T_C|^{z\nu}}, \tag{1.62}$$

where A is a constant, ν the correlation critical exponent, and z the dynamic exponent. From this expression, we see that as temperature T approaches to the transition temperature T_C, τ_L diverges. In the critical region around the transition temperature T_c, the system thus encounters the so-called "critical slowing down": the spin relaxation is extremely long due to the divergence of the spin-spin correlation. In our previous papers [60, 61, 62, 66, 67, 68, 69] we did not take into account the temperature dependence of τ_L. For the Ising spin model, $\nu = 0.638$ (3D Ising universality) and $z = 2.02$ [70]. We have previously shown that τ_L strongly affects the shape of ρ at T_C [64].

The itinerant spins move into the system at one end, travel in the x direction, and escape the system at the other end to reenter again at the first end under periodic boundary conditions. Note that periodic boundary conditions are used to ensure that the average density of itinerant spins remains constant with evolving time stationary regime.

Chapter 2

Phase Transitions and Spin Transport in Frustrated Systems

Using the method presented in chapter 1, we introduce in this chapter frustrated spin systems, and study two types of systems.

* The first one is a SC lattice with Ising spins interacting with each other via nearest and next-nearest neighbor antiferromagnetic interactions, J_1 and J_2 respectively ($J_1 - J_2$ model).

* The second one is a HCP lattice with both Ising and XY spins in which we suppose the in-plane interaction J_1 and inter-plane interaction J_2, both AF.

For each system, we determine the GS by the steepest-descent method and then we address the properties of its phase transitions. By extensive standard MC simulations described in chapter 1, we calculate different thermodynamic quantities such as the energy, magnetization, specific heat and susceptibility. The phase transition is indicated by anomalies in these quantities. The nature of phase transition is also determined by the histogram technique introduced in the last part of chapter 1. We have calculated the critical temperature T_c as a function of $\eta = J_2/J_1$ for the first case, and $\eta = J_1/J_2$ for the second one. The phase diagram in the space (T_c, η) is shown for both cases. Finally, the spin resistivity ρ is calculated for the Ising case for many values of parameters, so that we can estimate their effect.

2.1 Introduction

Historically, the first frustrated system was studied by G. H. Wannier [71] in 1950. It is the Ising model on a triangular lattice, with NN antiferromagnetic coupling. Ten years later, striking properties related to frustration were discovered in helical spin structures by A. Kaplan [72], A. Yoshimori [73], J. Villain [74] and R. J. Elliott [75]. However, at that time, the word "frustration" had not appeared. The name was first introduced by Toulouse in 1977 [76].

Frustrated spin systems have been the subject of intensive investigations during the last 30 years [17]. Frustration plays a very important role in spin systems, including Ising spin systems, classical vector spin systems such as the XY model, or the classical Heisenberg model, and also quantum spin systems. It is one of the most interesting issues in condensed matter physics.

These systems are very unstable due to the competition between antagonist interactions or to a geometrical frustration. A spin is said to be frustrated when it cannot find an orientation which "fully" satisfies all the interactions with its neighbors. The GS does not correspond to the minimum of the interaction energy of every spin pair.

We show in Fig. 2.1 an example of a system where four Ising spins are arranged in a tetrahedron, the interactions between them are antiferromagnetic. Their total energy is minimized when each spin is aligned opposite to its neighbors. As seen, in the figure there are six NN interactions, four of which are antiparallel and thus favorable, but two of which (between 1 and 2, and between 3 and 4) are unfavorable. Thus the system is frustrated.

We consider another situation where the spin system is frustrated by different kinds of conflicting interactions; in this case also, the GS does not correspond to the minimum energy of each kind of interaction. For instance, let us consider a spin chain where the NN interaction J_1 is ferromagnetic while the NNN interaction J_2 is antiferromagnetic. As long as $|J_2| << J_1$, the GS is ferromagnetic: every NN bond is

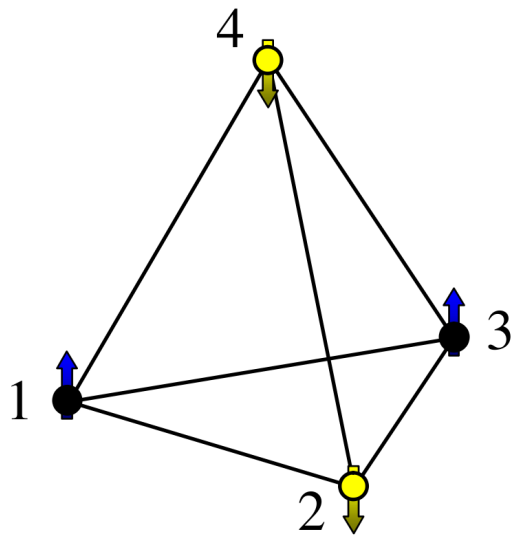

Figure 2.1: Example of frustration in 3D.

satisfied but the NNN ones are not. On the other hand, when $|J_2|$ exceeds a critical value, the ferromagnetic GS is no longer valid: neither NN nor NNN bonds are fully satisfied.

In general, we can say that a spin system is frustrated when one cannot find a configuration of spins to fully satisfy the interaction (bond) between every pair of spins. In other words, the minimum of the total energy does not correspond to the sum of the minimum energy of all bonds. This situation arises when there is a competition between different kinds of interactions between a spin and its neighbors, or when the lattice geometry does not allow to satisfy all the bonds simultaneously. With this definition, the chain with NN ferromagnetic and NNN antiferromagnetic interactions discussed above is frustrated even in the case where the ferromagnetic spin configuration is its GS ($|J_2| \ll J_1$) [77].

As a consequence of frustration, the GS is highly degenerate. In the Ising case, the GS degeneracy is often infinite as in the triangular, the face-centered cubic (FCC) and the HCP lattices with antiferromagnetic interactions. In the case of vector spins, the GS is non collinear such as the 120-degree configuration in the XY and Heisenberg

antiferromagnetic stacked triangular lattice. In 2D, several frustrated systems with Ising spins have been solved exactly [78, 17]. Among the most interesting models one can mention the frustrated generalized Kagome lattice and the honeycomb lattice [79] where exotic features such as the existence of several phase transitions, the reentrance, and the disorder lines have been exactly found by mapping these systems into vertex models [80]. In 3D, the situation is complicated. The renormalization group [12, 13, 81], which provided a good understanding of the nature of the phase transition in non frustrated systems, encounters many difficulties when applied to frustrated systems. Among the most studied subjects during the last 20 years, one can mention the nature of the phase transition in the XY and Heisenberg stacked triangular lattice. After a long debate [82] on whether it is a first- or a second-order transition, and or it belongs to a new universality class, the controversy has recently ended with the conclusion that it belongs to a first-order transition. Let us mention the early work of Itakura who, using MC and MC renormalization group, has identified a first-order behavior in the XY stacked triangular lattice case [83], the work of Bekhechi et al. [84] who, using a short-time critical dynamics, have come to the same conclusion, and finally the works of Ngo and Diep who put an end to the controversy [18, 19].

2.2 Phase Transition and Spin Transport in the $J_1 - J_2$ model

2.2.1 Model and Ground-state

We consider the SC lattice shown in Fig. 2.2, on which we consider the classical Ising model with spin magnitude $S = 1$. The lattice Hamiltonian is given by

$$\mathcal{H} = -J_1 \sum_{(i,j)} \mathbf{S}_i.\mathbf{S}_j - J_2 \sum_{(i,m)} \mathbf{S}_i.\mathbf{S}_m, \tag{2.1}$$

where $\mathbf{S}_i$ is the Ising spin at the lattice site i, $\sum_{(i,j)}$ is made over the NN spin pairs $\mathbf{S}_i$ and $\mathbf{S}_j$ with interaction J_1, while $\sum_{(i,m)}$ is performed over the NNN pairs with

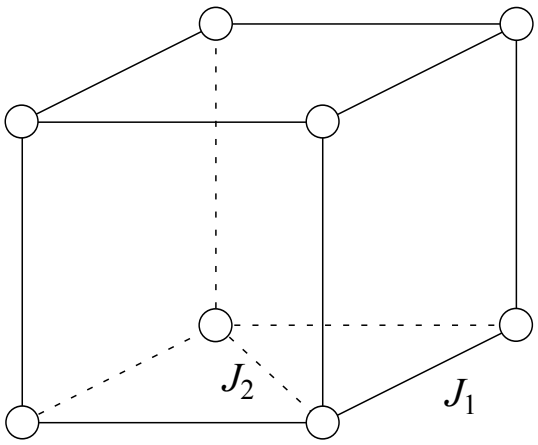

Figure 2.2: Simple cubic lattice with nearest and next-nearest neighbor interactions, J_1 and J_2, indicated.

interaction J_2. We are interested in the frustrated regime. Therefore, hereafter we suppose that $J_1 = -J$ ($J > 0$, antiferromagnetic interaction, and $J_2 = -\eta J$ where η is a positive parameter.

The GS can be determined by the steepest-descent method. This method can be summarized as follows:
(i) generate an initial configuration at random,
(ii) calculate the local field created at a site by its neighbors using (2.1),
(iii) align the spin of that site along the calculated local field to minimize its energy,
(iv) go to another site and repeat until all sites are visited: we say we make one sweep,
(v) do a large number of sweeps per site until a good convergence is reached.

One can also minimize the interaction energy as shown below to calculate the GS configuration. The steepest descent method with varying J_2 ($J_1 = -1$) gives two kinds of GS spin configuration: the first configuration is decomposed into two NNN tetrahedrons formed by the NNN sites and stacked as shown in Fig. 2.3(a), while the second one is collinear configurations (one line up, one line down) as in Fig. 2.3(b).

The transition between the two configurations is estimated as follows: one simply

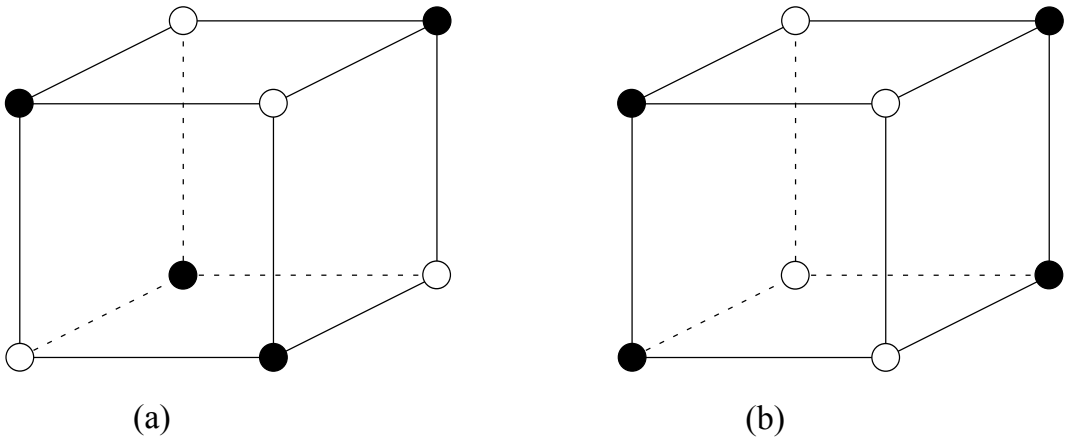

Figure 2.3: Simple cubic lattice. Up-spins: white circles; down-spins: black circles. (a): Ground state when $|J_2| < 0.25|J_1|$, (b): Ground state when $|J_2| > 0.25|J_1|$.

writes down the respective energies of an elementary cell and compares them:

$$E_1 = 3J_1 - 6J_2, \tag{2.2}$$

$$E_2 = J_1 + 2J_2. \tag{2.3}$$

One sees that $E_1 < E_2$ when $J_2 > 0.25J_1$, i.e. $|J_2| < 0.25|J_1|$. Thus the first configuration is more stable for $\eta < 0.25$.

Note that this latter configuration is three-fold degenerate by choosing the lines of parallel NN spins along x, y or z axis. With the permutation of black and white spins, the total degeneracy is thus six.

2.2.2 Phase transition: results

We consider a film with a thickness of N_z cubic cells in the z direction. Each of the xy planes contains $N_x \times N_y$ cells. Periodic boundary conditions are used on the xy planes.

The exchange interaction $|J_1| = 1$ is used as the unit of energy. At a given temperature, the system reaches equilibrium and average physical quantities over several millions of MC steps per spin are obtained.

The averaged energy $\langle U \rangle$ and the heat capacity C_V are calculated by

$$\langle U \rangle = \langle \mathcal{H} \rangle, \tag{2.4}$$

$$C_V = \frac{\langle U^2 \rangle - \langle U \rangle^2}{k_B T^2}, \tag{2.5}$$

where $\langle ... \rangle$ indicates the thermal average taken over microscopic states at the temperature T.

The order parameter M is defined from the sublattices magnetizations by

$$M = \sum_K |\sum_{i \in K} \mathbf{S}_i|, \tag{2.6}$$

where $\mathbf{S}_i$ belongs to the sublattice K.

The susceptibility is defined by

$$\chi = \frac{\langle M^2 \rangle - \langle M \rangle^2}{k_B T}. \tag{2.7}$$

In MC simulations, we work at finite sizes, so for each size we have to determine the "pseudo" transition which corresponds in general to the maximum of the specific heat or of the susceptibility. The maxima of these quantities need not be at the same temperature. Only for infinite sizes, they should coincide. The theory of finite-size scaling which we have introduced in section 1.3.2 of chapter 1 permits one to deduce the properties of a system at its thermodynamic limit. In order to check the first-order nature of the transition, we used the histogram technique which is very efficient in detecting weak first-order transitions and in calculating critical exponents of second-order transitions (see section 1.3 of chapter 1 for details). The main idea of this technique is to make an energy histogram at a temperature T_0 as close as possible to the transition temperature. One has often to try at several temperatures in the transition region. Using histogram method described in chapter 1, one obtains energy histograms in a range of temperature around T_0. In second-order transitions, these histograms are Gaussian. This allows us to calculate averages of physical quantities as well as the critical exponents using the finite-size scaling. In first-order transitions, the energy histogram shows a double-peak structure.

In the following, our results are shown in Fig. 2.4 to Fig. 2.8 with $N_x = N_y = 20$ and $N_z = 6$.

Since the GS changes at $\eta_c = 0.25$, we show samples on both sides of this value. Fig. 2.4 shows the energy per spin E, the order parameter M, the specific heat C_V and the susceptibility χ, for $\eta = 0.20$. The transition is second order.

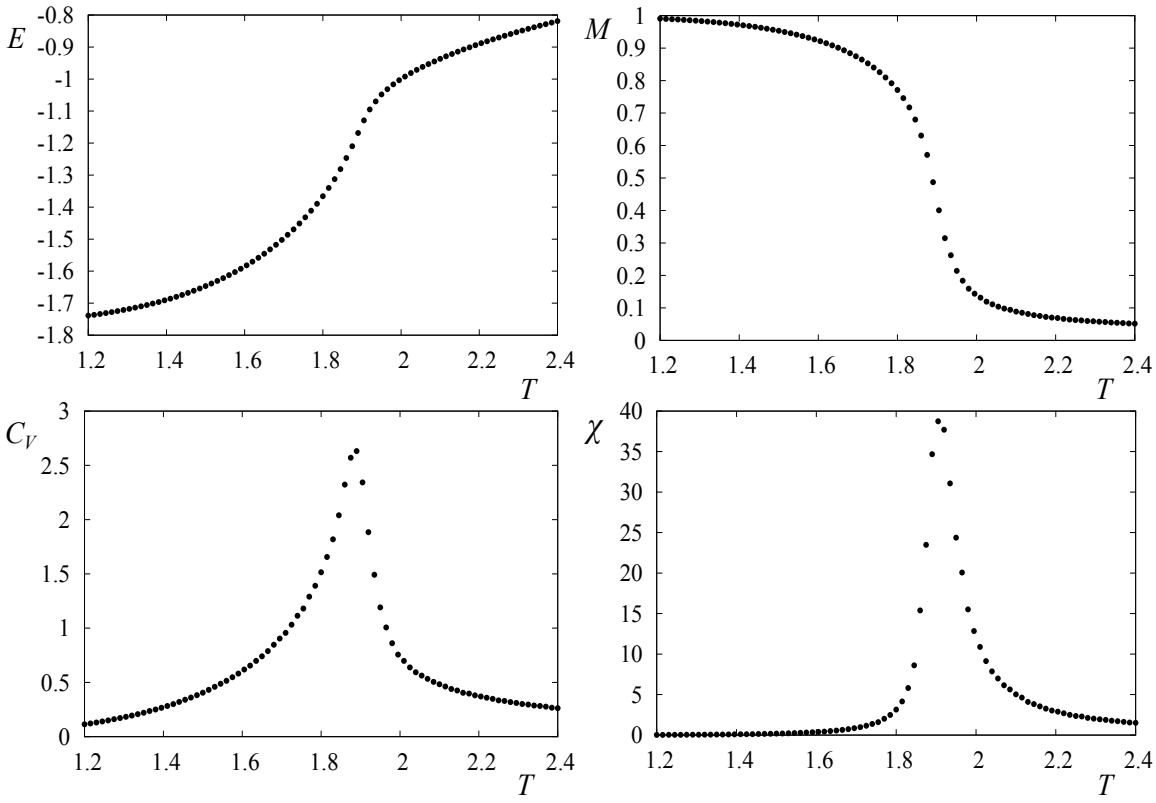

Figure 2.4: Energy per spin E, order parameter M, specific heat C_V and susceptibility χ versus temperature T for $\eta = J_2/J_1 = 0.20$. See text for comments.

On the other side, we show in Fig. 2.5 the energy per spin E, the order parameter M, the specific heat C_V and the susceptibility χ, for $\eta = 0.26$ and 0.30. We find a strong first-order transition in both cases. The discontinuity of E and M at the transition is very large.

In Fig. 2.6 and Fig. 2.7 we show the energy histogram taken for $\eta = 0.20$, 0.26, and 0.3 at the transition temperatures. As seen, the first case is a Gaussian distribu-

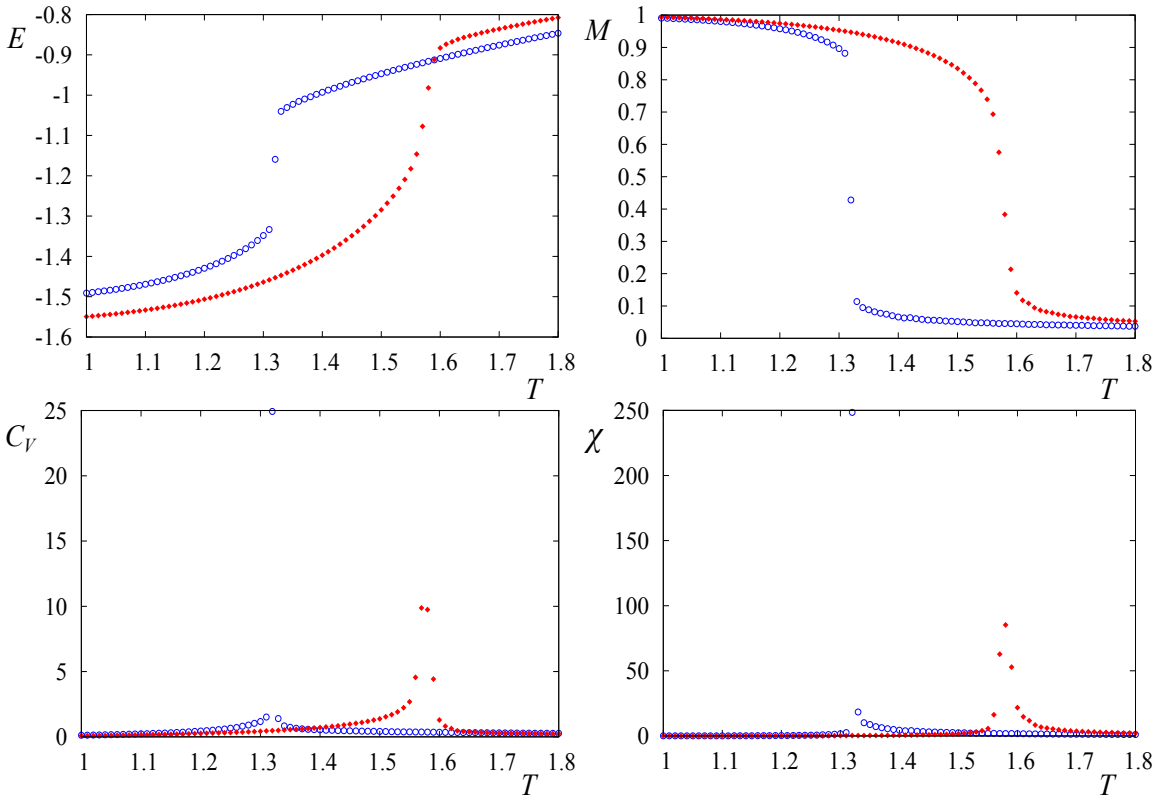

Figure 2.5: (Color online). Energy per spin E, order parameter M, specific heat C_V and susceptibility χ versus temperature T for $\eta = J_2/J_1 = 0.26$ (blue open circles) and 0.30 (red diamonds). See text for comments.

tion indicating a second-order transition, while the last two cases show a double-peak structure indicating a first-order transition. The distance between two peaks represents the latent heat.

We have calculated the critical temperature T_C as a function of η. The phase diagram is shown in Fig. 2.8 where (1) and (2) indicate the ordering of the first, and second kinds, respectively. (P) indicates the paramagnetic phase. Note that the transition line between (1) and (P) is a second-order line, while that between (2) and (P) is a first-order line.

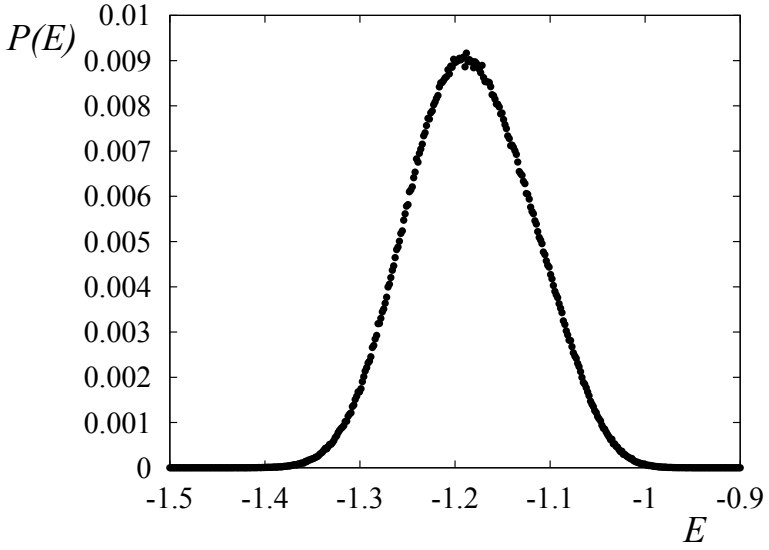

Figure 2.6: Energy histogram $P(E)$ versus energy E for $\eta = 0.2$ at $T_c = 1.884$. See text for comments.

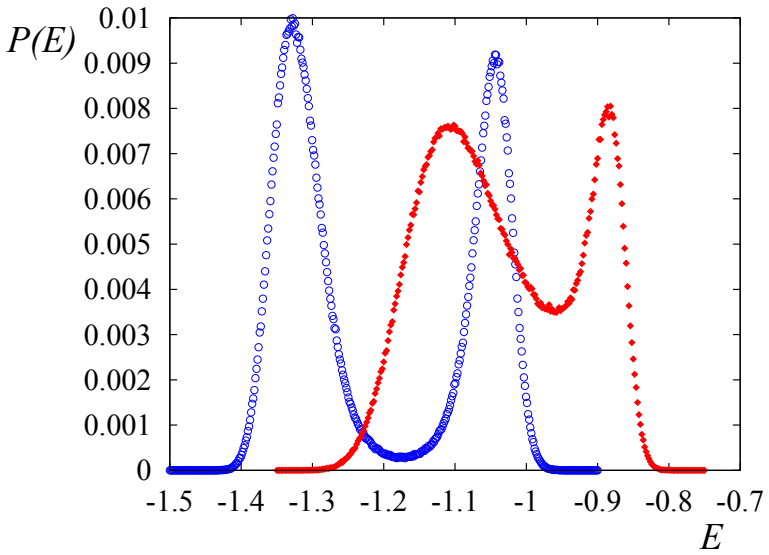

Figure 2.7: (Color online). Energy histogram $P(E)$ versus energy E for $\eta = 0.26$ (blue open circles) at $T_c = 1.3195$ and 0.3 (red diamonds) at $T_c = 1.5754$. See text for comments.

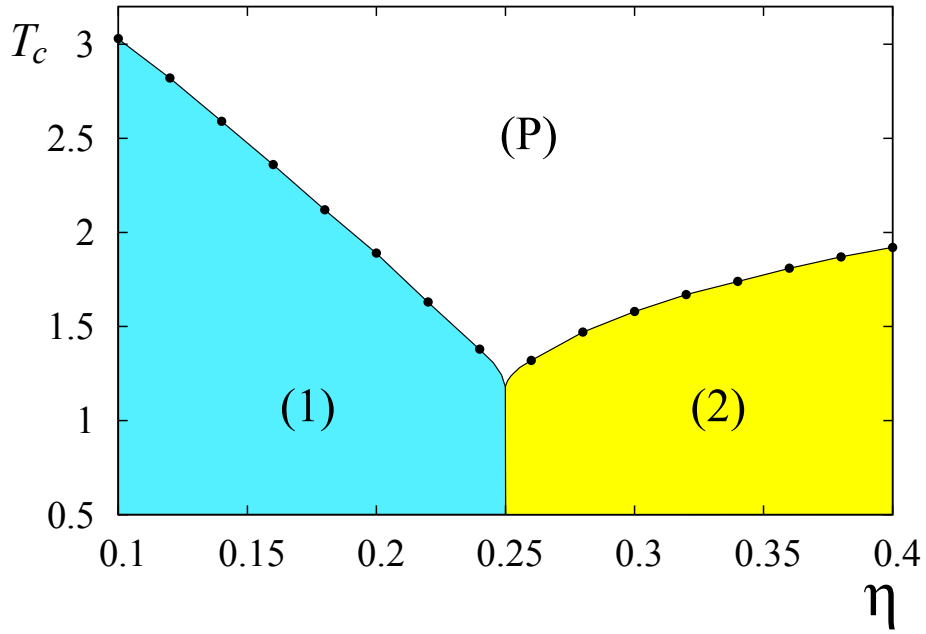

Figure 2.8: (Color online). Phase diagram of the lattice in the space (T_c, η). (1), (2) and (P) denote the first, second and paramagnetic phases, respectively. See text for comments.

2.2.3 Spin transport: results

The method has been described in detail in section 1.4 of chapter 1.

We will show below results obtained for typical values of parameters. The choice of the parameters has been made after numerous test runs. We describe the principal requirements which guide our choice:

i) We choose the interaction between lattice spins as unity, i. e. $|J_1| = 1$.

ii) We choose the interaction between an itinerant spin and its surrounding lattice spins so as its energy E_i in the low temperature region is of the same order of magnitude as that between lattice spins. To simplify, we take $C_1 = 1$ in Eq. 1.55.

iii) The interaction between itinerant spins is chosen so that this contribution to the itinerant spin energy is smaller than E_i in order to highlight the effect of the lattice ordering on the spin current. To simplify, we take $C_2 = 1$ in Eq. 1.57.

iv) The choice of D in Eq. 1.58 is made in such a way as to avoid the formation of clusters of itinerant spins (collapse) due to their attractive interaction.

v) The electric field in Eq. 1.59 is chosen not too strong in order to avoid its dominant effect that would mask the effects of thermal fluctuations and of the magnetic ordering.

vi) The density of the itinerant spins in Eq. 1.58 is chosen in a way that the contribution of interactions between themselves is neither too weak nor too strong with respect to E_i.

With these requirements, a variation of each parameter does not change qualitatively the results shown below. As will be seen, only the variation of D_1 changes drastically the results. This is the reason why we will study in detail the effect of this parameter. For larger densities of itinerant spins, the resistivity is larger as expected because of additional scattering processes between itinerant spins.

We fix $J_1 = -J = -1$ (AF interaction) for NN coupling of lattice spins as said above. The energy is thus measured in the unit of J. The temperature is expressed in the unit of J/k_B. The distances (D_1, D_2) are in the unit of a, the lattice constant.

We perform the simulation by taking into account the relaxation time of the lattice spins which is given by Eq. 1.62 with choosing $A = 1$. We fix $\tau_L = 1$ at $T = 2T_C$ deep inside the paramagnetic phase far above T_C. This value is what we expect for thermal fluctuations in the disordered phase.

As far as the interaction between itinerant spins is attractive, we need a chemical potential to avoid the collapse of the system. The strength of the chemical potential D depends on K_0. We show in Fig. 2.9 the collapse phase diagram which allows to choose for a given K_0, an appropriate value of D.

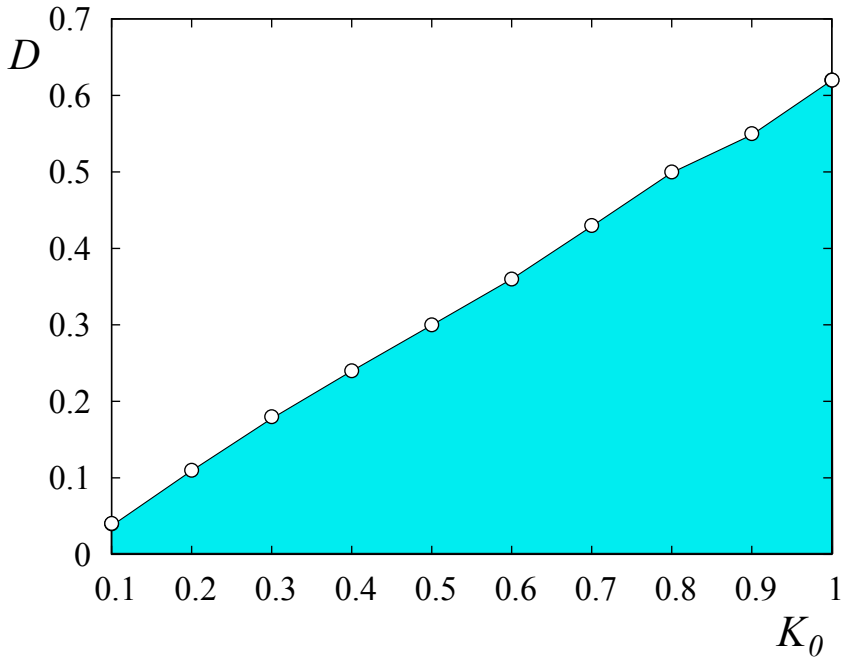

Figure 2.9: Phase diagram in the plane (K_0, D). The collapse region is in blue, for $\eta = 0.26$. Other parameters are $D_1 = D_2 = 1$, $I_0 = 0.5$, $\epsilon = 1$.

In order to see the reflection of the spin resistivity on the nature of phase transition, we focus in the following on two cases: $\eta = 0.2$ and $\eta = 0.26$, the values correspond

to the second and the first order transition, respectively.

A. For $\eta = 0.2$:

We show in Fig. 2.10 the resistivity at two temperatures, below and above the transition temperature T_C, as functions of D_1. At low temperature, we observe an oscillatory behavior of the resistivity ρ. By analyzing the ratio of numbers of up spins and down spins in the sphere of radius D_1, Magnin and Diep [68] found that this ratio oscillates with varying D_1: the maxima (minima) of ρ correspond to the largest (smallest) numbers of parallel (antiparallel) spins in the sphere. At high temperature, the lattice spins are disordered, the ratio of numbers of up spins and down spins in the sphere of interaction should be constant and equal to 1. There are nevertheless very slight oscillations due to the finite value of D_1 and the distance not far from Néel temperature T_N. Indeed, note that the amplitude of fluctuations is reduced as D_1 or T increases. In the limit where $D_1 \to \infty$, the different sizes do not exhibit oscillations.

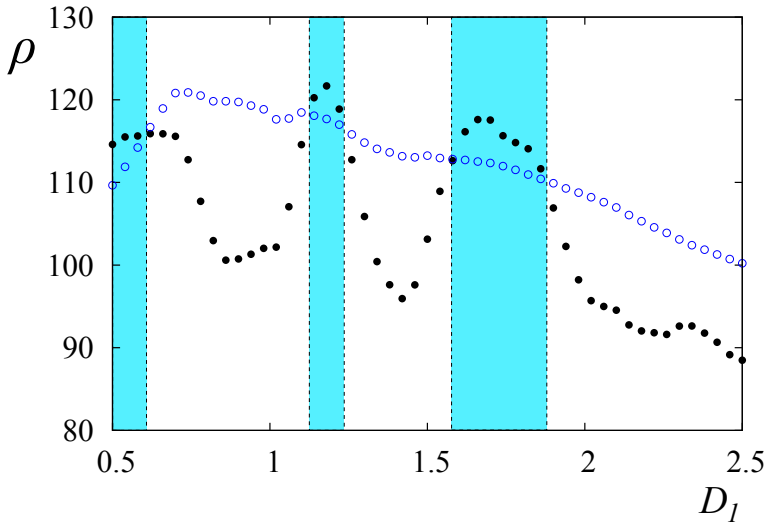

Figure 2.10: (Color online). Spin resistivity versus D_1 for $\eta = 0.2$ at $T = 1.5$ (black circles) and 2.1 (blue open circles). Other parameters are $N_x = N_y = 20, N_z = 6$, $I_0 = K_0 = 0.5$, $D_2 = 1$, $D = 1$, $\epsilon = 1$.

On the other hand, one observes a crossover of low temperature and high tem-

perature resistivities at different positions of D_1. Depending on D_1, the low temperature resistivity can be smaller (white zones) or larger (blue zones) than that at high temperature. So, at the transition temperature, resistivity ρ can jump upward or downward, depending on the value of D_1.

We show in Fig. 2.11 the resistivity as a function of temperature for $D_1 = 1.2$. In this case, the resistivity is bigger below than above the transition temperature. This has been experimentally observed on $La_{0.4}Ca_{0.6}MnO_3$ by Lu et al. [1] (see Fig. 2.12).

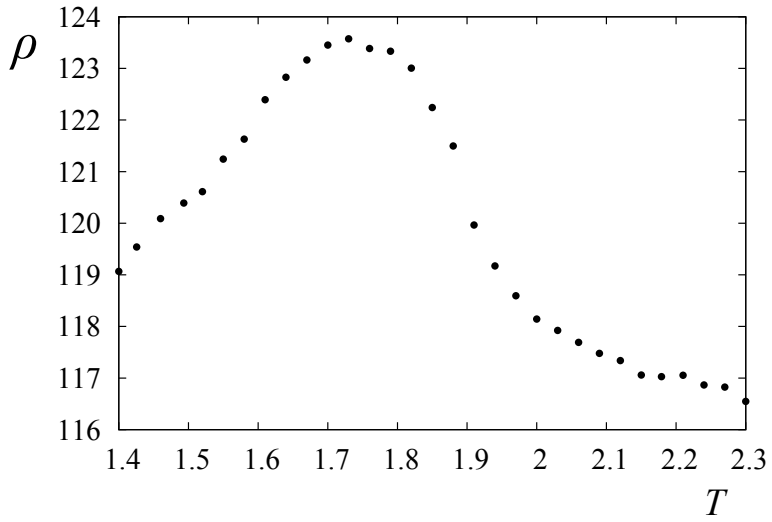

Figure 2.11: Spin resistivity versus temperature for $\eta = 0.2$, $D_1 = 1.2$. Other parameters are $N_x = N_y = 20, N_z = 6$, $I_0 = K_0 = 0.5$, $D_2 = 1$, $D = 1$, $\epsilon = 1$.

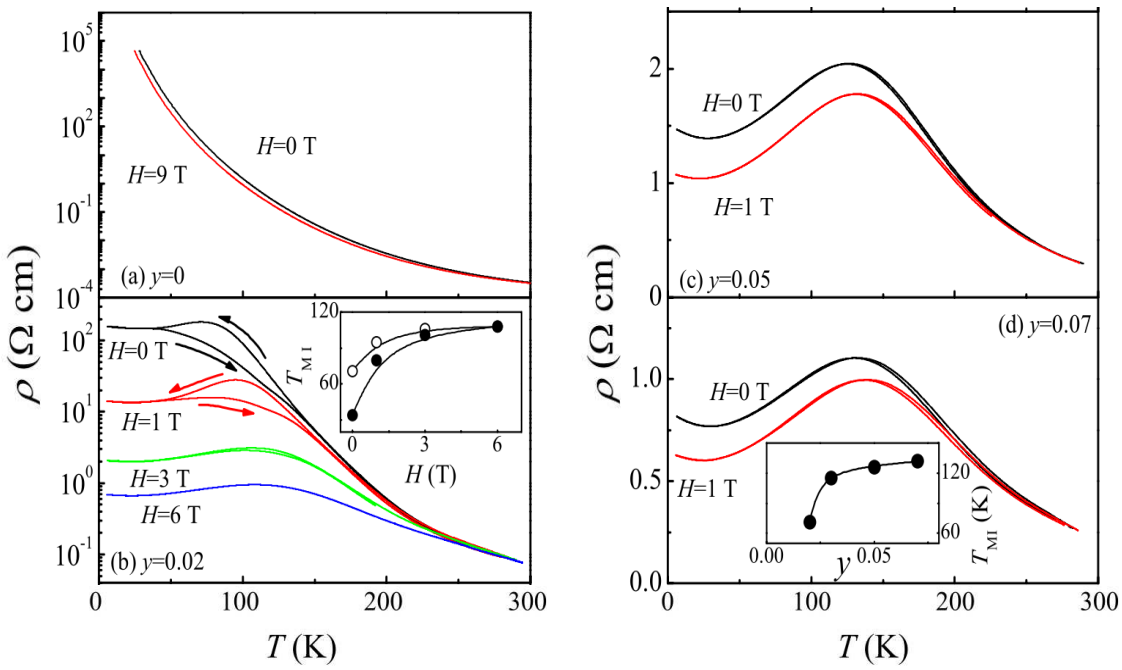

Figure 2.12: Resistivity versus temperature at various external magnetic fields in charge-ordered $La_{0.4}Ca_{0.6}MnO_3$. The figures presented are taken from Fig. 2 of [1].

In contrast, for $D_1 = 0.8$ or $D_1 = 1$, the resistivity is smaller below than that above the transition temperature, as seen in Fig. 2.13.

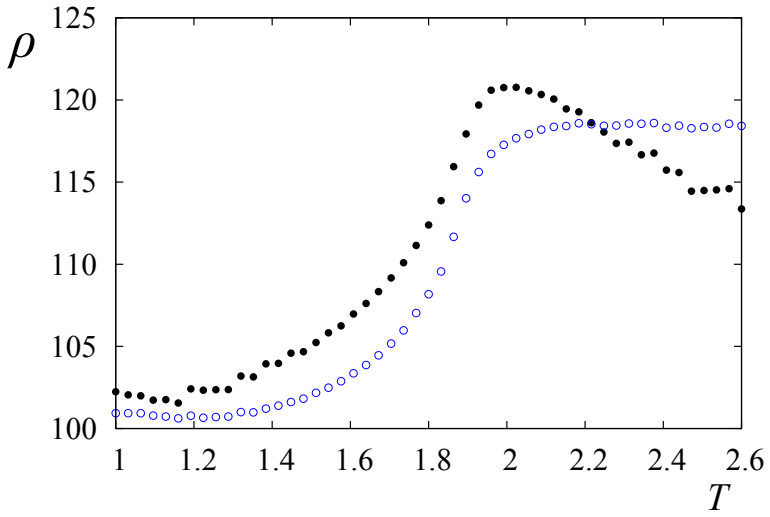

Figure 2.13: (Color online). Spin resistivity versus temperature for $\eta = 0.2$ with $D_1 = 0.8$ (black circles) and 1 (blue open circles). Other parameters are $N_x = N_y = 20, N_z = 6$, $I_0 = K_0 = 0.5$, $D_2 = 1$, $D = 1$, $\epsilon = 1$.

B. For $\eta = 0.26$:

We show in Fig. 2.14 the resistivity at two temperatures, below and above the transition temperature T_C, as a function of D_1. We observe a similar behavior to the second phase transition.

The resistivity ρ can make a down fall or an upward jump at the transition temperature T_C depending on the value of D_1, as shown in Fig. 2.15. Note the discontinuity of ρ at T_C. This behavior has been observed and analyzed in terms of the averaged magnetization in the sphere of radius D_1 in the frustrated FCC antiferromagnet [68]. In our previous work [69], we did not take into account the temperature dependence of τ_L, the results are shown in Fig. 2.16.

From the results shown above for $J_1 - J_2$ model, we conclude that the spin resistivity reflects the nature of the lattice transition: In a second-order transition of the magnetic lattice ordering, the resistivity has a rounded maximum in the region

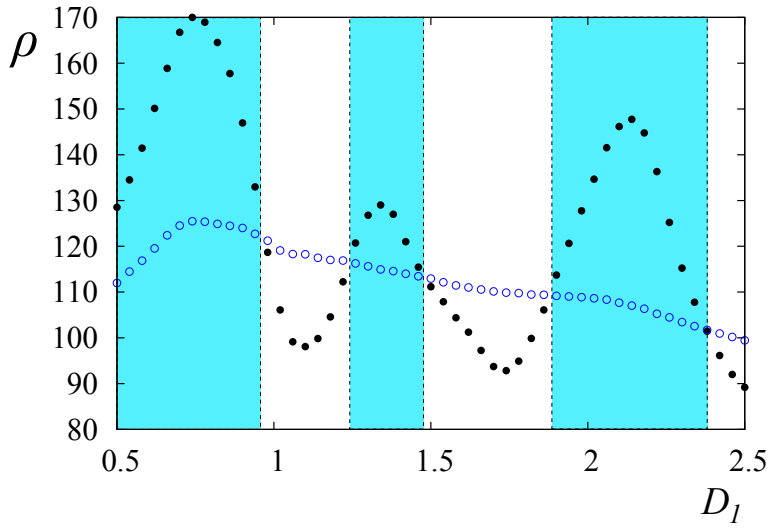

Figure 2.14: (Color online). Spin resistivity versus D_1 for $\eta = 0.26$ at $T = 1.2$ (black circles) and 1.5 (blue open circles). Other parameters are $N_x = N_y = 20, N_z = 6$, $I_0 = K_0 = 0.5$, $D_2 = 1$, $D = 1$, $\epsilon = 1$.

close to the transition while in a first-order transition, the resistivity undergoes a discontinuity at the transition temperature.

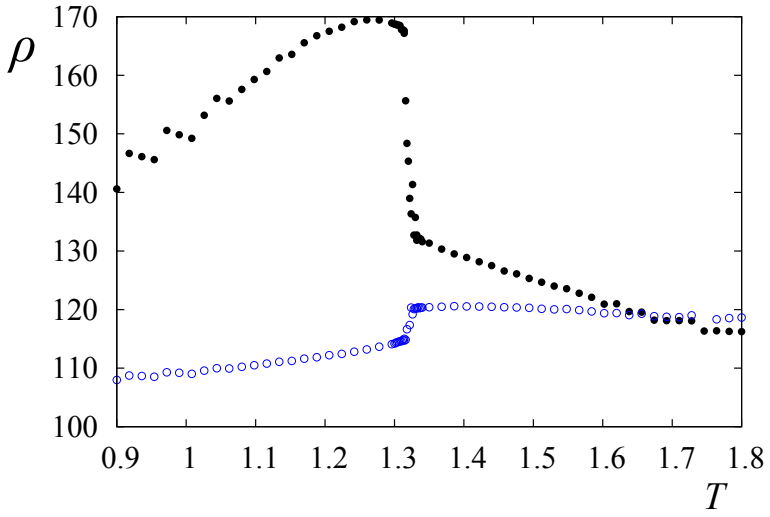

Figure 2.15: (Color online). Spin resistivity versus temperature for $\eta = 0.26$ with $D_1 = 0.8$ (black circles) and 1 (blue open circles). Other parameters are $N_x = N_y = 20, N_z = 6$, $I_0 = K_0 = 0.5$, $D_2 = 1$, $D = 1$, $\epsilon = 1$.

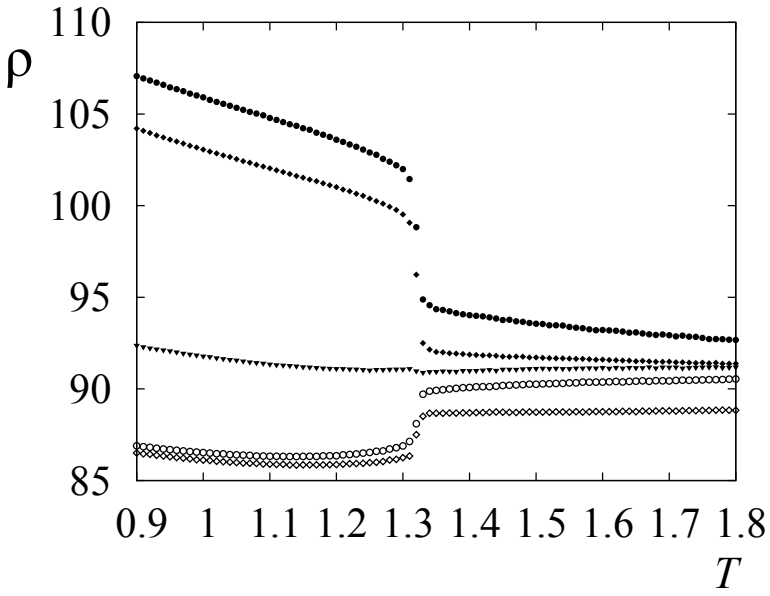

Figure 2.16: Spin resistivity calculated with temperature-independent relaxation versus T for $\eta = 0.26$ for several values of D_1: from up to down $D_1 = 0.7, 0.8, 0.94, 1, 1.2$. Other parameters are $N_x = N_y = 20, N_z = 6$, $I_0 = K_0 = 0.5$, $D_2 = 1$, $D = 1$, $\epsilon = 1$.

2.3 Phase Transition and Spin Transport in the Hexagonal-Close-Packed Lattice

In this section, we are interested in the HCP antiferromagnet with Ising and XY spin models. Our purpose is to study its properties such as the GS, the phase transition and the spin transport, in the case of anisotropic exchange interactions. The isotropic NN antiferromagnetic interaction has been studied for Ising [85], XY, and Heisenberg spins [86]. These isotropic cases have been shown to undergo a phase transition of first order, and the infinite GS degeneracy is reduced to 6 at low temperatures [85, 86]. The effect of anisotropic interaction and anisotropy on the GS in the case of vector spins has also been studied [87].

2.3.1 Model and Ground-state

We consider the HCP lattice shown in Fig. 2.17. The stacking direction is z. The

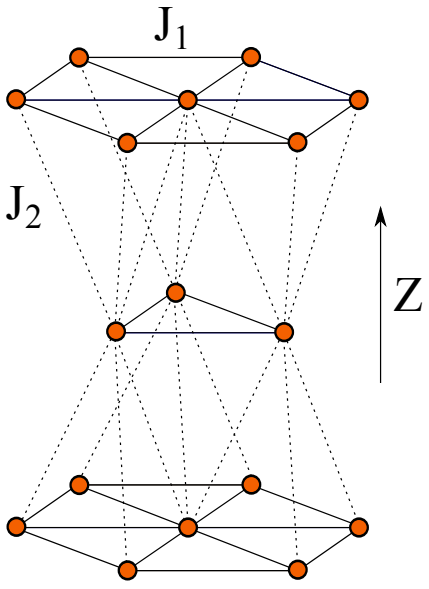

Figure 2.17: HCP lattice. The in-plane and inter-plane interactions are indicated by J_1 and J_2.

lattice Hamiltonian is given by

$$\mathcal{H} = -\sum_{(i,j)} J_{ij}\mathbf{S}_i \cdot \mathbf{S}_j, \tag{2.8}$$

where $\mathbf{S}_i$ is the spin at lattice site i and J_{ij} is the antiferromagnetic interaction between NN. We suppose that $J_{ij} = J_1$ if the NN are on the xy triangular plane, and $J_{ij} = J_2$ if the NN are on two adjacent planes (see Fig. 2.17). The GS can be determined by the steepest-descent method. This method has been described in section 2.2.1.

However, one can also minimize the interaction energy as shown below to calculate the GS configuration. Since both interactions are antiferromagnetic (negative), we fix $J_2 = -1$ for simplicity, and vary J_1. The unit of energy is taken as $|J_2|$ and the temperature T is in the unit of $|J_2|/k_B$ where k_B is the Boltzmann constant.

Let us recall the GS in the case of isotropic interactions, namely, $J_1 = J_2$ [86]. For the HCP lattice, each spin is shared by eight tetrahedra (four in the upper half-space and four in the lower half-space along the z axis) and an NN bond is shared by two tetrahedra. The GS spin configuration of the system is formed by stacking neighboring tetrahedra. In the GS, one has two pairs of antiparallel spins on each tetrahedron. Their axes form an arbitrary angle α. The degeneracy is thus infinite (see Fig. 2(a) of Ref. [86]). Of course, the periodic boundary conditions will reduce a number of configurations, but the degeneracy is still infinite. Of these GS's, one particular family of configurations of interest for both XY and Heisenberg cases is when $\alpha = 0$. The GS is then collinear with two spins up and the other two down. The stacking sequence is then simplest: there are three equivalent configurations since there are three ways to choose the parallel spin pair in the original tetrahedron.

We now examine the case where $J_1 \neq J_2$:

A. Ising case

The steepest descent method with varying J_1 ($J_2 = -1$) gives two kinds of GS spin configuration: The first consists of xy ferromagnetic planes stacked antiferromagnetically along the z direction, while the second one is the stacking of xy antiferromagnetic

planes such that each tetrahedron has two up and two down spins. The transition between the two configurations is determined as follows. One simply writes down the respective energies of a tetrahedron and compares them:

$$E_1 = 3(-J_1 + J_2), \tag{2.9}$$

$$E_2 = J_1 + J_2. \tag{2.10}$$

One sees that $E_1 < E_2$ when $J_1 > 0.5J_2$, that is $|J_1| < 0.5|J_2|$. The first configuration is thus more stable when $|J_1| < 0.5|J_2|$.

B. XY case

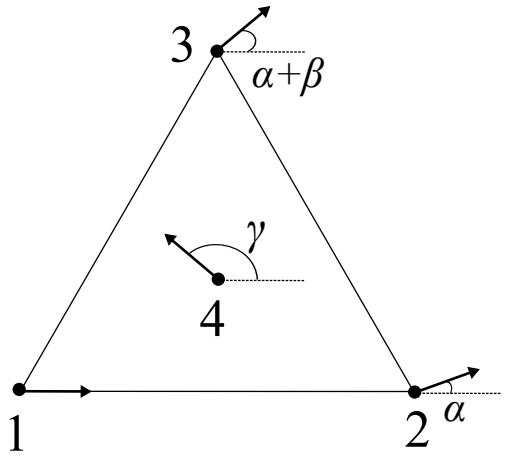

Figure 2.18: Ground state in the XY case. The tetrahedron is projected on the xy plane. The spins are numbered from 1 to 4. See text for comments.

Let us consider a single tetrahedron of the HCP lattice. The Hamiltonian for this cell is given by

$$\begin{aligned} \mathcal{H}_c = & -J_1(\mathbf{S}_1 \cdot \mathbf{S}_2 + \mathbf{S}_2 \cdot \mathbf{S}_3 + \mathbf{S}_3 \cdot \mathbf{S}_1) \\ & -J_2(\mathbf{S}_1 \cdot \mathbf{S}_4 + \mathbf{S}_2 \cdot \mathbf{S}_4 + \mathbf{S}_3 \cdot \mathbf{S}_4). \end{aligned} \tag{2.11}$$

Suppose that $|\mathbf{S}_i| = 1$, one has

$$\begin{aligned} \mathcal{H}_c = & -J_1 \left[\cos\alpha + \cos\beta + \cos(\alpha+\beta)\right] \\ & -J_2 \left[\cos\gamma + \cos(\gamma-\alpha) + \cos(\gamma-\alpha-\beta)\right], \end{aligned} \tag{2.12}$$

where the angles are defined in Fig. 2.18. The steepest descent method shows that while β and γ have unique values for a given J_1/J_2, α is arbitrary, just as in the case of the isotropic interaction [86] discussed above. To simplify the formulas, we take $\alpha = 0$ in the following. The energy of the cell is written as

$$\mathcal{H}_c = -J_1 \left[1 + 2\cos\beta\right] - J_2 \left[2\cos\gamma + \cos(\gamma - \beta)\right]. \tag{2.13}$$

The critical values of β and γ are determined from the relations,

$$\frac{\partial \mathcal{H}_c}{\partial \beta} = 2J_1 \sin\beta - 2J_2 \sin(\gamma - \beta) = 0, \tag{2.14}$$

$$\frac{\partial \mathcal{H}_c}{\partial \gamma} = 2J_2 \sin\gamma + J_2 \sin(\gamma - \beta) = 0. \tag{2.15}$$

We find the following solutions:
(i) $\beta = 0$, $\gamma = 0$,
(ii)$\beta = 0$, $\gamma = \pi$,
(iii) $\beta = \pi$, $\gamma = 0$,
(iv) $\beta = \pi$, $\gamma = \pi$,
and (v) $\cos\beta = \frac{1}{4(J_1/J_2)^2} - \frac{5}{4}$, $\cos\gamma = -\frac{1+3(J_1/J_2)^2}{4(J_1/J_2)}$.

By comparing the energy values at these solutions, we obtain the minimum energy with the last solution: one has

$$\mathcal{H}_c = -\frac{1 + 3(J_1/J_2)^2}{2(J_1/J_2)}, \tag{2.16}$$

where $\cos\beta$ and $\cos\gamma$ are given above.

Because $-1 \leq \cos\beta \leq 1$ and $-1 \leq \cos\gamma \leq 1$, the above solution is valid for $\frac{1}{3} \leq J_1/J_2 \leq 1$.

We plot $\cos\beta$, $\cos\gamma$, β, and γ in Fig. 2.20 where we observe that the non collinear GS configuration occurs in the interval $1/3 \leq \eta = J_1/J_2 \leq 1$.

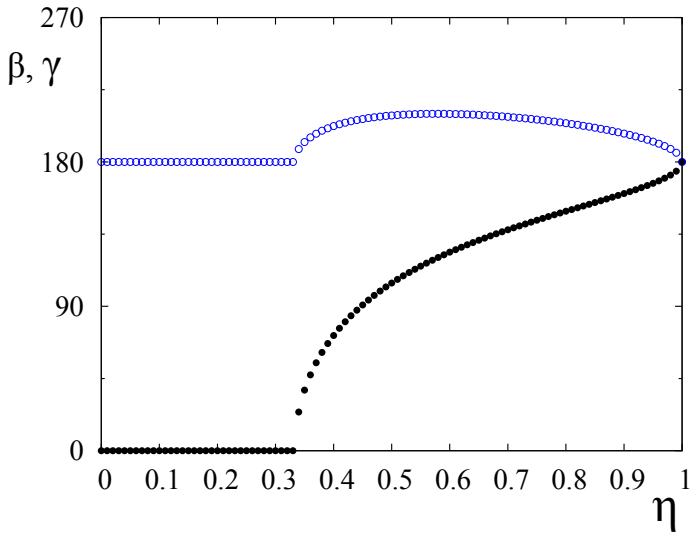

Figure 2.19: (Color online). Ground state in the XY case. The angles β (black circles) and γ (blue open circles) are shown as functions of $\eta = J_1/J_2$. Non collinear GS configurations occur in the region $1/3 \leq \eta \leq 1$. See text for comments.

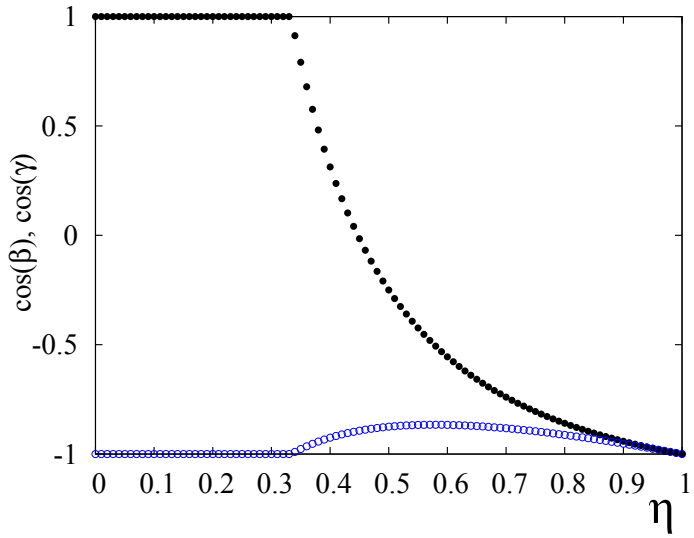

Figure 2.20: (Color online). Ground state in the XY case. The $\cos(\beta)$ (black circles) and $\cos(\gamma)$ (blue open circles) are shown as functions of $\eta = J_1/J_2$.

2.3.2 Phase Transition: results

In this paragraph, we show the results obtained by MC simulations with the Hamiltonian from Eq. (2.8). The size of the lattice is $N_x \times N_y \times N_z$ where $N_x = N_y = 18$ and $N_z = 8$ (16 atomic planes along z). Periodic boundary conditions are used for the three-dimensional lattice. The time for reaching equilibrium is about 10^6 MC steps per spin and the averaging times is 10^6 MC steps per spin. The exchange interaction $|J_2| = 1$ is used as the unit of energy.

A. Ising case

Since the GS changes at $\eta_c = 0.5$, we show here examples on both sides of this value. We show in Fig. 2.21 the averaged energy per spin, the order parameter, the heat capacity, and the susceptibility for $\eta = 0.3$. The transition is of second order. On the other side, we show in Fig. 2.22 the energy per spin and the order parameter versus T, for $\eta = 0.85$ and 1. We find a strong first-order transition in both cases. The discontinuity of E and M at the transition is very large.

We show in Fig. 2.23 the energy histogram taken at the transition temperature for three values $\eta = 0.3$ (black), 0.85 (blue) and 1 (red). As seen, the first case is a Gaussian distribution indicating a second-order transition, while the last two cases show a double-peak structure indicating a first-order transition.

Fig. 2.24 shows the phase diagram in the space (T_C, η) where zone (1) and zone (2) denote the ordering of the first, and second kinds, respectively; (P) indicates the paramagnetic phase. Note that the transition line between (1) and (P) is a second-order line, while that between (2) and (P) is a first-order line.

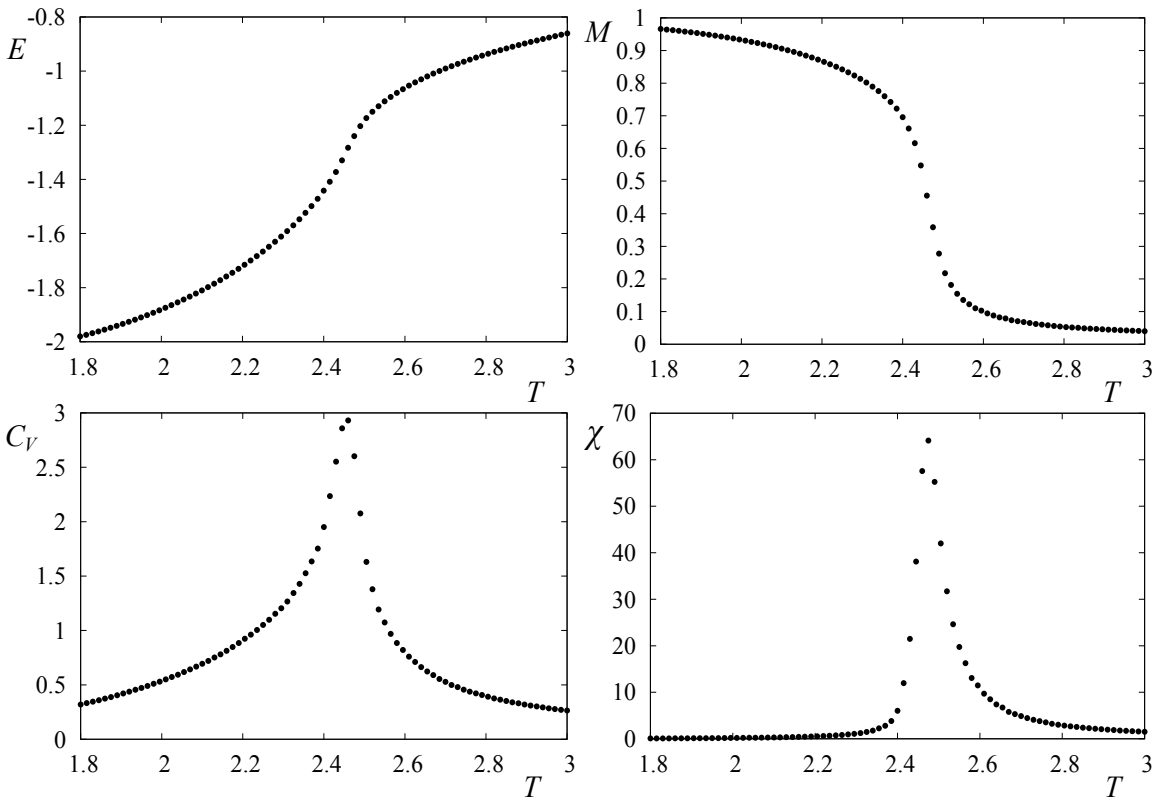

Figure 2.21: Ising case: Energy per spin E, order parameter M, specific heat C_V and susceptibility χ versus temperature T for $\eta = J_1/J_2 = 0.30$. See text for comments.

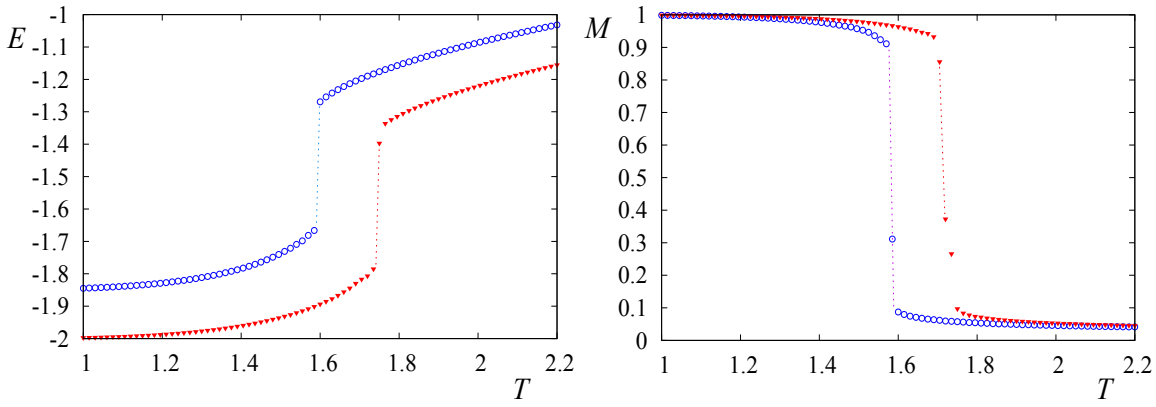

Figure 2.22: (Color online). Ising case: Energy per spin E and order parameter M versus temperature T for $\eta = J_1/J_2 = 0.85$ (blue open circles) and 1 (red triangles). See text for comments.

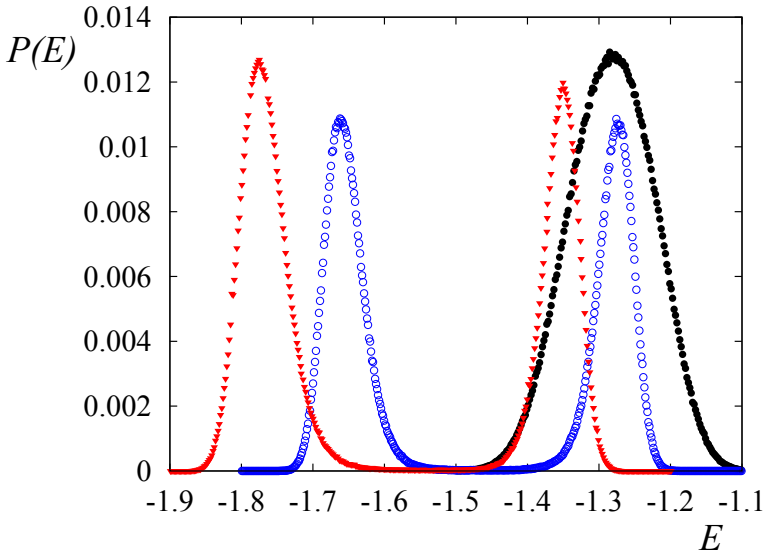

Figure 2.23: (Color online). Ising case: Energy histogram $P(E)$ versus E for $\eta = 0.3$ (black circles), 0.85 (blue open circles), and 1(red triangles). See text for comments.

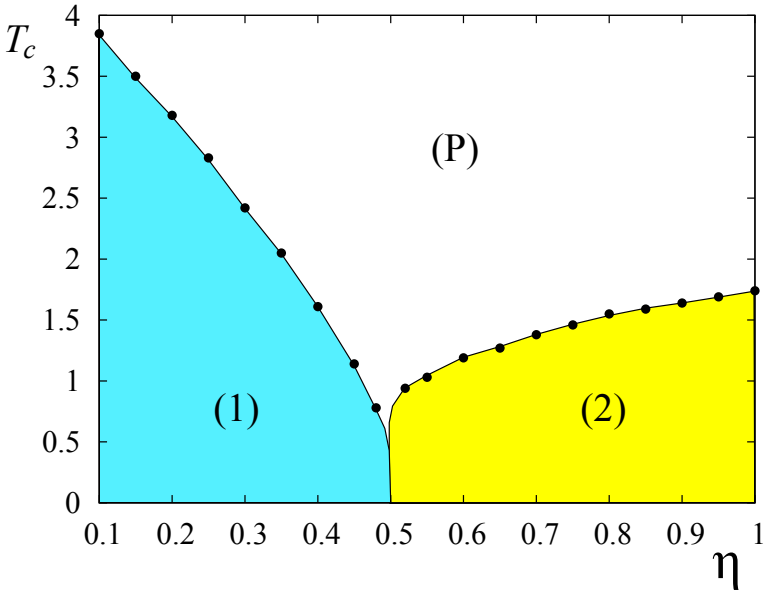

Figure 2.24: (Color online). Ising case: Critical temperature T_C versus η. (1), (2) and (P) denote the first, second and paramagnetic phases, respectively. See text for comments.

B. XY case

In the XY case, the change of the GS takes place at $\eta = 1/3$. We show in Fig. 2.25 the result for $\eta = 0.3$ where the GS is composed of ferromagnetic planes antiferromagnetically stacked in the z direction. The transition is of second order.

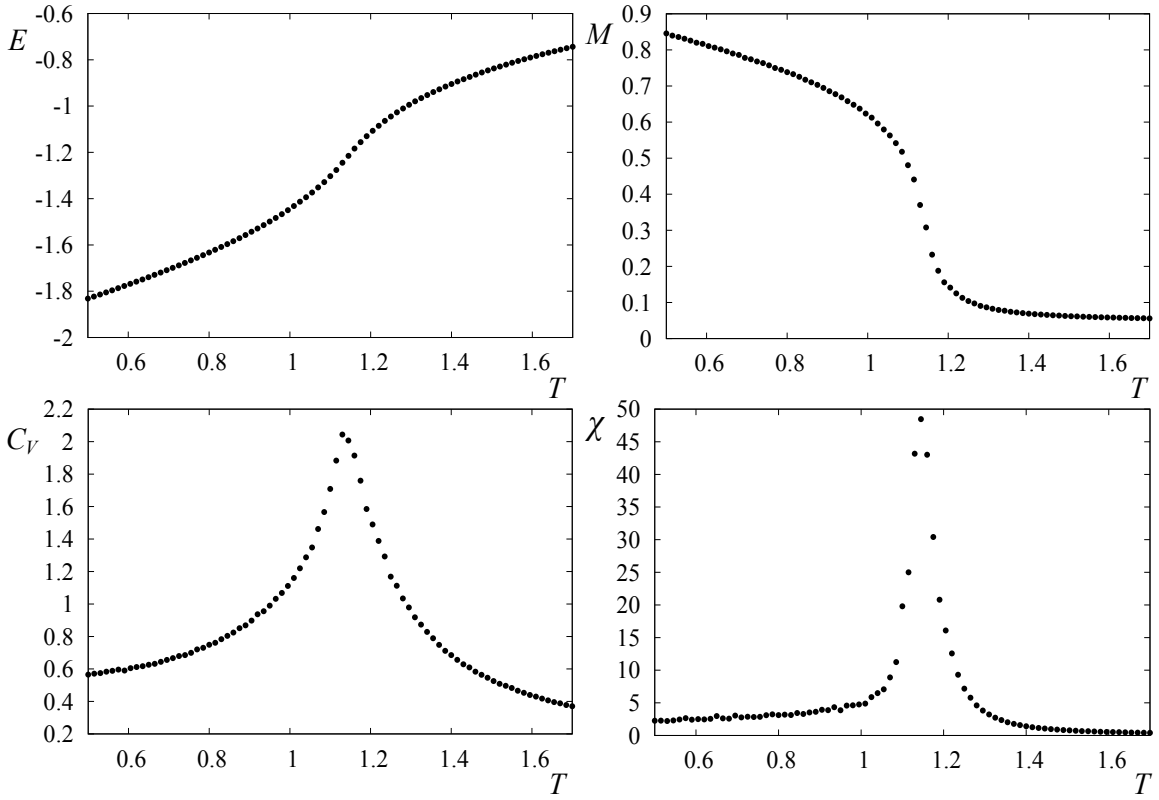

Figure 2.25: XY case: Energy per spin E, order parameter M, specific heat per spin C_V and susceptibility χ versus T for $\eta = 0.3$. See text for comments.

We show now the result for the non collinear GS region in Fig. 2.26. The energy and the order parameter show clearly a discontinuity at the transition for $\eta = 0.58$ and 1.

Using the histogram method, we have also calculated the histogram shown in Fig. 2.27 for $\eta = 0.3$, 0.58 and 1. For $\eta = 0.3$ which is in the collinear region of the GS, the histogram is Gaussian, confirming the second-order transition observed in the data shown above. For $\eta = 0.58$ and 1 belonging to the non collinear region, the histogram

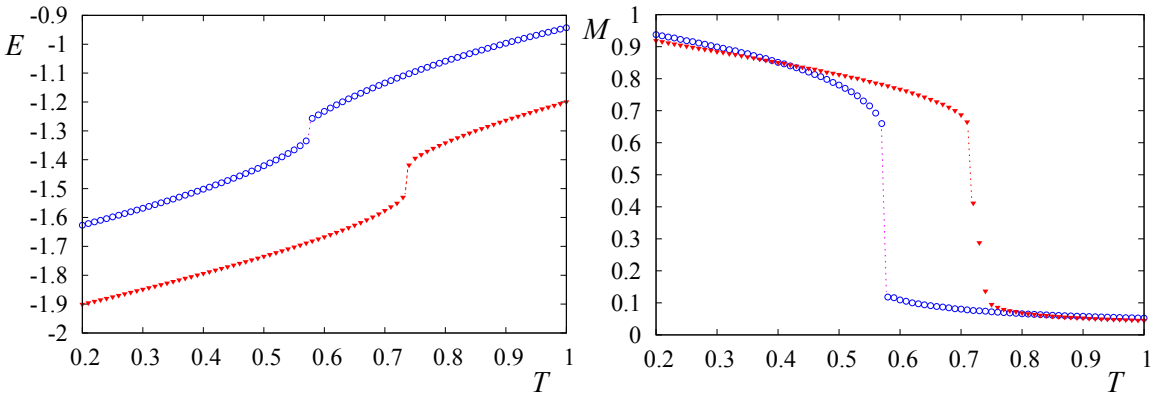

Figure 2.26: (Color online). XY case: Energy per spin E and order parameter M versus T for $\eta = 0.58$ (blue open circles) and 1 (red triangles). See text for comments.

shows a two-peak structure which confirms the first-order character of the transitions in this region. The two peaks are very well separated with the dip going down to zero, indicating an energy discontinuity. The distance between the two peaks is the latent heat ΔE.

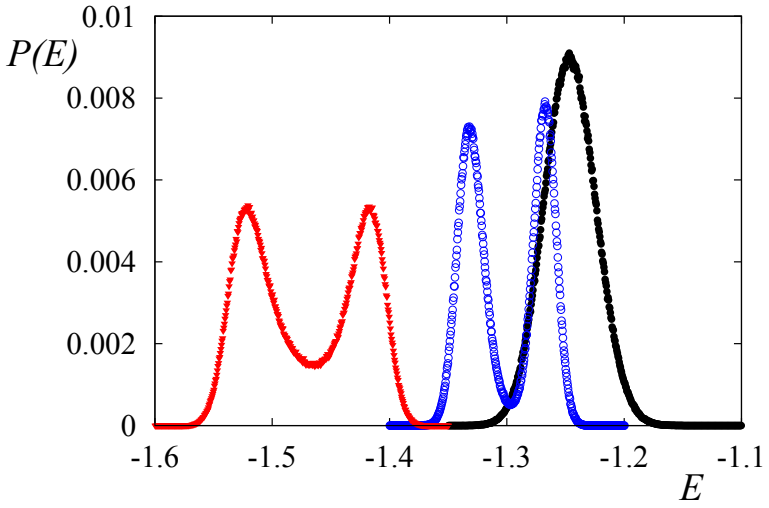

Figure 2.27: (Color online). XY case: Energy histogram P versus E for $\eta = 0.3$ (black circles), 0.58 (blue open circles), 1 (red triangles) at the respective transition temperatures. See text for comments.

We show in Fig. 2.28 the transition temperature versus η where (1) and (2)

indicate the collinear and non collinear phases, respectively. (P) denotes the paramagnetic state. The line separating (1) and (P) is a second-order transition line, while that separating (2) and (P) is the first-order one.

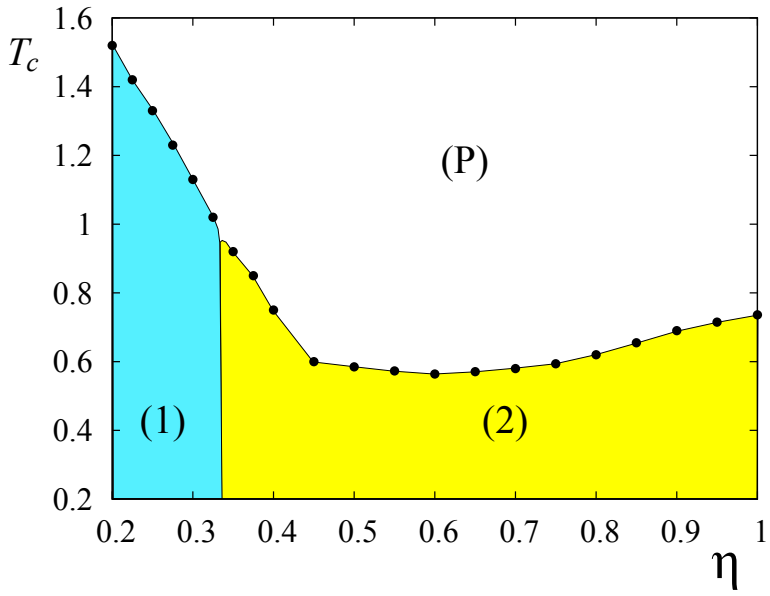

Figure 2.28: (Color online). XY case: Critical temperature T_C versus η. (1), (2) and (P) denote the collinear, non collinear and paramagnetic phases, respectively. See text for comments.

To close this section, we emphasize that all 3D frustrated systems known so far undergo a first-order transition: Let us mention the antiferromagnetic stacked triangular lattice [83, 84, 18, 19], the FCC antiferromagnets [88], the simple cubic fully frustrated lattices [89, 90, 91, 92], helimagnets [93], and the HCP lattice studied here.

2.3.3 Spin Transport in the Ising case

Using the method which has been described in detail in section 1.4 of chapter 1, we study spin resistivity in the Ising case. In Fig. 2.29 and 2.30, for the two different GS ($\eta = 0.3$ and $\eta = 1$), we show the resistivity at two temperatures, below and above the transition temperature, as functions of D_1. Similar to the case of $J_1 - J_2$ model considered in section 2.2, one observes here an oscillatory behavior of the resistivity ρ at low temperature. However, for all values of D_1, the resistivity ρ at low temperature is smaller than that at high temperature.

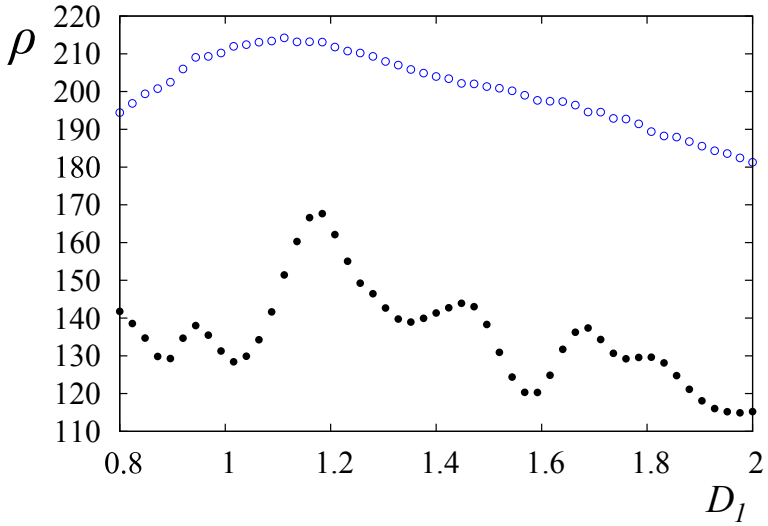

Figure 2.29: Spin resistivity versus D_1 for $\eta = 0.3$ at $T = 1.6$ (black circles) and 2.8 (open circles). Other parameters are $N_x = N_y = 18$, $N_z = 8$ (16 planes in the z direction), $D_2 = 1$, $I_0 = 2$, $K_0 = 0.5$, $C_1 = C_2 = 1$, $A = 1$, $D = 0.5$, $\epsilon = 1$.

The spin resistivity ρ versus T for the two typical cases $\eta = 0.3$ and 1 is shown in Fig. 2.31 where distances D_1 and D_2 are in unit of the NN distance, energy constants I_0, K_0 and D are in unit of $|J_2| = 1$. We observe here that in the second-order region ρ has a rounded maximum and in the first-order region it undergoes an almost discontinuous jump at the transition. In both cases, we see that:

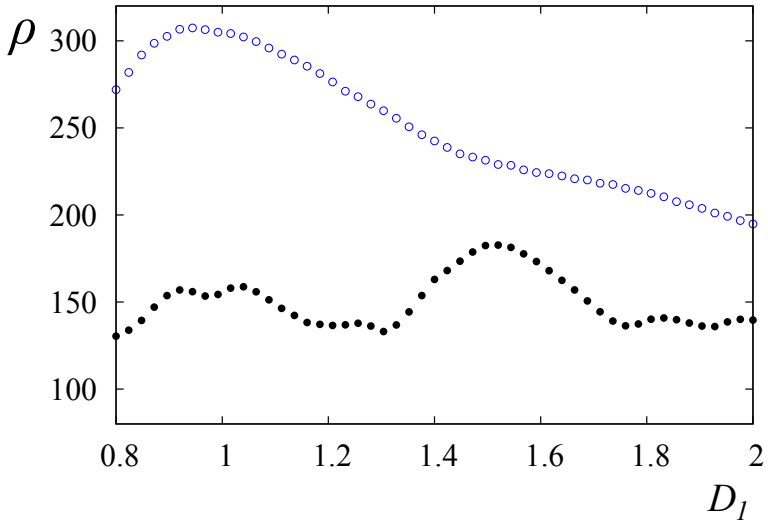

Figure 2.30: Spin resistivity versus D_1 for $\eta = 1$ at $T = 1.5$ (black circles) and 1.9 (open circles). Other parameters are $N_x = N_y = 18$, $N_z = 8$ (16 planes in the z direction), $D_2 = 1$, $I_0 = 2$, $K_0 = 0.5$, $C_1 = C_2 = 1$, $A = 1$, $D = 0.5$, $\epsilon = 1$.

i) At very low temperature, the resistivity increases with decreasing temperature. The origin of this behavior comes from the freezing of the itinerant spins due to their interactions with the lattice spins and with the other itinerant spins. The itinerant spins search to minimize energy by occupying low-energy positions in the periodic lattice. Since the thermal energy and the electric field are not strong enough to make them move, the itinerant spins are somewhat frozen in almost periodic positions; namely a pseudo crystallization occurs. This is very similar to the crystallization of interacting particles at low temperature. Note that the increase of resistivity at very low temperature was observed in many experiments on various materials and is not limited to ferromagnets [43, 5, 41, 2].

ii) When temperature increases, thermal energy progressively unfreezes the itinerant electrons, the resistivity slightly decreases and then increases up to the transition temperature.

iii) At the transition temperature, resistivity exhibits a peak. We can explain the existence of the peak by the following argument: In recent works [62], it was found

from MC simulations that the resistivity's peak is due to scattering by antiparallel-spin clusters which exist when one enters the critical region. Below the transition temperature, there exists a single large cluster of lattice spins with some isolated "defects" (i. e. clusters of antiparallel spins), so that the resistivity decreases with decreasing temperature just below the transition temperature.

iv) Above the transition temperature, in the paramagnetic phase, as temperature increases, small clusters will be broken more and more into single disordered spins, so that there is no energy barrier between successive positions of itinerant spins on their trajectory. The resistivity, though high, is thus decreasing with increasing temperature and saturates as $T \to \infty$.

We have varied the radius D_1 to see its effect on the resistivity ρ at the transition. We observe the same effect as in some other antiferromagnets [64, 69]: at a given temperature, resistivity ρ oscillates slightly with distance. We have found that this oscillation comes from the oscillatory behavior of the difference between the numbers of up and down spins in the sphere as D_1 varies.

Let us recall the experimental results in ferromagnets and antiferromagnets as seen in Fig. 2.32 by Du et al. on ε-$(Mn_{1-x}Fe_x)_{3.25}Ge$ antiferromagnets [2], by McGuire et al. on antiferromagnetic superconductors LaFeAsO [3], by Chandra et al. on thin $Cd_{1-x}Mn_xTe$ films [4], and in Fig. 2.33 by Santos et al. on antiferromagnetic $La_{1-x}Sr_xMnO_3$ [5].

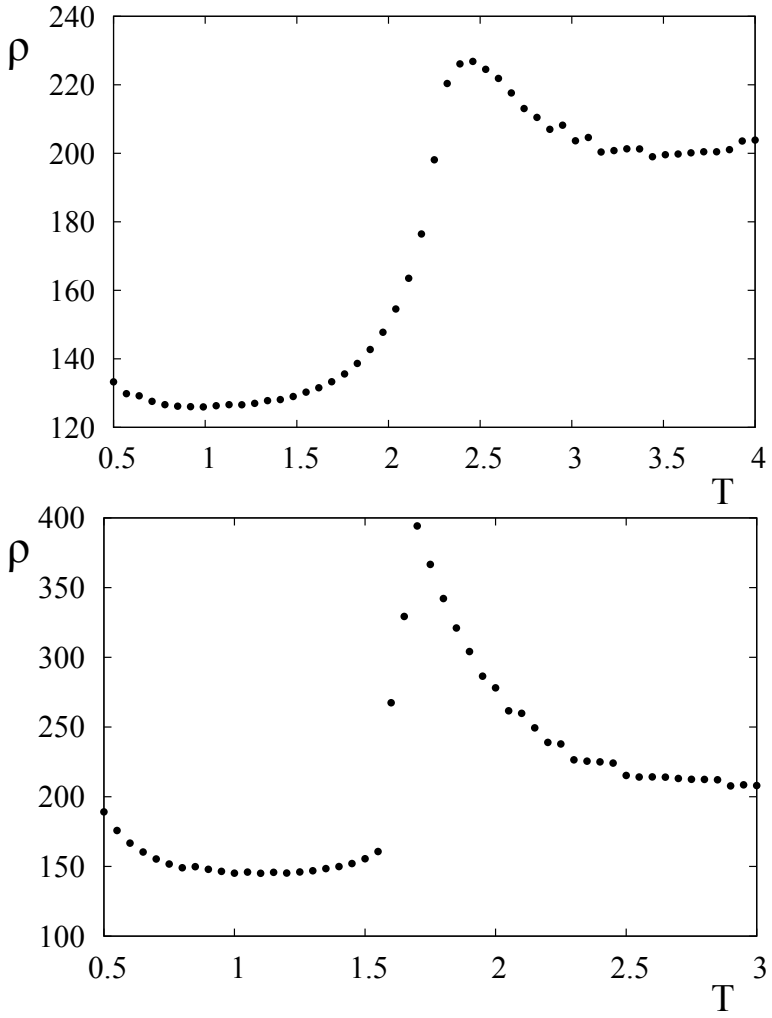

Figure 2.31: Ising case: Spin resistivity ρ versus temperature T for $\eta = 0.3$ (upper) and 1 (lower). $N_x = N_y = 18$, $N_z = 8$ (16 planes in the z direction), $D_1 = D_2 = 1$, $\epsilon = 1$, $I_0 = 2$, $K_0 = 0.5$, $C_1 = C_2 = 1$, $A = 1$, $D = 0.5$. All distances are in unit of the NN distance, energy constants are in unit of $|J_2| = 1$. See text for comments.

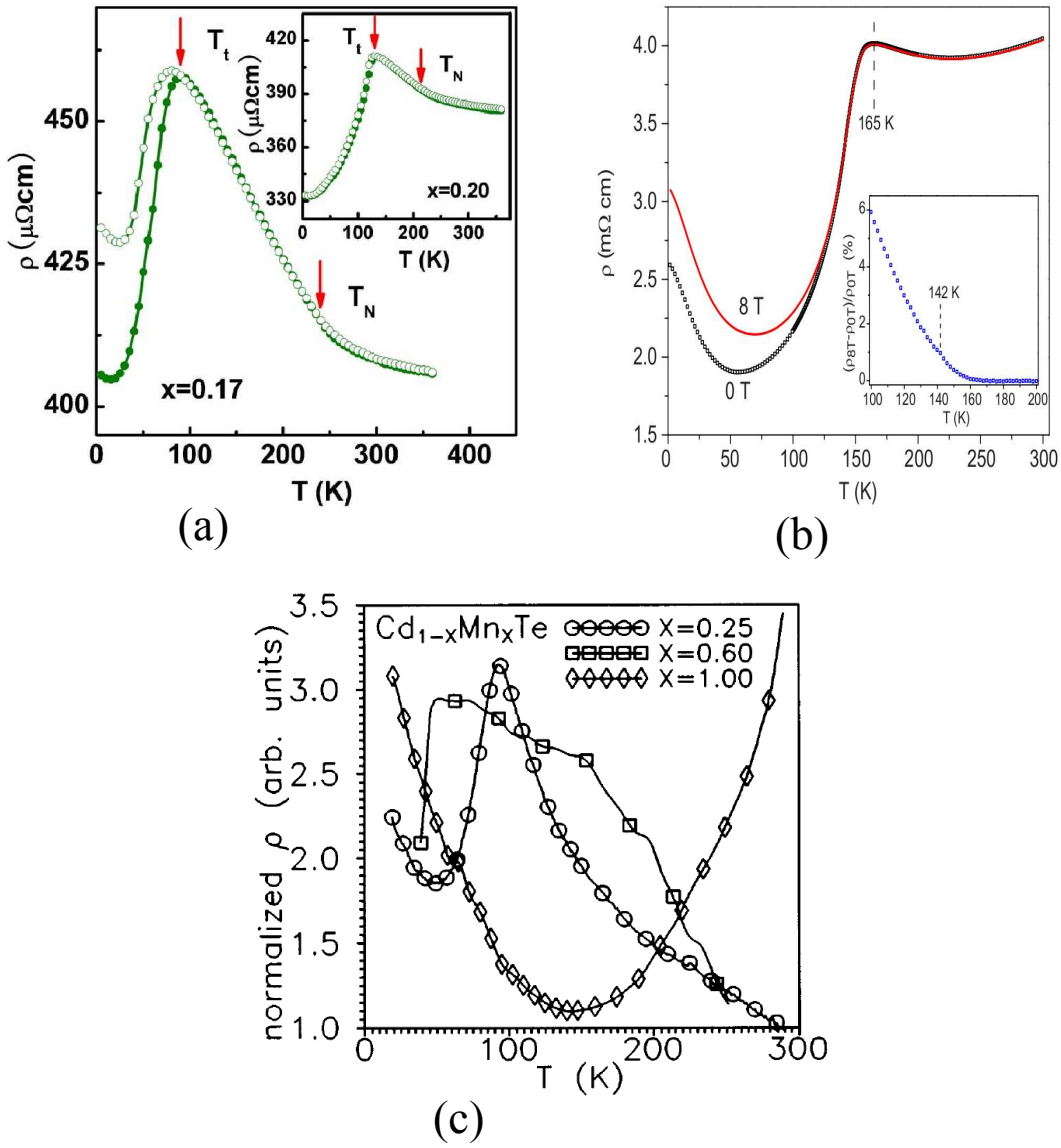

Figure 2.32: Resistivity versus temperature in the experimental results: (a) by Du et al on ε-$(Mn_{1-x}Fe_x)_{3.25}Ge$ antiferromagnets [2], (b) by McGuire et al. on antiferromagnetic superconductors LaFeAsO [3], and (c) by Chandra et al. on thin $Cd_{1-x}Mn_xTe$ films [4].

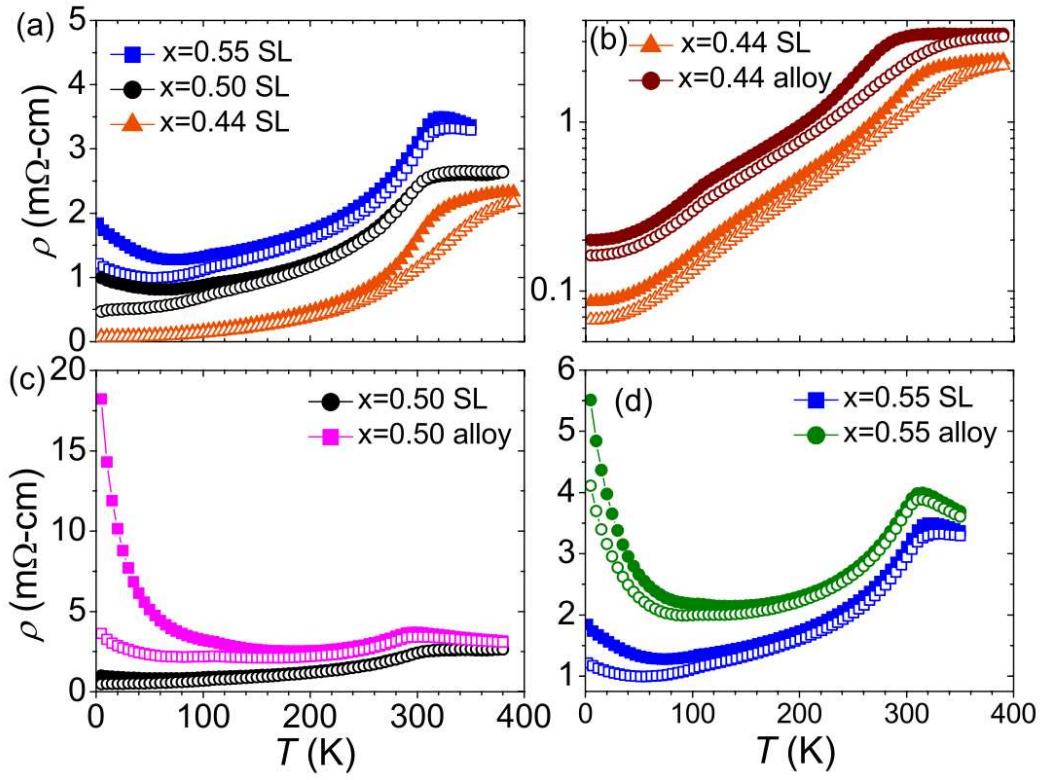

Figure 2.33: Resistivity versus temperature on antiferromagnetic $La_{1-x}Sr_xMnO_3$. The figures presented are taken from Fig. 7 of [5].

2.4 Conclusion

In this chapter, we have studied phase transitions and spin transport in two frustrated systems: the $J_1 - J_2$ model and the HCP lattice.

The $J_1 - J_2$ model is a SC lattice with Ising spins interacting with each other via nearest and next-nearest neighbor antiferromagnetic interactions, J_1 and J_2 respectively. We show that the GS depends on the ratio $\eta = J_2/J_1$. There exists a critical value $\eta_c = 0.25$ where the GS changes. For $\eta < 0.25$, the GS is composed of two stacked tetrahedra formed by the NNN sites, while for $\eta > 0.25$, the GS is a collinear configuration (one line of spin up, one line of spin down). The nature of the transition changes from a second order below η_c to a first order above η_c. We have also calculated the resistivity ρ of the itinerant spins and shown that the resistivity ρ varies continuously as a function of temperature in the region displaying a second order transition and discontinuously in the first order region. In particular, the resistivity ρ can make a down fall or an upward jump at the transition temperature, depending on the value of D_1.

The HCP lattice is considered with both Ising and XY spins with an in-plane interaction J_1 and an inter-plane interaction J_2, both antiferromagnetic. As a result, the GS spin configuration depends on the ratio $\eta = J_1/J_2$. We show that there exists a critical value η_c where the GS changes. For the Ising case, we find $\eta_c = 0.5$ below (above) which the spins in the xy planes are ferromagnetic (antiferromagnetic). For the XY case, the GS is collinear below $\eta_c = 1/3$, and is non collinear above that value. The nature of the transition changes from a second order below η_c to a first order above η_c for both Ising and XY cases. We also studied the spin resistivity in the Ising case. We found that the shape of ρ depends on the nature of the transition: in the second-order region, a rounded maximum is observed at the transition while in the first-order region, the resistivity ρ undergoes a discontinuity at the transition as we have observed in other frustrated cases. These findings may help to understand the nature of the transition and the spin transport in different compounds with a

HCP structure.

Chapter 3

Phase transition in molecular crystals by Potts model with dipolar interaction

We investigate in this chapter the GS and the nature of the transition from an orientational ordered phase at low temperature to the disordered state at high temperature in a molecular crystal. Our model is a Potts model which takes into account the exchange interaction J between NN molecules and a dipolar interaction between molecular axes in three dimensions. The dipolar interaction is characterized by two parameters: its amplitude D and the cutoff distance r_c. If the molecular axis at a lattice site has three orientations, say the x, y or z axes, then when $D = 0$, the system is equivalent to the 3-state Potts model: the transition to the disordered phase is known to be of first order. When $D \neq 0$, the GS configuration is shown to be composed of two independent interpenetrating layered subsystems which form a sandwich whose periodicity depends on D and r_c. We show by extensive MC simulation with a histogram method that the phase transition remains of first order at relatively large values of r_c.

We are also interested in the phase transition in thin films with taking into account a single-ion perpendicular anisotropy of amplitude A. We show that the GS depends on the ratio D/A and r_c. For a single layer, for a given A, there is a critical value D_c below (above) which the GS configuration of molecular axes is perpendicu-

lar (parallel) to the film surface. When the temperature is increased, a re-orientation transition occurs near D_c: the low temperature in-plane ordering undergoes a transition to the perpendicular ordering at a finite temperature, below the transition to the paramagnetic phase. The same phenomenon is observed in the case of a film with a thickness. We show that the surface phase transition can occur below or above the bulk transition depending on the ratio J_s/J. Surface and bulk order parameters as well as other physical quantities are shown and discussed.

3.1 Introduction

In this chapter, we are interested in the phase transition in molecular crystals which has been a subject of intensive investigations for 40 years. This spectacular development was due to numerous applications of liquid crystals in daily life [56, 94]. Liquid crystals are somewhere between solid and liquid states where molecules have some spatial orientations which, under some conditions, can order themselves into some structures such as nematic and smectic phases. This subject will be introduced in more detail in chapter 4.

In spite of the large number of applications using experimental findings, theoretical understanding in many points is still desirable. One of the most important aspects of the problem is the origin of layered structures observed in smectic ordering: in smectic phases the molecules are ordered layer by layer with periodicity.

Experiments have discovered, for example, smectic phases of 3-layer, 4-layer, or 6-layer periodicity. Smectic-C* with 6-layer periodicity (SmC^*_{d6}) was discovered by Shun Wang et al. on ternary mixture $(73\%10\text{OHF}-27\%11\text{OHF})_{0.85}\text{C9}_{0.15}$ and binary mixture 89%10OHF−11%C11 [6] (see Fig. 3.1(a) and (b)).

In paper [7], P. M. Johnson et al. have presented the structure with 4- and 3-layer periodicity respectively in SmC^*_{FI2} phase at 69.65°C and SmC^*_{FI1} phase [1] at 67.12°C

[1] The SmC^*_{FI1} and SmC^*_{FI2} phases are also named SmC^*_{d3} and SmC^*_{d4} phases, respectively.

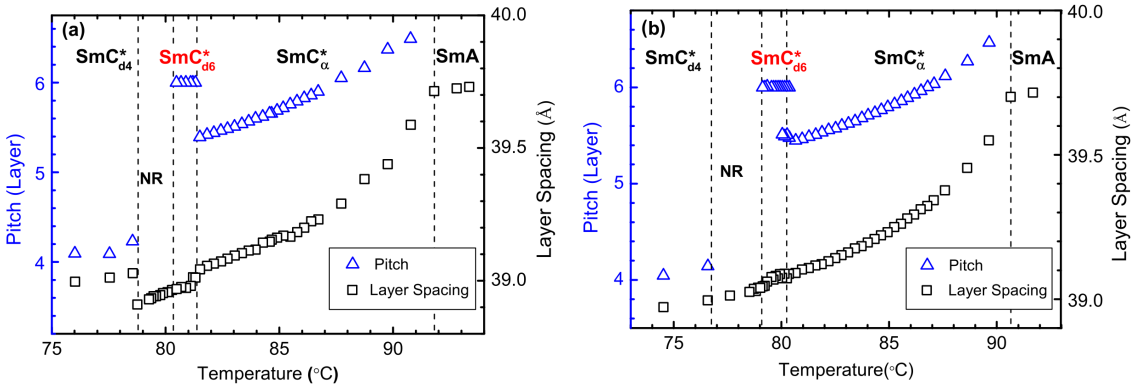

Figure 3.1: Temperature dependence of pitch (triangles) and layer spacing (squares) for (a) ternary mixture $(73\%10OHF-27\%11OHF)_{0.85}C9_{0.15}$ and (b) binary mixture 89%10OHF−11%C11. The figures presented are taken from Fig. 2 of [6].

for MHPBC [SmA (76) SmC^*_α (72) SmC^*_{FI2} (68) SmC^*_{FI1} (65) SmC^*_A] (see Fig. 3.2(a) and (b)). They discovered also SmC^*_{FI2} phase at 82.51°C for MHDDOPTCOB [SmA (93) SmC^* (83) SmC^*_{FI2} (80) SmC^*_A] (see Fig. 3.3).

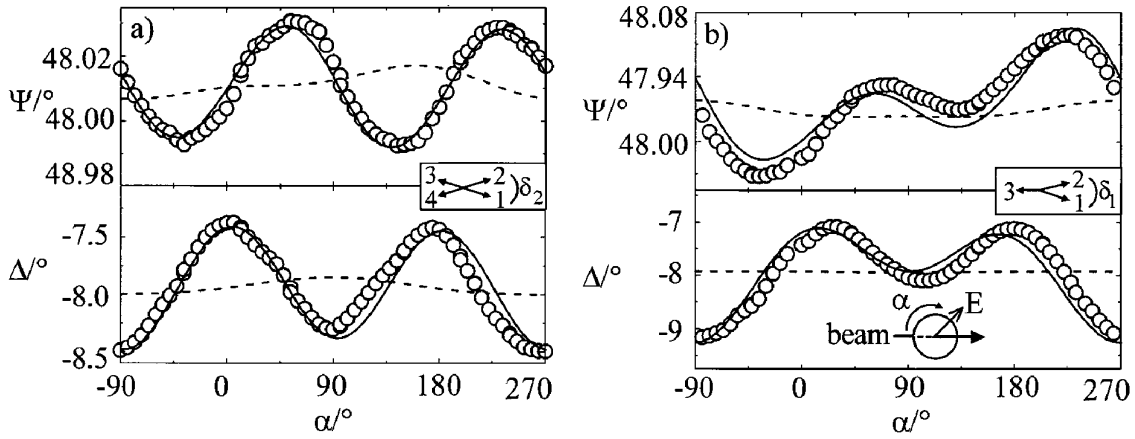

Figure 3.2: Ellipsometry results for MHPBC in the (a) SmC^*_{FI2} phase at 69.65^{o}C and (b) SmC^*_{FI1} phase at 67.12°C. The figures presented are taken from Fig. 1 of [7].

By resonant X-ray scattering performed upon free-standing films of a thiobenzoate liquid crystal compound, P. Mach et al. [8] have found the first direct structure evidence of distinct super lattice periodicities with 2-, 3-, 4- layer in SmC^*_A, SmC^*_{FI1}

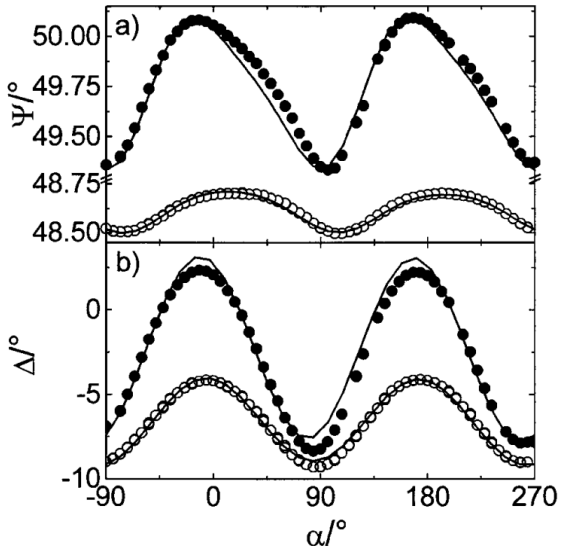

Figure 3.3: Ellipsometry results for MHDDOPTCOB in the SmC^*_{FI2} phase at 82.51°C. The figures presented are taken from Fig. 2 of [7].

and SmC^*_{FI2} phases, respectively. Their results are shown in Fig. 3.4. We can see that in Fig. 3.4(b), there exist 4 satellite peaks at $1.25Q_0$,$1.5Q_0$,$1.75Q_0$ and $2.25Q_0$ which correspond with 4−layer superlattice periodicity, i.e. SmC^*_{FI2} phase. In Fig. 3.4(c), one third integer peaks are evident, implying a three-layer periodicity, i.e. SmC^*_{FI1} phase.

Orientation of molecules with 3− and 4−layer have been investigated for several materials contain sulfur and selenium by L. S. Hirst et al. in paper [95]. Different theories have been suggested to interpret these observations [96, 97, 98, 99, 100, 101, 102].

One of the unanswered questions is what is the origin of the long-period layered structure in observed smectic phases? Hamaneh et al. [103, 104] suggested that the effective long-range interaction is due to bend fluctuations of the smectic layers which may stabilize commensurate structures in particular the six-layer phase. This suggestion is too qualitative to allow a clear understanding of the long-period layered structure in smectic phases. To our opinion, we should distinguish long-range correlation and long-range interaction. We know that long-range correlation can be a

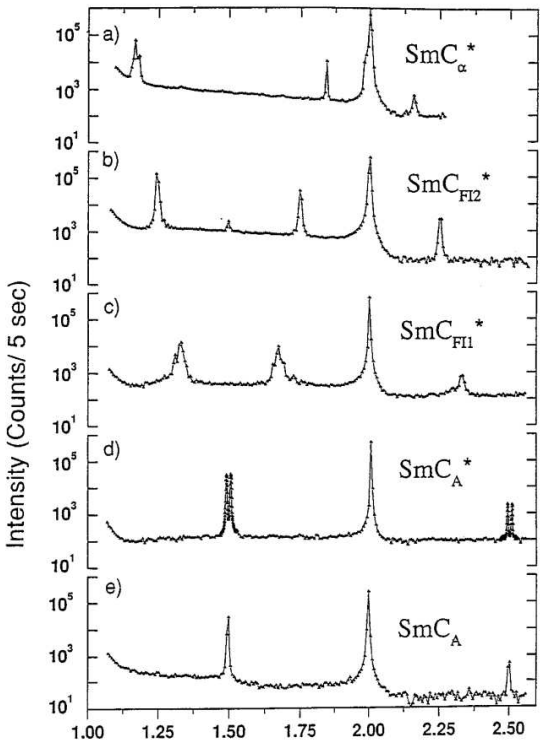

Figure 3.4: X-ray intensity scans in the indicated phase of (R)-enantiomer (plot $a-d$) and racemic 10OTBBB1M7 (plot e). The figures presented are taken from Fig. 3 of [8]. See [8] for comments.

consequence of short-range interactions, not necessarily of long-range ones, as it is well known in theory of critical phenomena [81, 13]. However, a long-range correlation does not imply a particular long-period configuration.

To look for a physical origin of long-period structures, we concentrate ourselves in the present chapter the effect of a dipolar interaction in a Potts model, in addition to an exchange interaction between NN. We suppose that each molecule has a molecular axis which can lie on one of the three principal directions. An example of such a molecule is the ammoniac molecule NH_3. Without the dipolar interaction, the interaction between neighboring molecules gives rise to an orientational order of molecular axes at low temperature. In this situation, the system can be described by a 3-state Potts model in 3D. The Potts model is very important in statistical physics.

It is in fact a class of models each of which is defined by the number of states q that an individual particle or molecule can have. The interaction between two neighboring molecules is negative if they are in the same state, and zero otherwise. Exact solutions are found for many Potts models in 2D [80]. In 2D, the phase transition is of second order for $q \leq 4$ and of first order for higher q. In 3D, a number of points are well understood. For example, the phase transition is of first order for $q > 2$. The molecular crystal described above undergoes therefore a first-order transition in the absence of a dipolar interaction.

The purpose of this chapter is to investigate the effect of the dipolar interaction on the GS structure and on the nature of the phase transition. The dipolar interaction is a long-range interaction which yields different GS structures depending on the shape of the sample as will be discussed in the next section. To carry out our purpose, we use a steepest descent method for the GS determination and the MC simulation combined with the histogram technique to distinguish first- and second-order characters.

In section 3.2, we show our model and analyze the GS. Results of MC simulations are shown and discussed in section 3.3. Concluding remarks are given in section 3.5.

3.2 Model and Ground-State Analysis

We consider a simple cubic lattice where each site is occupied by an axial molecule. The molecular axis can be in the x, y or z direction. Let us denote the orientation of the molecule at the lattice site i by a unit segment, not a vector, which can lie in the x, y or z direction. We attribute the Potts variable σ=1, 2 or 3 when it lies in the x, y or z axes, respectively, in the calculation. By the very nature of the model shown below, the results do not depend on these numbers as in the standard q-state Potts model.

We suppose that the interaction energy between two nearest molecules is $-J$ ($J > 0$) if their axes are parallel, zero otherwise. With this hypothesis, the Hamiltonian is

given by the following 3-state Potts model:

$$\mathcal{H} = -J \sum_{(i,j)} \delta(\sigma_i, \sigma_j) \tag{3.1}$$

where σ_i is the 3-state Potts variable at the lattice site i and $\sum_{(i,j)}$ is made over the nearest sites σ_i and σ_j.

The dipolar interaction between Potts variables is written as

$$\mathcal{H}_d = D \sum_{(i,j)} \{ \frac{\mathbf{S}(\sigma_i) \cdot \mathbf{S}(\sigma_j)}{r_{i,j}^3} - 3 \frac{[\mathbf{S}(\sigma_i) \cdot \mathbf{r}_{i,j}][\mathbf{S}(\sigma_j) \cdot \mathbf{r}_{i,j}]}{r_{i,j}^5} \} \delta(\sigma_i, \sigma_j) \tag{3.2}$$

where $\mathbf{r}_{i,j}$ is the vector of modulus $r_{i,j}$ connecting the site i to the site j, D a positive constant depending on the material, $\mathbf{S}(\sigma_i)$ is defined as the unit vector lying on the axis corresponding to the value of σ_i. The sum is limited at some cutoff distance r_c. Without the Kronecker condition and in the case of classical XY or Heisenberg spins, the dipolar interaction gives rise to spin configurations which depend on the sample shape. For example, in 2D or in rectangular slabs spins lie in the plane to minimize the system energy.

The origin of the frustration comes from the competition between the first term and the second term in the brackets of the dipolar interaction given by Eq. (3.2). The first term is positive or zero, while the second term can be positive, zero or negative, depending on the orientations of the molecular dipoles $\mathbf{S}(\sigma_i)$ and $\mathbf{S}(\sigma_j)$ with respect to the vector $\mathbf{u}_{ij}$ which connects these dipoles. For examples, if $\mathbf{u}_{ij}$ is on the x axis, the second term is:
(i) equal to zero if the dipoles $\mathbf{S}(\sigma_i)$ and $\mathbf{S}(\sigma_j)$ are on y or z axes since they are perpendicular to $\mathbf{u}_{ij}$, the scalar products are then zero,
(ii) equal to $-3/r_{ij}^3$ if $\mathbf{S}(\sigma_i)$ and $\mathbf{S}(\sigma_j)$ lie on the x axis.

Note that the calculation of the minimum of the dipolar interaction is very complicated, it cannot be done by hand because of the very large number of neighbors. However, it can be done numerically by the steepest-descent method used in this thesis.

Let us first discuss the GS in the Potts model introduced above. When $D = 0$ the GS is uniform with one orientation value, namely it is 3-fold degenerate. However, for a nonzero D, the ground state changes with varying r_c. To determine the GS, we use the steepest descent method which is described in the section 2.2 of chapter 2.

We show some examples in Fig. 3.5. For very small D, the GS is uniform for any r_c as shown in Fig. 3.5a. For increasing D, the GS has layered structures with period $p = 1$ (alternate single layers), $p = 2$ (double layers), $p = 3$ (triple layers),... depending on r_c and D. Note that this work was motivated by the observation that in most experimental systems very long-ranged interaction can be neglected. The concept that the interaction range between particles can go to infinity is a theoretical concept. Models in statistical physics limited to interaction between nearest neighbors are known to interpret with success experiments [13]. Therefore, we wish to test how physical results depend on r_c in the dipolar interaction. If we know for sure that in a system the interaction is dipolar and that a triple-layer structure is observed, we can suggest the interaction range beyond which interaction can be neglected.

We note that in Fig. 3.5 there are only two kinds of molecular orientations represented by two colors (on line) in spite of the fact that we have three possible orientations. Let us discuss the single-layer structure shown in Fig. 3.5b. It is very important to note that each layer has no coupling with two nearest layers whose molecules lie on another axis. However, it is coupled to two next-nearest layers of the same color, namely the same molecular axis, lying within r_c. In other words, the GS is composed of two interpenetrating "independent" subsystems. The same is true for other layered structures: in a double-layer structure molecules of the same orientation (same color on line) interact with each other but they are separated by a double layer of molecules of another orientation. To our knowledge, this kind of GS has never been found before. It may have important applications at macroscopic levels.

Note also that if the molecules of the single-layer structure are successively in x-oriented and y-oriented planes, then the stacking direction of these planes is the z

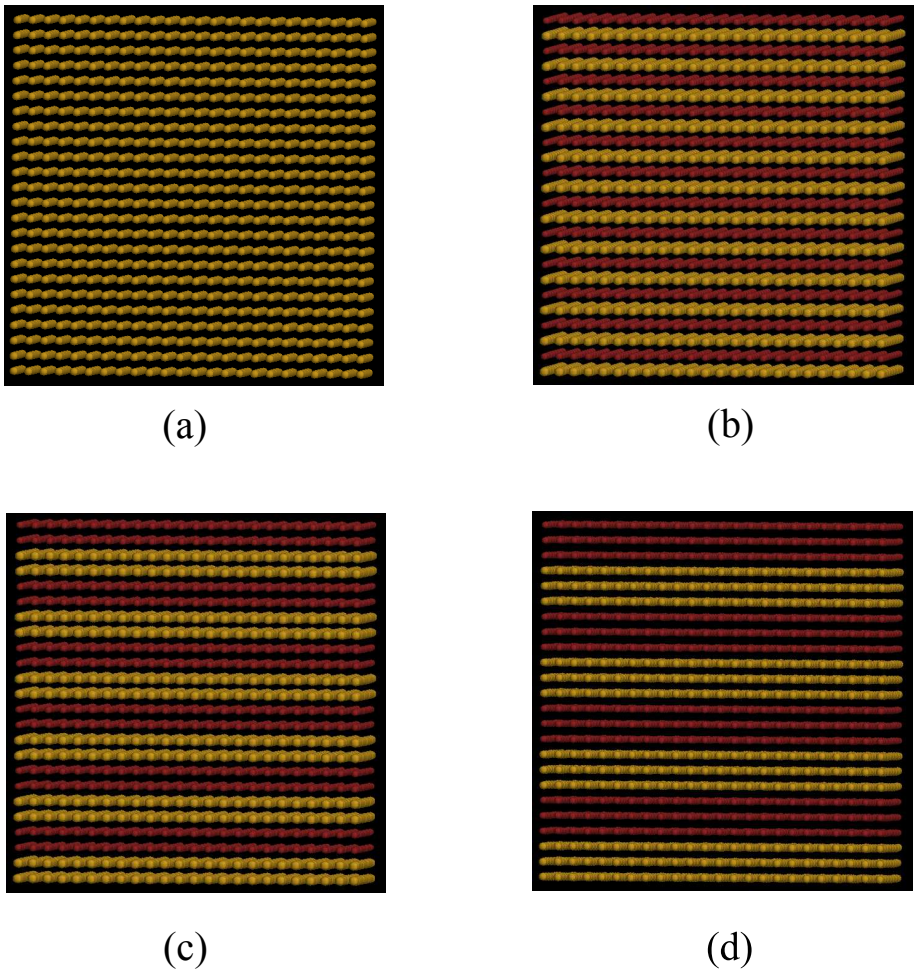

Figure 3.5: (Color online) Ground state in the case where a) $D/J = 0.4$, $r_c = 2.3$: uniform configuration; b) $D/J = 2$, $r_c = 2.3$: single-layer structure; c) $D/J = 1$, $r_c = 2.3$: double-layer structure; d) $D/J = 0.4$, $r_c = \sqrt{10} \simeq 3.16$: triple-layer structure. See text for comments.

direction. The molecules can choose the x and z orientations or the y and z directions. In those cases the stacking directions are respectively the y and x directions. These three possibilities are equivalent if the sample is cubic. In rectangular shapes, the stacking direction is along the smallest thickness.

In order to understand how such GS configurations found by the steepest descent method depend on D and r_c, we have considered the structures 121212...(single-

layer structure), 11221122... (2-layer structure), 111222111222... (3-layer structure) and carried out the calculations of the energy of a molecule σ_i interacting with its neighbors σ_j. The case where the configuration is uniform, i. e. there is only one kind of molecular orientation, say axis x, the dipolar energy of σ_i is

$$E_i = D \sum_j [\frac{1}{r_{ij}^3} - 3\frac{x_{ij}^2}{r_{ij}^5}] \tag{3.3}$$

Note that with the use of the Potts model for the dipolar term in Eq. 3.2, the energy depends only on the axis, not on its direction as seen by the square term $(u_{ij}^x)^2$. In this sense, the model is suitable to describe axial, but non-directed, interacting molecules.

If we transform the sum into integral, the sum in the first term gives $4\pi \ln r_c$ (integrating from 1 to r_c), while the second term gives $-4\pi \ln r_c$, which cancels the first term. This is valid for r_c larger than 1. Thus the dipolar energy $E_d = D[4\pi \ln r_c - 4\pi \ln r_c]$ is zero for the uniform configuration in 3D space in the framework of our model. The energy of the system comes from the short-range exchange term, Eq. 3.1.

The energy per site of other layered structures with periodicity $p = 2$ and 3 is numerically calculated and shown in Fig. 3.6 for $D/J = 0.8$ and 2. In each figure, the GS is the structure which corresponds to the lowest energy. One sees in Fig. 3.6 a the following GS configurations with varying r_c:

- uniform GS: for $1 \leq r_c \leq 1.3$ (zone (0))

- single-layer structure: for $1.3 \leq r_c \leq 1.8$ (zone (1))

- double-layer structure: for $1.8 \leq r_c \leq 3.65$ (zone (2))

- triple-layer structure: for $r_c \geq 3.65$ (zone (3))

For $D/J = 2$ there are only two possible GS with varying r_c as shown in Fig. 3.6b.

We summarize in table 3.1 the different GS in the space (r_c, D) with $J = 1$. We note that for a given D, for example $D = 0.8$, the GS configuration starts with uniform configuration then with period 1, 2, 3, ... for increasing r_c. At large D,

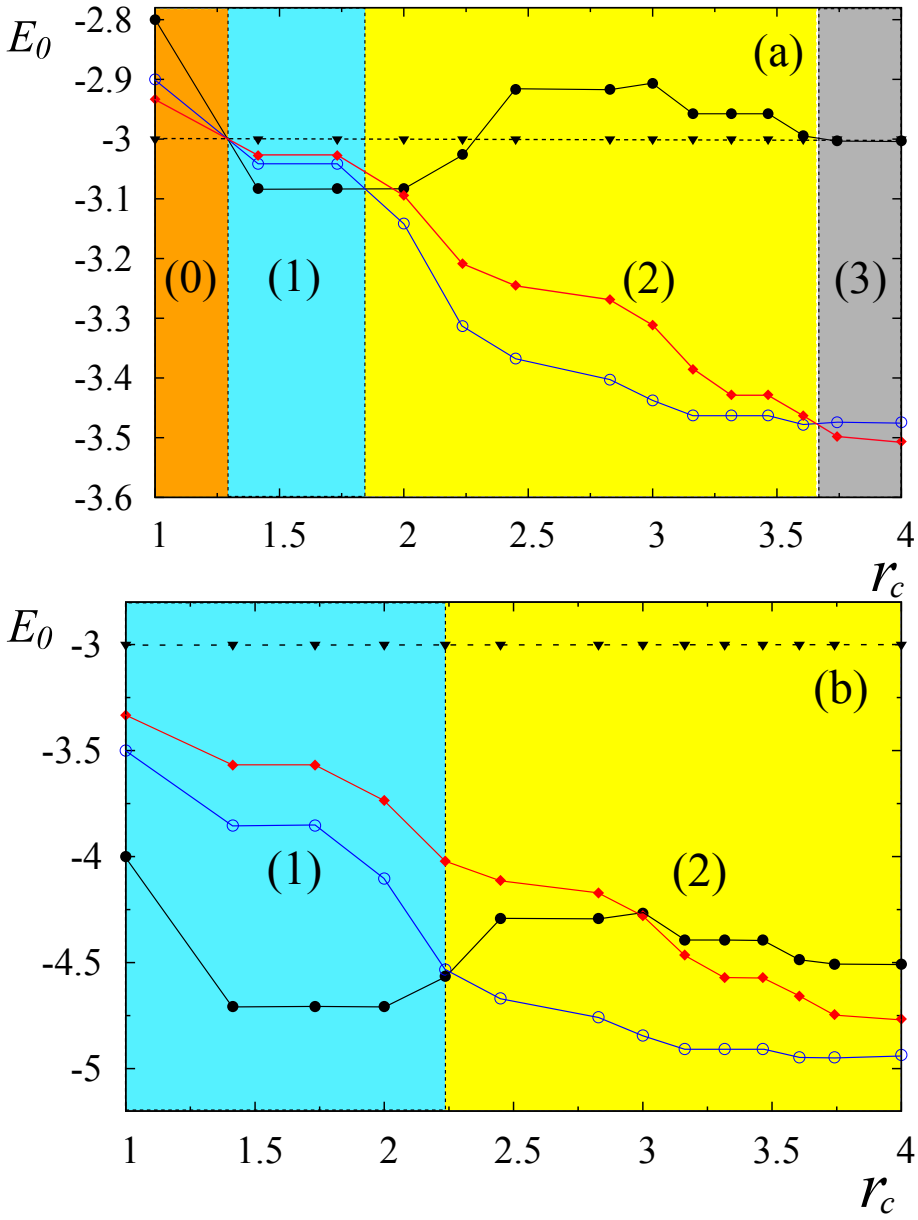

Figure 3.6: (Color online) Ground state energy versus r_c in the case where (a) $D/J = 0.8$ (b) $D/J = 2$. Black dashed, black solid, blue and red lines represent GS energy of the uniform, single-layer, double-layer and triple-layer structures, respectively. Zones (0), (1), (2), (0) indicate these respective different GS. See text for comments.

uniform configuration is not possible at any r_c. Long-period configurations are on the other hand favored at small D and large r_c.

r_c \ D	**0**	**0.2**	**0.4**	**0.6**	**0.7**	**0.8**	**0.9**	**1.0**	**1.2**	**1.5**	**2.0**	**5.0**
1.0 (6)	0	0	0	0	0	0	0	01	1	1	1	1
$\sqrt{2}$ (18)	0	0	0	0	0	1	1	1	1	1	1	1
$\sqrt{3}$ (26)	0	0	0	0	0	1	1	1	1	1	1	1
2.0 (32)	0	0	0	0	2	2	2	1	1	1	1	1
$\sqrt{5}$ (56)	0	0	0	2	2	2	2	2	2	2	1	1
$\sqrt{6}$ (80)	0	0	0	2	2	2	2	2	2	2	2	2
$\sqrt{8}$ (92)	0	0	0	2	2	2	2	2	2	2	2	2
3.0 (122)	0	0	0	2	2	2	2	2	2	2	2	2
$\sqrt{10}$ (146)	0	0	3	2	2	2	2	2	2	2	2	2
$\sqrt{11}$ (170)	0	0	3	3	2	2	2	2	2	2	2	2
$\sqrt{12}$ (178)	0	0	3	3	2	2	2	2	2	2	2	2
$\sqrt{13}$ (202)	0	0	3	3	3	2	2	2	2	2	2	2
$\sqrt{14}$ (250)	0	0	3	3	3	3	3	2	2	2	2	2
4.0 (256)	0	0	3	3	3	3	3	2	2	2	2	2

Table 3.1: Ground state in space (r_c, D): the numbers 0, 1, 2 and 3 denote the uniform, single-layer, double-layer and triple-layer structures, respectively. The first column displays the values of r_c with the number of neighbors indicated in the parentheses.

3.3 Phase Transition: results

We consider a sample size of $N \times N \times N_z$ where N and N_z vary from 24 to 48 but N_z can be different from N in order to detect the shape-dependence of the ground state.. The 3-state Potts model with NN exchange interaction $J = 1$ is used to describe the three molecular orientations. For the dipolar term, a cutoff distance r_c is taken up to $\sqrt{10} \simeq 3.16$ lattice distance. At this value, each molecule has a dipolar interaction with 146 neighbors. Periodic boundary conditions in all directions are employed.

We have used the standard MC method with the system size from 24^3 to 48^3. The

equilibrating time N_1 is about 10^6 MC steps per site, and the averaging time N_2 is between 10^6 and 10^7 MC steps per site. The averages of the internal energy $< U >$ and the specific heat C_V are defined by

$$\langle U \rangle = < \mathcal{H} + \mathcal{H}_d > \tag{3.4}$$

$$C_V = \frac{\langle U^2 \rangle - \langle U \rangle^2}{k_B T^2} \tag{3.5}$$

where $< ... >$ indicates the thermal average taken over N_2 microscopic states at T.

We define the Potts order parameter Q by

$$Q = [q \max(Q_1, Q_2, ..., Q_q) - 1]/(q-1) \tag{3.6}$$

where Q_n is the spatial average defined by

$$Q_n = \sum_j \delta(\sigma_j - n)/(N \times N \times N_z) \tag{3.7}$$

$n(n = 1, ..., q)$ being the value of the Potts variable at the site j. For $q = 3$, one has $n = 1, 2, 3$ representing respectively the molecular axis in the x, y and z directions. The susceptibility is defined by

$$\chi = \frac{\langle Q^2 \rangle - \langle Q \rangle^2}{k_B T} \tag{3.8}$$

A. Effect of D

We first show in Fig. 3.7 the energy per site $E \equiv < U > /(N \times N \times N_z)$ and the order parameter $M = < Q >$ versus T for the cases: i) absence of the dipolar interaction, i. e. $D = 0$ and ii) with dipolar interaction at $r_c = 2$ for $D = 0.8$ and $D = 1$. We find a very sharp transition.

In order to check the first-order nature of this transition, we have calculated the histogram shown in Fig. 3.8 for the values. We show that the two peaks are well separated with the dip going down to zero, indicating a tendency toward an energy discontinuity. The distance between the two peaks is the latent heat ΔE.

We have calculated the critical temperature T_c as a function of D for the case $r_c = 2, N_z = N = 48, J = 1$. The phase diagram is shown in Fig. 3.9 where $(0), (1),$

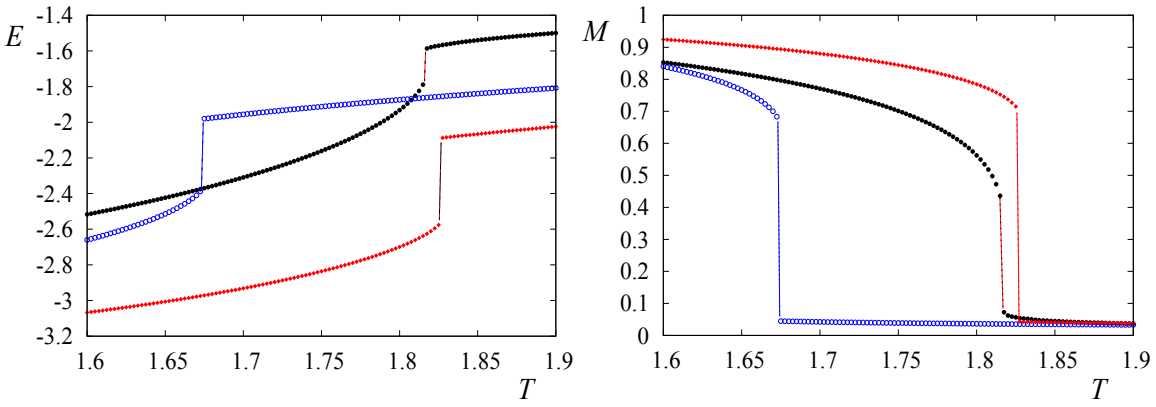

Figure 3.7: (Color on line) Energy per spin E and order parameter $M =< Q >$ versus temperature T without ($D = 0$, black circles) and with ($r_c = 2$) dipolar interaction, for several values $D = 0.8$ (blue void circles), 1 (red diamonds). $N_z = N = 48$, $J = 1$.

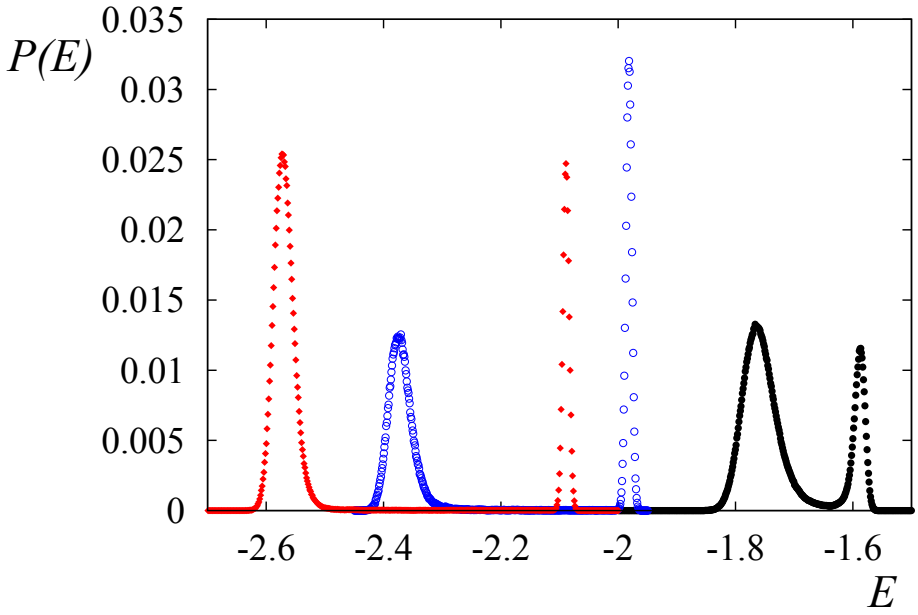

Figure 3.8: (Color on line) Energy histogram at the transition temperature without ($D = 0$, black circles) and with ($r_c = 2$) dipolar interaction, for several values $D = 0.8$ (blue void circles), 1 (red diamonds). $N_z = N = 48$, $J = 1$.

and (2) indicate the uniform, the single-layer and the double-layer GS, respectively. (P) denotes the paramagnetic phase.

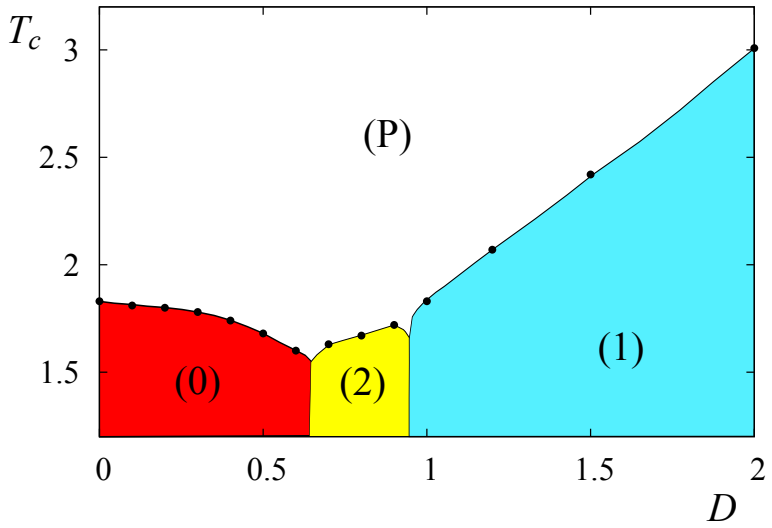

Figure 3.9: (Color on line) Phase diagram in the space (T_c, D) for $r_c = 2, N_z = N = 48, J = 1$. Zones $(0), (1), (2)$ indicate the uniform, single-layer, double-layer GS, respectively. (P) denotes the paramagnetic phase

B. Effect of cutoff distance r_c

In order to see the progressive effect of cutoff distance r_c, we perform simulations with fixing value of D, changing value of r_c and follow the change of the characteristics of the phase transition. We show in Fig. 3.10 the energy per spin E and the order parameter M versus T respectively for $D = 2$ and several values of r_c: $\sqrt{2}$, 2, and $\sqrt{10}$. The transition is still very sharp but the strong first-order character diminishes.

We show in Fig. 3.11 the energy histogram for several values of r_c with $D = 2$. As seen the latent heat becomes small at $r_c = \sqrt{10}$. We observe that the latent heat ΔE diminishes with increasing r_c. However, we cannot conclude that the first-order disappears at large r_c. To check that point we need to go to larger r_c which will take a huge CPU time because of the increasing number of neighbors (we recall that for $r_c = \sqrt{10}$, we have 146 neighbors for each molecules). We observe from Fig. 3.11 that the latent heat does not change significantly with r_c up to $r_c \simeq 2.85$, meaning that the first order transition is dominated by the short-range 3-state Potts interaction. The latent heat decreases rather strongly afterward but we do not know if it tends to

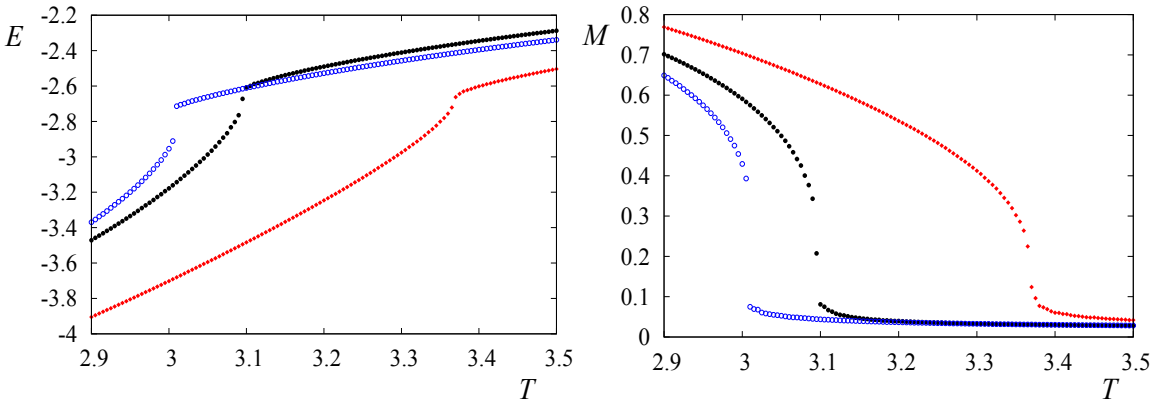

Figure 3.10: (Color on line) Energy per spin E and order parameter $M =< Q >$ versus temperature T for $D = 2$ at several values of r_c: $r_c = \sqrt{2}$ (black circles), 2 (blue void circles), and $\sqrt{10}$ (red diamonds). $N_z = N = 48$, $J = 1$.

zero or not.

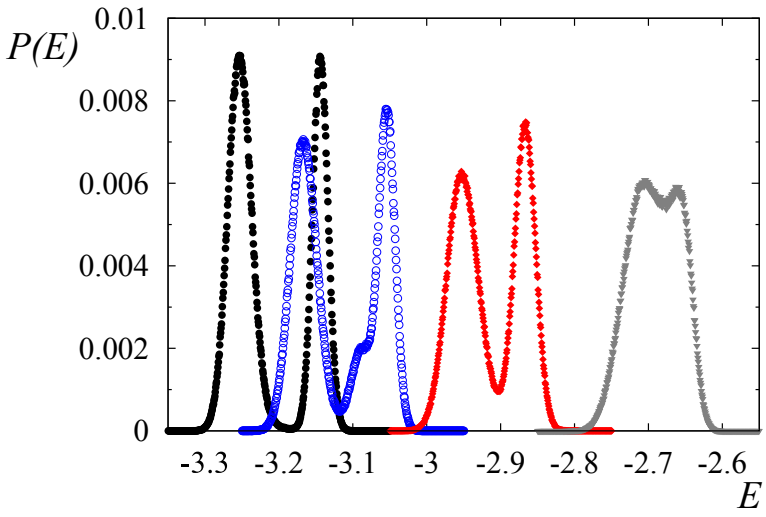

Figure 3.11: (Color on line) Energy histogram showing double-peak structure for $D = 2$ at several values of r_c: from left to right $r_c = \sqrt{6}$ (black circles), $\sqrt{8}$ (void circles), 3 (red stars) and $\sqrt{10}$ (grey triangles). $N_z = N = 48$, $J = 1$.

As said, even numerically we cannot prove that the first order will disappear for large D and large r_c, we conjecture that the first-order should disappear in this limit. The physical argument for this conjecture is based on the observation of two

limiting cases (i) when J=1 and $D = 0$ (no dipolar interaction), the transition is a strong first-order 3-state Potts model (ii) when $J = 0$, and D is not zero with infinite r_c, the transition is of dipolar origin. In this limit spin models such as Ising, XY and Heisenberg are known to yield a continuous (second-order) transition in 3D. We think that for the 3-state Potts model it should be of continuous type. If this is true, the nature of the transition should depend on the ratio $a = D/J$: when $a << 1$, the transition is of first-order and when $a >> 1$, the transition should become of a continuous type. This explains why at $D/J = 2$, the first-order transition is "weakened" as shown in Fig. 3.10. It is noted that the weakening is stronger for larger r_c as seen in Fig. 3.11 because one tends to the limiting case (ii) mentioned above.

The phase diagram in the space (T_c, r_c) is shown in Fig. 3.12 for $D = 2, N_z = N = 48$, $J = 1$. Phases $(1), (2)$ and (P) correspond, respectively, to GS single-layer, double-layer and paramagnetic phases.

In order to see the relationship between the transition temperature and GS energy, we plot in Fig. 3.13 the GS energy as a function of r_c for $D = 2$. We see that the variation of T_c depends on the variation of E_0: T_c increases when E_0 decreases, and vice-versa.

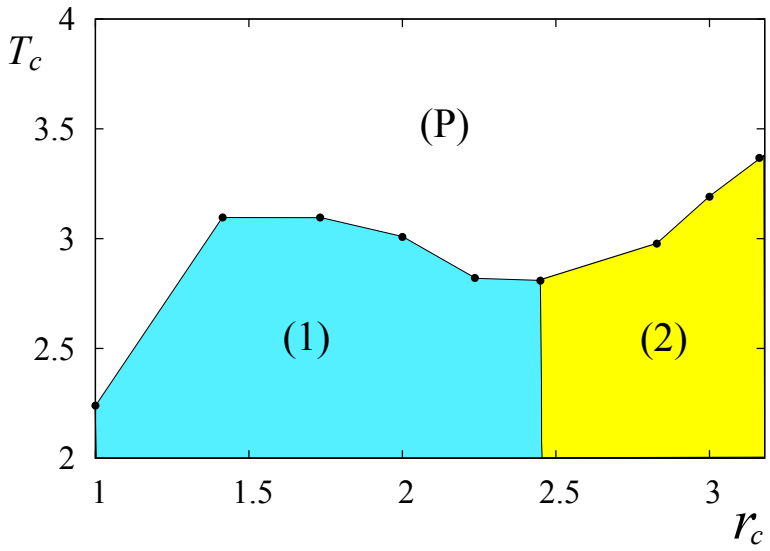

Figure 3.12: (Color on line) Phase diagram in the space (T_c, r_c) for $D = 2, N_z = N = 48$, $J = 1$. Phases $(1), (2)$ and (P) correspond, respectively, to the single-layer, the double-layer and the paramagnetic phases.

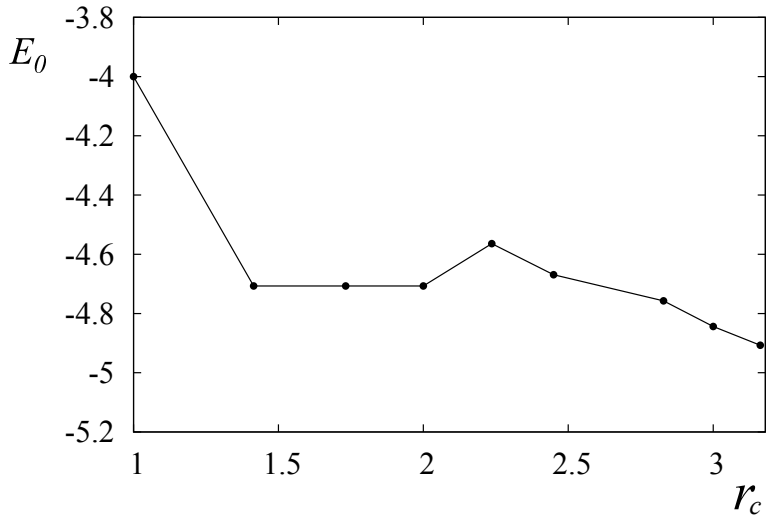

Figure 3.13: Ground state energy versus r_c for $D = 2, N_z = N = 48$, $J = 1$.

3.4 Surfaces effect

Surface physics has been intensively developed during the last 30 years. Among the main reasons for that rapid and successful development we can mention the interest in understanding the physics of low-dimensional systems and an immense potential of industrial applications of thin films [20, 21, 105]. In particular, theoretically it has been shown that systems of continuous spins (XY and Heisenberg) in 2D with short-range interaction cannot have long-range order at finite temperature [106]. In the case of thin films, it has been shown that low-lying localized spin waves can be found at the film surface [107, 108] and effects of these localized modes on the surface magnetization at finite temperature and on the critical temperature have been investigated by the Green's function technique [109, 110]. Experimentally, objects of nanometric size such as ultrathin films and nanoparticles have also been intensively studied because of numerous and important applications in industry. An example is the so-called giant magnetoresistance used in data storage devices, magnetic sensors, etc. [31, 30, 33]. Recently, much interest has been attracted towards practical problems such as spin transport, spin valves and spin-torques transfer, due to numerous applications in spintronics.

The dipolar interaction, however, is very special because it contains two competing terms which yield complicated orderings depending on the sample shape. For example, the dipolar interaction favors an in-plane ordering in films and slabs with infinite lateral dimensions. Many studies have been done with the dipolar interaction in thin films with the Heisenberg spin model [111, 112].

3.4.1 Model and method

We consider a thin film of simple cubic lattice. The film is infinite in the xy plane and has a thickness L_z in the z direction. The perpendicular anisotropy is introduced

by the following term

$$\mathcal{H}_a = -A \sum_i s_z(i)^2 \tag{3.9}$$

where A is a constant.

In the absence of D, the GS configuration is perpendicular to the film surface due to the term $\mathcal{H}_a$. In the absence of A, the GS is an in-plane configuration due to D. When both A and D are present, the GS depends on the ratio D/A. We shall use MC simulation to calculate properties of the system at finite T. Periodic boundary conditions are used in the xy planes for sample sizes of $L \times L \times L_z$ where L_z is the film thickness. Free symmetric surfaces are assumed for simplicity.

In order to appreciate finite-size effects, we carried out simulations in the 2D case for sizes from $L \times L = 24 \times 24$ to 60×60 and in the case of thin films from $L \times L \times L_z = 12 \times 12 \times 4$ to $48 \times 48 \times 6$. Results for the largest size are not significatively different from those of smaller sizes, excepted for the thickness. We will show therefore in the following results for lateral lattice size $L = 60$ for the 2D case, and $L = 24$ for thin films with thicknesses $L_z = 4$ and 6. In order to check the first-order nature of a weak first-order transition, the histogram technique is very efficient. But in our case as will be seen below, the re-orientation is a very strong first-order transition. The discontinuity of energy and magnetization is clearly seen at the transition. We just use the histogram technique to check the 2D case for a demonstration.

3.4.2 Two dimensions

In the case of 2D, for a given A, the steepest-descent method gives the "critical value" D_c of D above (below) which the GS is the in-plane (perpendicular) configuration. D_c depends on r_c. Let us take $A = 0.5$ and vary D and r_c in the following. The GS obtained numerically is shown in table 3.2 for several sets of (D, r_c). For instance, when $r_c = \sqrt{6} \simeq 2.449$, we have $D_c = 0.100$.

$\mathbf{r_c}$ \ **D**	**0.080**	**0.090**	**0.093**	**0.096**	**0.101**	**0.113**	**0.124**	**0.167**
1.0	I	I	I	I	I	I	I	II
$\sqrt{3}$	I	I	I	I	I	I	II	II
2.0	I	I	I	I	I	II	II	II
$\sqrt{6}$	I	I	I	I	II	II	II	II
3.0	I	I	I	II	II	II	II	II
$\sqrt{12}$	I	I	II	II	II	II	II	II
4.0	I	II	II	II	II	II	II	II

Table 3.2: Ground states as functions of (D, r_c), with $A = 0.5$, $J = 1$: the number (I) stands for the perpendicular configuration and the number (II) for the in-plane configuration (spins pointing along x or y axis).

We show in Fig. 3.14 the energy per site $E \equiv < U > /(L \times L \times L_z)$, the order parameter $M = < Q >$, the specific heat C_V and the susceptibility χ as functions of T in the case of $r_c = \sqrt{6}$, for $D = 0.09$ and $D = 0.11$ on two sides of $D_c = 0.100$. We observe one transition of second order for these values of D. Note that the transition for larger D is sharper.

It is interesting to examine the region very close to D_c, namely close to the frontier of two different GS. We have seen in the past that many interesting phenomena occur at the boundaries of different phases: we can mention the reentrance phenomenon in frustrated spin systems [17, 113] and the re-orientation transition in the Heisenberg film with a dipolar interaction similar to the present model [112]. We have carried out a simulation for values close to D_c. We find indeed a transition from the in-plane ordering to the perpendicular one when D increases in the region $D \in [0.100, 0.104]$. We show an example at $D = 0.101$ in Fig. 3.15 where we observe that in the low temperature phase ($0 \leq T < 0.93$) the spins align parallel to the x axis and in the intermediate temperature phase ($0.93 < T < 1.05$) the spins point along the z axis perpendicular to the film. The system becomes disordered at $T > 1.05$. Note that in the disordered phase, each "state" of the Potts spin (along one of the three axes) has 1/3 of the total number of spins. This explains why M_x and M_z tend to 1/3 at

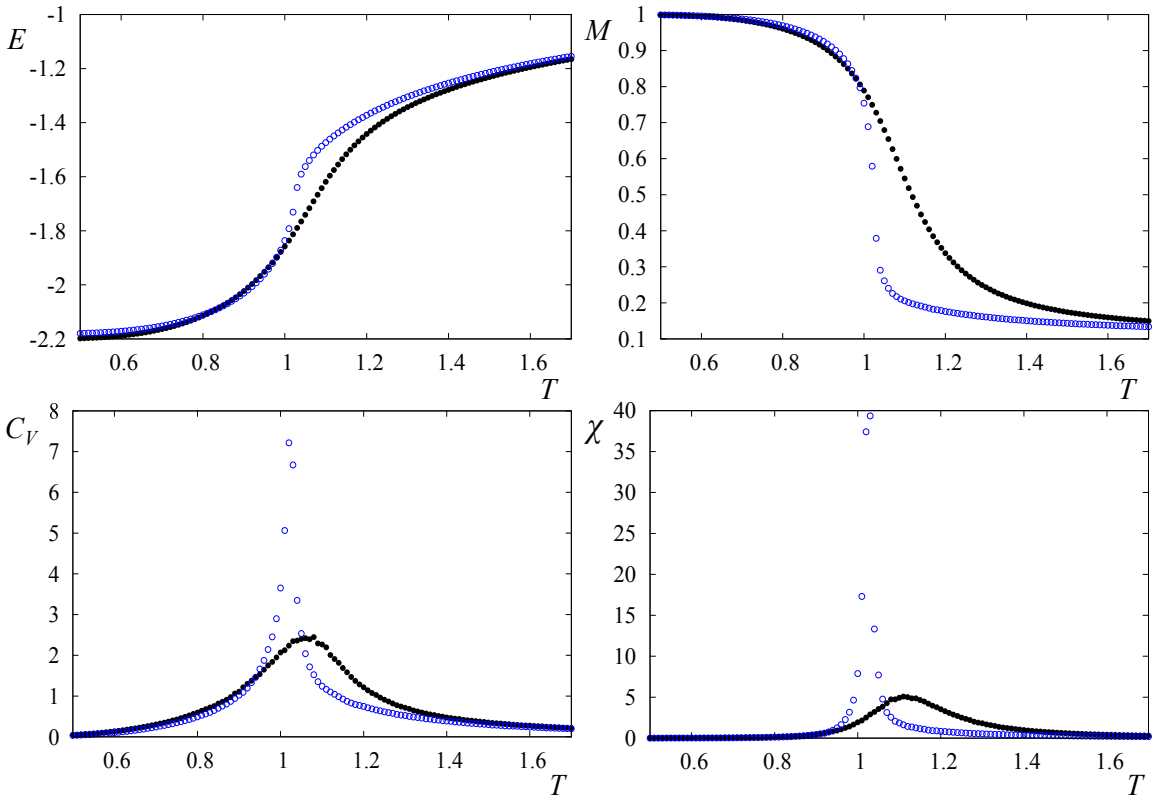

Figure 3.14: (Color online) Energy per spin E, order parameter M, specific heat C_V and susceptibility χ versus temperature T for D =0.09 (black solid circles) and 0.11(blue void circles). Note that M for $D = 0.09$ is the perpendicular magnetization while M for $D = 0.11$ is the in-plane magnetization, $L = 60$, $A = 0.5$, $J = 1$, $r_c = \sqrt{6}$.

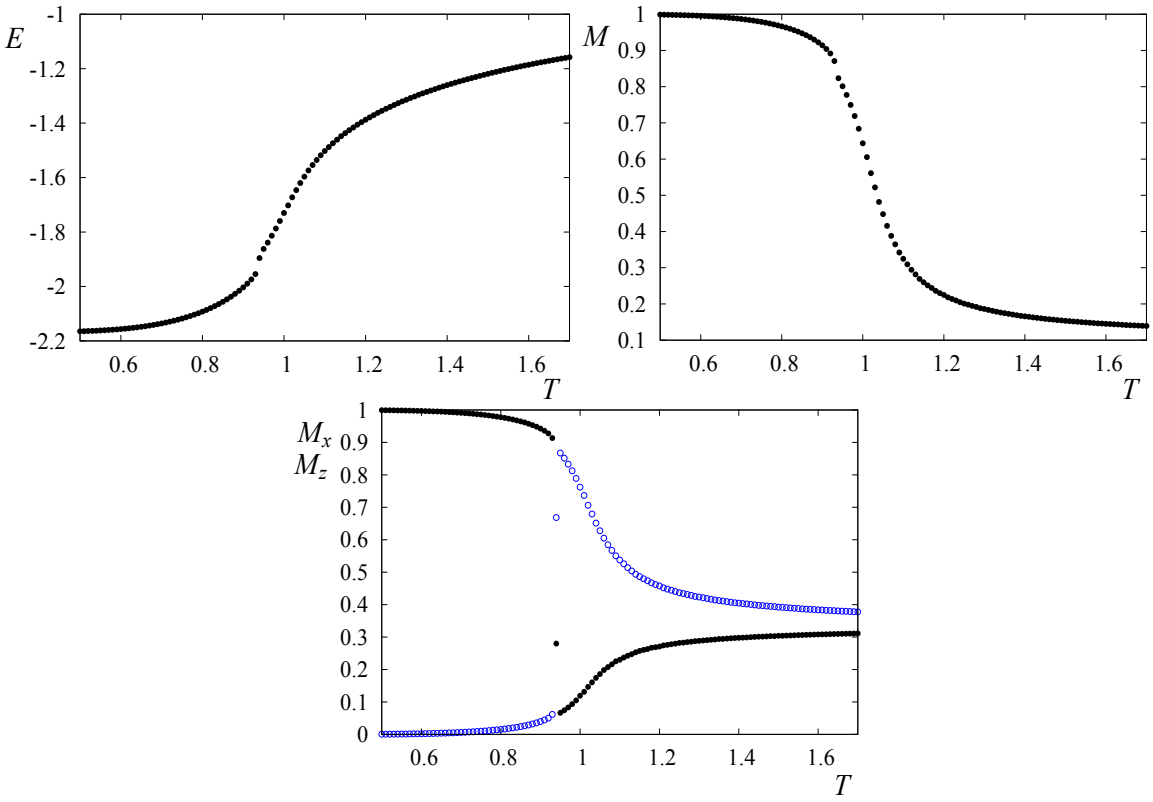

Figure 3.15: (Color online) Energy per spin E, total magnetization M, M_x (black solid circles) and M_z (blue void circles) versus temperature T for D =0.101 in the re-orientation transition region, $L = 60$, $A = 0.5$, $J = 1$, $r_c = \sqrt{6}$.

high temperature in Fig. 3.15. The transition from the in-plane to the perpendicular configuration is of first order as seen in Fig. 3.15 by the discontinuity of M_x, M_z, the energy and the magnetization at the transition point. The first-order character has been confirmed by the double-peaked energy histogram at the re-orientation transition temperature as shown in Fig. 3.16.

We show in Fig. 3.17 (top) the phase diagram in the space (D, T) for $r_c = \sqrt{6}$ where the line of re-orientation transition near D_c is a line of first order. Let us discuss the effect of changing r_c. Increasing r_c will increase the dipolar energy at each site. Therefore, a smaller value of D suffices to "neutralize" the effect of perpendicular anisotropy energy. The critical value of D_c is thus reduced as seen in the phase diagram established with $r_c = 4$ shown in Fig. 3.17 (bottom) where $D_c = 0.090$

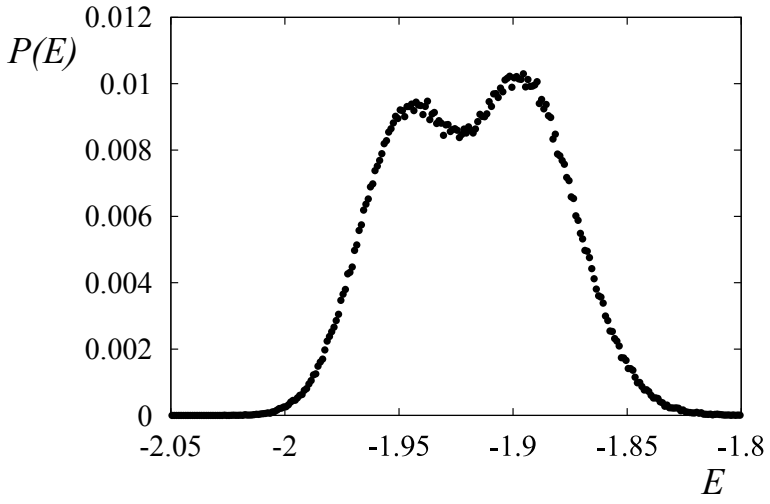

Figure 3.16: Energy histogram P versus energy E at the re-orientation transition temperature $T = 0.930$, for D =0.101, $A = 0.5$, $J = 1$, $r_c = \sqrt{6}$ ($L = 60$).

compared to $D_c = 0.100$ when $r_c = \sqrt{6}$ (top).

It is interesting to compare the present system using the 3-state Potts model with the same system using the Heisenberg spins [112]. In that work, the re-orientation transition line is also of first order but it tilts on the left of D_c, namely the re-orientation transition occurs in a small region below D_c, unlike what we find here for the Potts model. To explain the "left tilting" of the Heisenberg case, we have used the following entropy argument: the Heisenberg in-plane configuration has a spin-wave entropy larger than that of the perpendicular configuration at finite temperature, so the re-orientation occurs in "favor" of the in-plane configuration, it goes from perpendicular to in-plane ordering with increasing temperature. Obviously, this argument for the Heisenberg case does not apply to the Potts model because we have here the inverse re-orientation transition. We think that, due to the discrete nature of the Potts spins, spin-waves cannot be excited, so there is no spin-wave entropy as in the Heisenberg case. The perpendicular anisotropy A is thus dominant at finite temperature for D slightly larger than D_c.

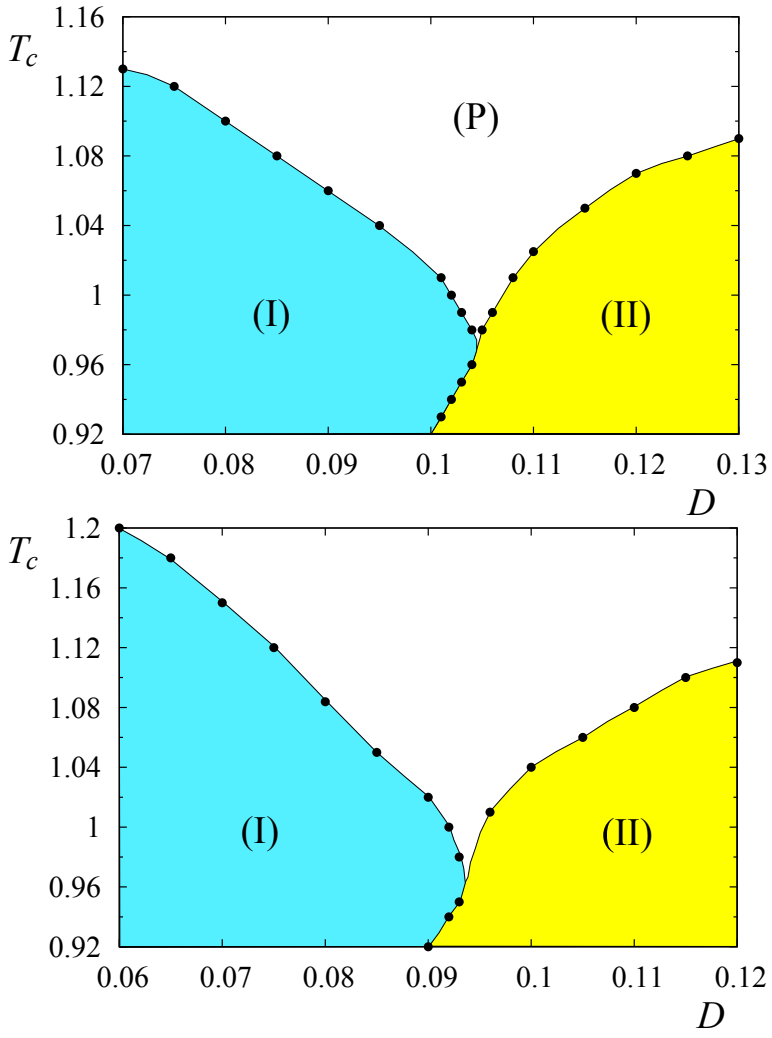

Figure 3.17: (Color online) Phase diagram in 2D: Transition temperature T_C versus D, with $A = 0.5$, $J = 1$, $r_c = \sqrt{6}$ (top) and $r_c = 4$ (bottom). Phase (I) is the perpendicular spin configuration, phase (II) the in-plane spin configuration and phase (P) the paramagnetic phase. See text for comments.

3.4.3 Thin films

The case of thin films with a thickness L_z where L_z goes from a few to a dozen atomic layers has a very similar re-orientation transition as that shown above for the 2D case.

Let us show results for $J_s = J$ in Figs. and tables 3.3-3.20 below. The effect of surface exchange integral J_s will be shown in the following subsection.

Let us show in table 3.3 the GS obtained by the steepest-descent method with $A = 0.5$ and $J = 1$ as before, for two thicknesses $L_z = 4$ and $L_z = 6$. Changing the film thickness results in changing the dipolar energy at each lattice site. Therefore, the critical value D_c will change accordingly. We note the periodic layered structures at large D and r_c for both cases. In the case $L_z = 4$, for $r_c = \sqrt{6}$ the critical value D_c above which the GS changes from the perpendicular to the in-plane configuration is $D_c = 0.305$.

As in the 2D case, we expect interesting behaviors near the critical value D_c. For example, when $L_z = 4$, $r_c = \sqrt{6}$ and $A = 0.5$, we find indeed a re-orientation transition which is shown in Fig. 3.18. The upper curves show clearly a first-order transition from in-plane x ordering to perpendicular ordering at $T \simeq 1.41$. The total magnetization (middle curve) and the energy (bottom curve) show a discontinuity at that temperature.

The whole phase diagram is shown in Fig. 3.19. Note that the line separating the uniform in-plane phase (II) and the periodic single-layered phase (1) is vertical.

To close this subsection, let us show in Fig. 3.20 the transition at values of D far from the critical values of D. There is only one transition from the ordered phase to the paramagnetic phase. As seen the transition from the in-plane ordering [phases (II) and (1)] to the paramagnetic phase is sharper than that from the perpendicular one [phase (I)], as in the 2D case.

r_c \ D	0.2	0.28	0.3	0.4	0.45	0.6	0.8	1.5
1.0	I	I	I	I	I	I	II	1
$\sqrt{3}$	I	I	I	I	I	II	1	1
2.0	I	I	I	I	II	II	2	1
$\sqrt{6}$	I	I	I	II	II	2	2	2
3.0	I	II	II	II	2	2	2	2
$\sqrt{12}$	I	II	II	II	2	2	2	2
4.0	I	II	II	II	2	2	2	2

r_c \ D	0.3	0.4	0.45	0.6	0.8	1.5
1.0	I	I	I	I	I	1
$\sqrt{3}$	I	I	I	I	1	1
2.0	I	I	I	I	2	1
$\sqrt{6}$	I	I	I	2	2	2
3.0	I	I	2	2	2	2
$\sqrt{12}$	I	3	3	2	2	2
4.0	I	3	3	2	2	2

Table 3.3: Ground states in a thin film as functions of (D, r_c), for thickness L_z = 4(top) and 6 (bottom), with $A = 0.5$ and $J = 1$: the number (I) stands for the perpendicular configuration, the number (II) for the in-plane configuration (spins pointing along x or y axis), the number (1) for alternately one layer in x and one layer in y direction (periodic single-layered structure), the number (2) stands for the configuration with alternately 2 layers in x alignment and 2 layers in y alignment (periodic bi-layered structure), and the number (3) for alternately three layers in x and three layers in y direction (periodic tri-layered structure).

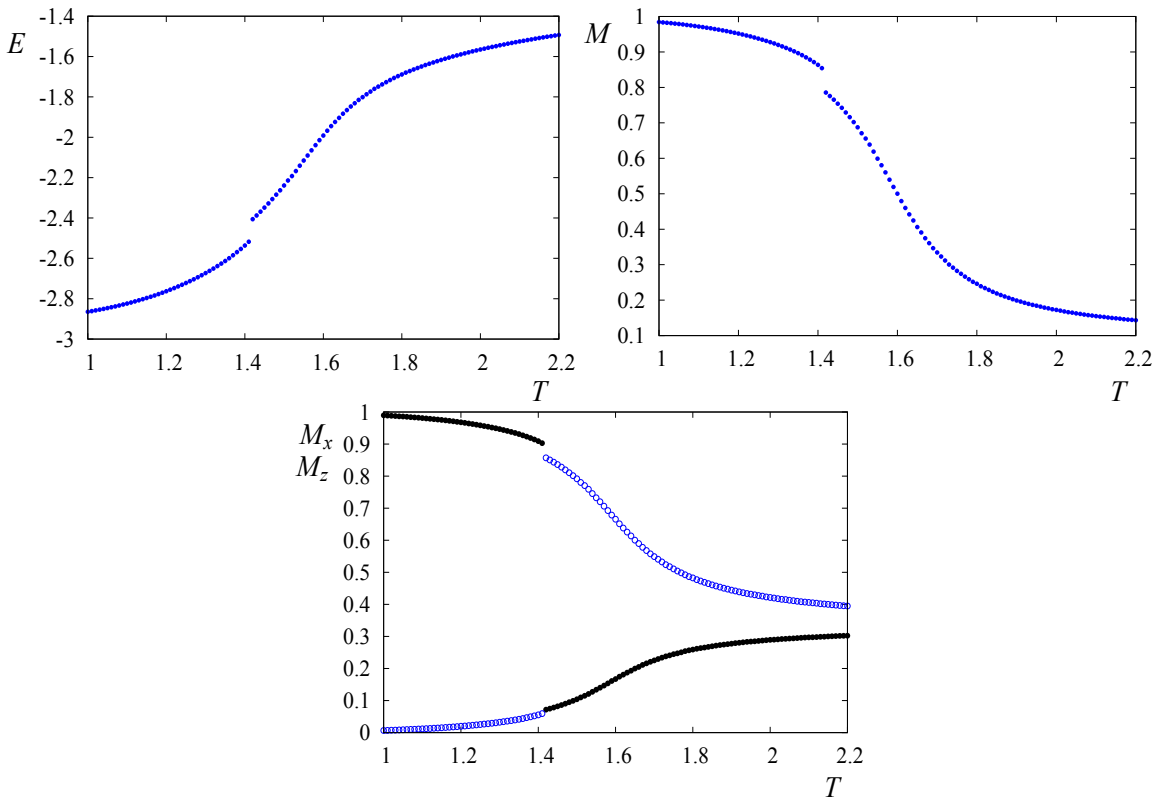

Figure 3.18: (Color online) Film with thickness $L_z = 4$ ($L = 24$). Energy per spin E, total magnetization M, M_x (black solid circles) and M_z (blue void circles) versus T for D =0.31 in the re-orientation transition region. See text for comments.

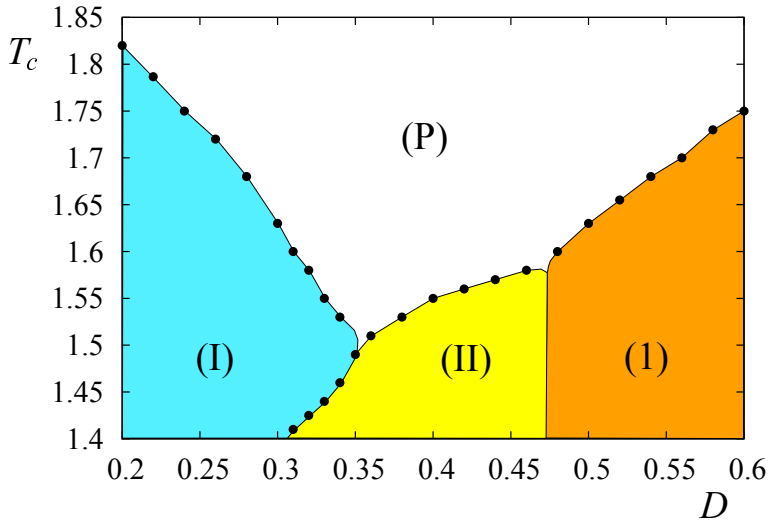

Figure 3.19: (Color online) Phase diagram in thin film of 4-layer thickness: Transition temperature T_C versus D, with $A = 0.5$, $J = 1$ and $L = 24$. Phases (I), (II),(1) and (P) are defined in the caption of table 3.3. See text for comments.

3.4.4 Effect of surface exchange interaction

We have calculated the effect of J_s by taking its values far from the bulk value ($J = 1$) for several values of D. In general, when J_s is smaller than J the surface spins become disordered at a temperature T below the temperature where the interior layers become disordered. This case corresponds to the soft surface (or magnetically "dead" surface layer) [110]. On the other hand, when $J_s > J$, we have the inverse situation: the interior spins become disordered at a temperature lower that of the surface disordering. We have here the case of a magnetically hard surface. We show in Fig. 3.21 an example of a hard surface in the case where $J_s = 3$ for $D = 0.6$ with $L_z = 4$. The same feature is observed for $D = 0.4$. Note that the surface and bulk transitions are seen by the respective peaks in the specific heat and the susceptibility. In the re-orientation region, the situation is very complicated as expected because the surface transition occurs in the re-orientation zone.

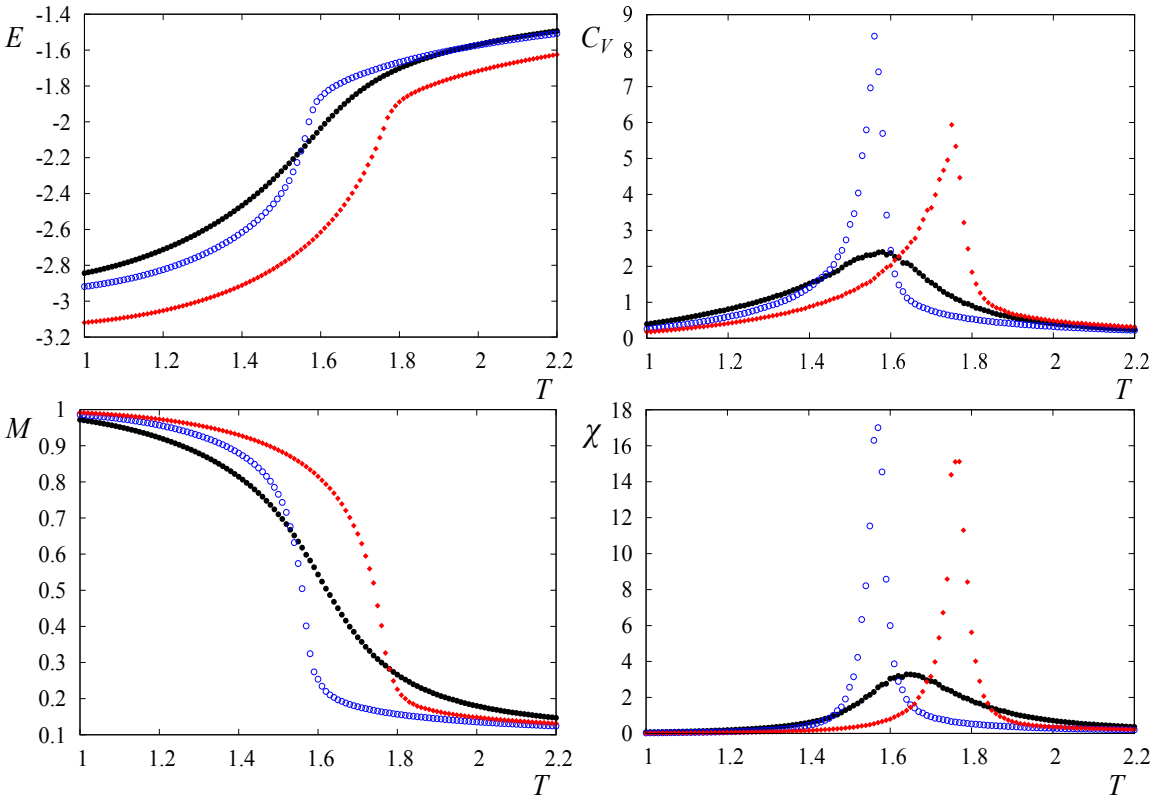

Figure 3.20: (Color online) Energy per spin E, order parameter M, specific heat C_V and susceptibility χ versus temperature T for D =0.3 (black solid circles), 0.4 (blue void circles) and 0.6 (red diamonds), $L_z = 4$, $L = 24$.

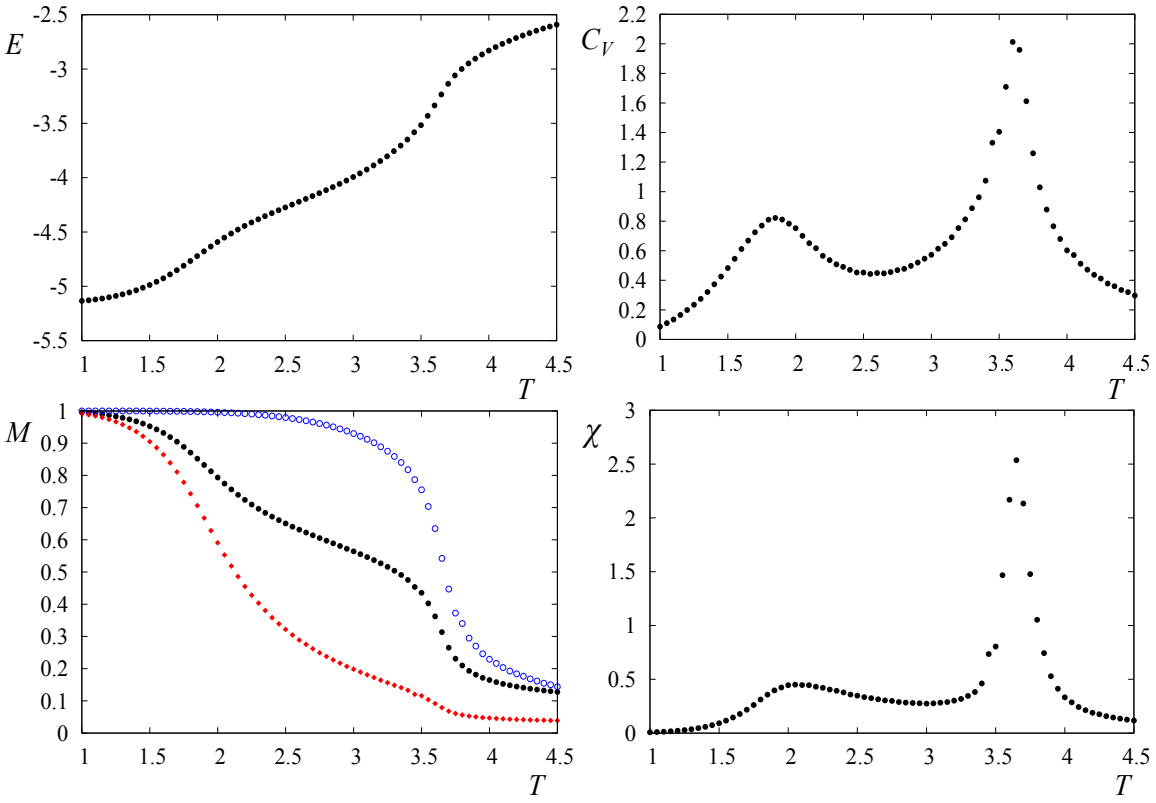

Figure 3.21: (Color online) Energy per spin E, order parameter M, specific heat C_V and susceptibility χ of a 4-layer film versus temperature T for D =0.6 with $J_s = 3$ ($L = 24$). The surface magnetization is shown by blue void circles, the bulk magnetization by red diamonds and the total curves by black solid circles.

3.4.5 Discussion

Note that for a given D, the effect of the cutoff distance r_c is to move the critical value of D_c as seen in tables 3.2 and 3.3. At $r_c = \sqrt{10} \simeq 3.16$ one has 146 neighbors for each interior spin (not near the surface). This huge number makes MC simulations CPU-time consuming. We therefore performed simulations at finite temperature only with two values of r_c in the 2D case. As seen in Fig. 3.17, the change of r_c does not alter our conclusion on the re-orientation transition. Therefore, we wanted to test in this work how physical results depend on r_c in the dipolar interaction. If we know for sure that in a thin film the interaction is dipolar and that a double-layered structure for example is observed, from what is found above we can suggest the interaction range between spins in the system.

Finally, we note that if we change A, the value of D_c will change. The choice of A=0.5 which is a half of J is a reasonable choice to make the re-orientation happen. A smaller A will induce a smaller D_c but again, the physics found above will not change.

3.5 Conclusion

We have studied in this chapter a molecular crystal characterized by three possible orientations of the molecular axes. The model is described by a short-range 3-state Potts model and a dipolar Potts interaction. We have analyzed in section 3.2 the GS as functions of the dipolar interaction strength D and its cutoff distance r_c. The GS is shown that: For very small D, the GS is uniform for any r_c. For increasing D, the GS has layered structures with period $1, 2, 3, ...$ depending on D and r_c. To our knowledge, such a GS has not been seen in systems with uniformly interacting molecules. The stacking of independent ordered layers is reminiscent of a smectic ordering. Note that the model is applied to smectic phases where tilted angles are uniform: it can be of type A as supposed here or of type C if the molecular axis does

not coincide with the x, y or z axis of the lattice. The coupling between adjacent different ordered planes is here strictly zero at $T = 0$, due to the Potts condition in the model.

We have used the MC histogram method to study the phase transition in this system. In the absence of the dipolar interaction, the model which is a 3-state Potts model is known to undergo a first-order phase transition from the orientational ordered phase to the disordered state. Upon the introduction of a dipolar interaction of sufficient strength into the Potts model, the GS is broken into layers as described above. We have shown that the transition remains of first order as the cutoff distance is increased at least up to $r_c = \sqrt{10}$.

In section 3.4, we have also shown MC results for the phase transition in thin magnetic films with taking into account a single-ion perpendicular anisotropy of amplitude A. Among the striking results, we mention the re-orientation transition which occurs in 2D and in thin films at a finite temperature below the overall disordering. This re-orientation is a very strong first-order transition as seen by the discontinuity of the energy and the magnetization. We emphasize that the re-orientation is possible only because we have two competing interactions: the perpendicular anisotropy and the dipolar interaction.

Chapter 4

Phase Transition in Dimer Liquids

We study the phase transition in a system composed of dimers interacting with each other via a NN exchange J and a long-range dipolar coupling. In our model, each dimer occupies a link between two nearest sites of a simple cubic lattice. Dimers cannot touch each other. We suppose that dimers can have only three orientations which coincide with the x, y or z direction. The interaction J gives rise to a negative energy if the two dimers are parallel with each other at the NN distance, zero otherwise. The dipolar interaction is characterized by two parameters: its amplitude D and the cutoff distance r_c. We consider two cases: polarized dimers (namely, oriented dimers) and non polarized dimers. Using the steepest-descent method, we determine the GS configuration as functions of D and r_c. We next use extensive MC simulations to determine the characteristics of the phase transition from the orientationally-ordered dimer phase at low temperature to the disordered phase at high temperature. In particular, we show that when D is small, the transition is of second order but it becomes of first order for large enough D, for both polarized and non polarized dimers.

4.1 Introduction

The first observation of liquid crystals is thought to be around 160 years ago, although its importance was not understood until 100 years later.

Around 1850, when the German structural chemist Wilhelm Heinrich Heintz was studying natural fats, he observed that when heating stearin, it turns cloudy at 52°C, then completely opaque at 58°C, and becomes clear at 62.5°C [114]. These observations are very similar to the ones that 40 years later led to the discovery of liquid crystals.

Years later, European biologists Virchow, Mettenheimer and Valentin were studying nerve fibres. They found that a fluid substance from the nerve core, when dissolved in water, exhibited strange behavior when viewed in polarized light [114]. At that time it was believed that liquids could not exhibit such a behavior in the presence of polarized light, and yet the substance was clearly not a solid. They did not realize that this was a completely a new state of matter.

In 1877, the German physicist Otto Lehmann developed a polarizing microscope with a heated stage to investigate the phase transitions of several substances [115]. He found that some substances would change from a clear liquid to a cloudy liquid before crystallizing, and he thought that he was observing an imperfect phase transition from liquid to solid.

In 1888, the Austrian chemist Reinitzer investigated the phase transitions of various compounds using a polarizing microscope fitted with a heating stage. Over the course of his study, Reinitzer discovered that cholesteryl benzoate changed from a clear to a cloudy liquid before crystallizing. Unfortunately, he attributed the apparent occurrence of two melting points to an imperfect phase transition, at 145.5°C the solid crystal melted into a cloudy liquid which existed until 178.5°C, at which the cloudiness suddenly disappeared, giving way to a clear transparent liquid. Still puzzled, a year later Reinitzer wrote a letter with his findings to the German physicist Otto Lehmann

[115]. After conducting similar experiments, Lehmann suggested that the cloudy fluid was a new phase of matter which he called "Liquid Crystal" in the landmark paper entitled "Uber fliessende Krystalle" [116].

Liquid crystals are a state of matter intermediate between that of a crystalline solid and an isotropic liquid. They possess many of the mechanical properties of a liquid, e.g., high fluidity, inability to support shear, formation, and coalescence of droplets. At the same time they are similar to crystals in that they exhibit anisotropy in their optical, electrical, and magnetic properties.

Today liquid crystals appear in very many applications but the most common application is still LCDs, which rely on the different optical properties of liquid crystals in the presence and absence of an electric field. LCDs are used in many everyday devices, including TV and computer screens, mobile phones, cameras, watches, calculators and so on.

Two main classes of liquid crystal materials are distinguished: thermotropic and lyotropic liquid crystals. Lyotropic liquid crystals only form liquid crystal phases when mixed with a solvent, and they only change phase with concentration. Thermotropic liquid crystals are liquid crystals that change phase with temperature and are only stable within a certain temperature range.

My study concerns thermotropic liquid crystals. Depending on their structural properties, thermotropic liquid crystals can be classified into smectic (Sm), nematic (N), and cholesterics (or chiral nematic) (N*) [117].

A. Nematic

Nematic phase is the simplest liquid crystalline phase which is characterized by long-range orientational order. The molecules can translate freely and can rotate around their long axis (see Fig. 4.1).

B. Smectic

In the smectic phase, the molecules are organized in layers with a well-defined in-

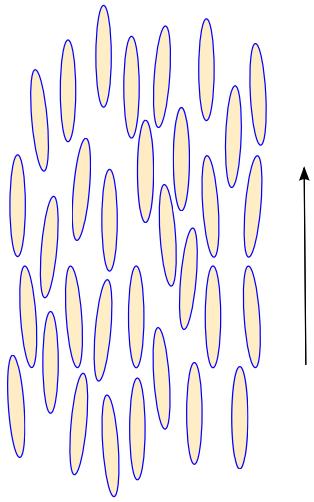

Figure 4.1: The arrangement of molecules in nematic phase.

terlayer spacing and exhibit some correlations in their positions in addition to the orientational ordering.

Many different smectic phases are known, each one differing in orientation and position of the mesogenic molecules [118]. They are distinguished by a letter and denoted as SmA, SmB, SmC, SmC*,etc.

- As shown in Fig. 4.2, in the smectic A phase the molecules are aligned perpendicular to the layer, with no long-range order within a layer. The layers can slide freely over one another.

- In the smectic C phase, the molecular orientations are constant in all smectic layers but the preferred axis is not perpendicular to the layer. In the smectic A and smectic C phases there is no long-range positional order in the arrangement of the molecules within the layers and thus each layer resembles a two-dimensional liquid. Adjacent layers may slip easily over one another.

- Smectic C* phase corresponds exactly to smectic C but the long axes are rotated around a cone generator.

C. Cholesteric

The cholesteric phase is essentially a nematic phase with an additional helical change in orientation of the director (see Fig. 4.3). Whereas the director in an ordinary

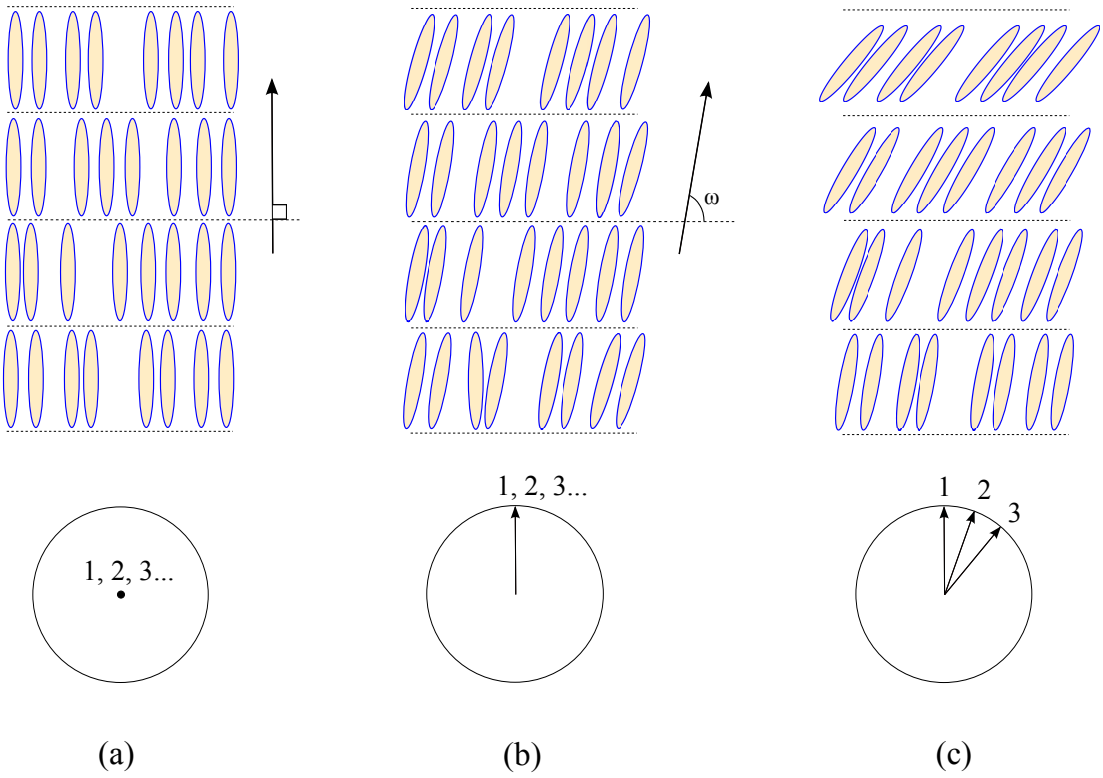

Figure 4.2: The arrangement of molecules in smectic phase: (a) Smectic A, (b) Smectic C and (c) Smectic C*. Numbers $(1, 2, 3, ...)$ denote subsequent layers.

nematic liquid crystal has a constant direction, in a cholesteric phase it changes direction in a helical fashion throughout the sample, perpendicular to the helix axis.

We show the schematic structures of crystalline solid, liquid crystal and isotropic liquid phases in Fig. 4.4. At lower temperatures, the matter compounds form solid crystals like ordinary organic substances (see Fig. 4.4a). Upon heating, a phase transition to a liquid crystal phase can occur (see Fig. 4.4b). With further heating, a phase transition to a isotropic liquid phase can occur the Matter possesses the same properties as ordinary liquids (see Fig. 4.4c).

We are interested here in the phase transition of a system composed of interacting dimers, a kind of axial molecules moving in space. At low temperatures these dimers are frozen in an orientational ordered phase and at high temperature they are in a

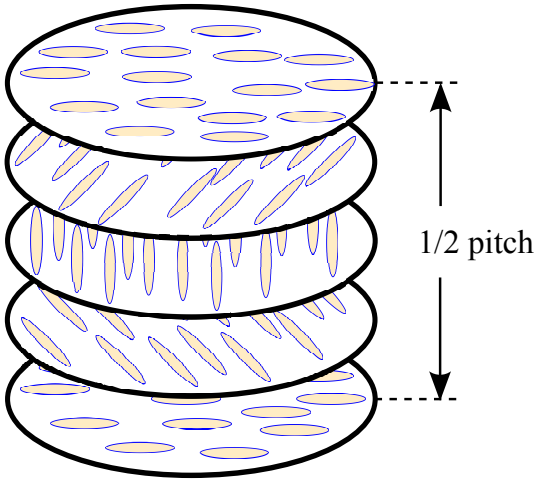

Figure 4.3: The arrangement of molecules in cholesteric phase.

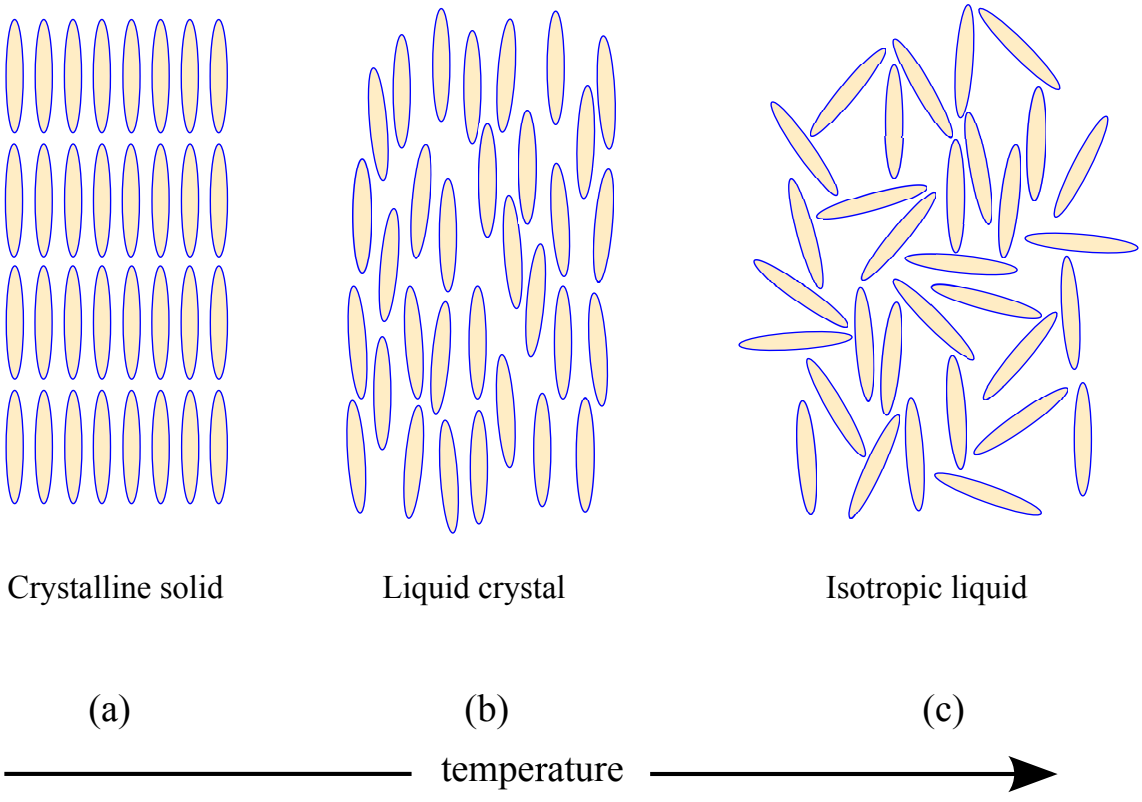

Figure 4.4: Thermotropic liquid crystal phase transition behavior. The axis indicates the direction of increasing temperature.

liquid state with or without orientational ordering. Liquid crystals are thus somewhere between solid and liquid states where molecules have some spatial orientations which under some conditions can order themselves into some ordered structures.

We study in this thesis a model of liquid crystal by taking into account the effect of a dipolar interaction and an exchange interaction between nearest neighboring (NN) dimers. The dipolar interaction in spin systems, and in particular in thin films [112], has been widely studied. Our purpose is to investigate the nature of the ordering and of the phase transition in a liquid crystal described by our model. This is motivated by recent experiments on periodic layered structures of ordered phases [119, 8, 120, 7, 95, 6] and on orientational phase transitions in various liquid crystals [121, 122, 123, 124, 125, 126, 127]. Some numerical investigations on orientational order have also been published [128, 129, 130].

Our model is described in detail in section 4.2. The GS analysis and results of MC simulations of polarized dimers are shown and discussed in section 4.3. The case of non polarized dimers are shown in section 4.4. Concluding remarks are given in section 4.5.

4.2 Model

We consider a system of dimers, each of which lies on a link between two nearest sites on a SC lattice. By definition, dimers do not touch each other. The dimer axis can be in the x, y or z direction. The Hamiltonian is given by the following 3-state Potts model [80]:

$$\mathcal{H} = -\sum_{(ij,mn)} J(ij,mn)\delta(\sigma_{ij},\sigma_{mn}) \tag{4.1}$$

where σ_{ij} is a variable defined for the link between nearest lattice sites i and j. σ_{ij} is equal to 1 if the dimer axis is x, 2 if it is y, and 3 if it is z. We suppose that the interaction energy between two dimers (ij) and (mn) is $-J(ij,mn)$ and it is equal to $-J$ $(J>0)$ if they occupy two parallel links on a square face of a cubic lattice cell,

zero otherwise. For a description purpose, we shall adopt the following notation to define a dimer: the dimer on the link (ij) is always written with i being the first end. In the case where the dimer is oriented (or polarized), the dimer is considered as a vector. In the case of non polarized dimers, each dimer is a non oriented segment. Periodic boundary conditions are applied in all directions.

The dipolar interaction between dimers is written as

$$\begin{aligned}\mathcal{H}_d &= D \sum_{(ij,mn)} \{\frac{\mathbf{S}(\sigma_{ij}) \cdot \mathbf{S}(\sigma_{mn})}{r^3_{(ij,mn)}} \\ &\quad -3\frac{[\mathbf{S}(\sigma_{ij}) \cdot \mathbf{r}_{(ij,mn)}][\mathbf{S}(\sigma_{mn}) \cdot \mathbf{r}_{(ij,mn)}]}{r^5_{(ij,mn)}}\} \end{aligned} \tag{4.2}$$

where $\mathbf{r}_{(ij,mn)}$ is the vector of modulus $r_{(ij,mn)}$ connecting the middle point A of the dimer (ij) and the middle point B of the dimer (mn). One has then: $\mathbf{r}_{(ij,mn)} \equiv \mathbf{r}_B - \mathbf{r}_A$. In Eq. (4.2), D a positive constant depending on the material, the sum $\sum_{(ij,mn)}$ is limited at pairs of dimers within a cut-off distance r_c. The dimer state is defined by a quantity $\mathbf{S}(\sigma_{ij})$ given by

$$\mathbf{S}(\sigma_{ij}) = (S_1, 0, 0) \text{ if } \sigma_{ij} = 1 \tag{4.3}$$

$$\mathbf{S}(\sigma_{ij}) = (0, S_2, 0) \text{ if } \sigma_{ij} = 2 \tag{4.4}$$

$$\mathbf{S}(\sigma_{ij}) = (0, 0, S_3) \text{ if } \sigma_{ij} = 3 \tag{4.5}$$

There are two cases:
i) the non polarized dimers: $\mathbf{S}(\sigma_{ij})$ is given by the following non algebraic components $S_1 = a$, $S_2 = a$, $S_3 = a$, a being the lattice constant.
ii) the polarized dimers: $\mathbf{S}(\sigma_{ij})$ is given a true three-component vector with $S_1 = \pm a$, $S_2 = \pm a$ and $S_3 = \pm a$.

In this work we study both non polarized and polarized dimers. a will be taken to be 1 in the following.

4.3 Polarized Dimers: Ground State Analysis and Phase Transition

4.3.1 Ground state

A. Without dipolar interaction $D = 0$

Without the dipolar interaction, the interaction between neighboring molecules will give rise to an orientational order of molecular axes at low temperature. This situation is similar to a 3-state Potts model in 3D, but the difference resides in the fact that dimers are moving from one bond to another while in the Potts model, the particle stays at its lattice site. The dynamics which leads to excited states is not the same: dimers have self-avoiding constraints. Note that the phase transition of the q-state Potts model in 3D is of first order for $q > 2$ [80]. We will see that the 3-state dimer crystal described above undergoes a second-order transition in the absence of a dipolar interaction.

It is easy to see that in the GS of the above Hamiltonian, all dimers are parallel, as shown by the dimer configuration of type 1 in Fig. 4.5. Note that if the lattice size is $L \times L \times L$, the number of links is $3L^3$, but the number of dimers n_d should be less than or equal to $N_d(\max) = L^3/2$ because each dimer takes two lattice sites and they do not touch each other. If $n_d = N_d(\max)$, then the dimers occupy the whole lattice as shown in Fig. 4.5. Now if we use a number of dimers less than $N_d(\max)$, for instance $n_d = N_d(\max)/2$, then in the GS the dimers will fully occupy the half of the lattice in which they are parallel, leaving the remaining half empty. In other words, dimers occupy the lattice space in a most compact manner. This GS is similar to that of a polymer on a lattice where it is "folded" to get a minimal energy at temperature $T = 0$. We emphasize that when $n_d = N_d(\max)$, dimers cannot move, the system is blocked. In order to study excitations of dimer systems at finite temperature, it is necessary to take n_d much less than $N_d(\max)$.

B. With dipolar interaction $D \neq 0$

We will see hereafter that when a dipolar interaction between dimers is introduced, the GS depends on D and r_c. We see that in the uniform dimer configuration such as the configuration of type 1 in Fig. 4.5, the dipolar energy is zero: when there is only one kind of dimer orientation, say axis z, the dipolar energy of σ_{ij} is

$$E_i = D \sum_{mn} [\frac{1}{r^3_{ij,mn}} - 3\frac{z^2_{ij,mn}}{r^5_{ij,mn}}] \tag{4.6}$$

If we transform the sum into integral, the sum in the first term gives $4\pi \ln r_c$ (integrating from 1 to r_c), while the second term gives -$4\pi \ln r_c$, which cancels the first term. This is valid for r_c larger than 1. The energy of the system comes from the short-range exchange term, Eq. (4.1).

In order to understand the GS found below as functions of D and r_c, let us consider a dimer σ_{ij} interacting with its neighbor σ_{mn}. If they have the same orientation, say the x axis for instance, the energy calculated with Eq. (4.2) is

$$E_i = D[\frac{1}{r^3_{ij,mn}} - 3\frac{x^2_{ij,mn}}{r^5_{ij,mn}}] \tag{4.7}$$

in which the first term is positive and the second one is negative. However when the first dimer is on x and the second one on y for example, the first term in Eq. (4.2) is zero, the dipolar energy for the perpendicular dimer pair is given by

$$E_i = D[-3\frac{S_1 x_{ij,mn} S_2 y_{ij,mn}}{r^5_{ij,mn}}] \tag{4.8}$$

where $S_1 = \pm 1$ and $S_2 = \pm 1$. This term can be positive or negative, depending on the signs of $x_{ij,mn}$, $y_{ij,mn}$, S_1 and S_2 of the dimer pair (ij, mn). So, in the GS, S_1 and S_2 take their signs which minimize this term. The difficulty of determining the GS comes from the choice of each dimer pair so as to have the minimum of the global energy. This cannot be done analytically.

Using the steepest descent method, we have calculated the GS configurations for various sets of (D, r_c). The results are shown in table 4.1. For each set (D, r_c),

r_C \ D	0.30	0.40	0.45	0.48	0.50	0.60
1.5	1	1	1	1	3	3
1.8	1	1	4	4	4	4
2.3	1	1	4	4	4	4
2.5	1	1	5	5	5	5
2.8	1	1	5	5	5	5
3.2	1	2	2	6	6	6
3.6	1	2	6	6	6	6

Table 4.1: Ground state configurations numbered from 1 to 6 obtained by the steepest-descent method in the space (D, r_c). These configurations are displayed in Figs. 4.5.

the configuration is indicated by a number. The configurations corresponding to the numbers from 1 to 6 are shown in Figs. 4.5. For a description commodity, let us call z the vertical axis of these figures, and x the horizontal axis. Note the GS degeneracy due to the permutation of the dimer axes. Let us now comment table 4.1. For small D and small r_c, the GS is of type 1 which is uniform just as in the case $D = 0$ discussed above. Larger values of D and r_c yield complicated configurations: for instance, type 2 consists of a three-layered structure of opposite dimer polarizations with a shift in z at their interface, type 3 consists of a single-layered structure of parallel polarization but with a shift in z. Types 4, 5 and and 6 are more complicated with larger dimer lattice cells.

4.3.2 Phase Transition

We consider a sample size of $L \times L \times L$ where L varies from 12 to 48. The NN exchange interaction is used as the unit of energy, i. e. $J = 1$. For the dipolar term, a cutoff distance r_c is taken up to $\sqrt{10} \simeq 3.15$ lattice distance. The algorithm is

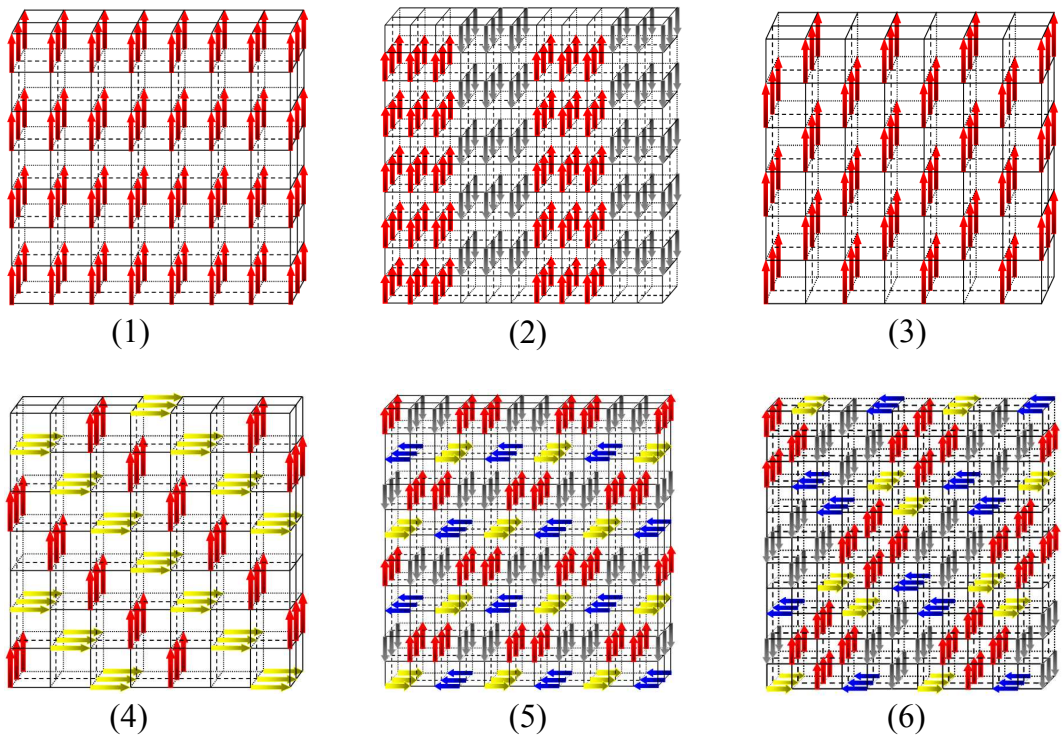

Figure 4.5: (Color on line) Ground-state dimer configurations of the type 1, 2, 3, 4, 5 and 6 as indicated in table 4.1 in the polarized case are shown ($J = 1$).

as follows: we consider a dimer and calculate its interaction energy E_1 with other dimers within r_c using Eqs. (4.1) and (4.2). We move this dimer to one of the links surrounding its two ends. There are such 10 links in the simple cubic lattice, but not all of them are "free" at the other end, namely unoccupied by another dimer. A random free link is chosen, and the new energy E_2 is calculated. If $E_2 \leq E_1$, the new position of the dimer is accepted, otherwise it is accepted with a probability $\exp[-(E_2 - E_1)/(k_B T)]$. We go next to another dimer and repeat the procedure until all dimers are visited, That is one MC step/dimer. A large number of steps has to be made to equilibrate the system and to average physical quantities. We use several millions of MC steps/dimer for equilibrating and for averaging. The averaged energy and the specific heat are defined by

$$\langle U \rangle = < \mathcal{H} + \mathcal{H}_d > \tag{4.9}$$

$$C_V = \frac{\langle U^2 \rangle - \langle U \rangle^2}{k_B T^2} \tag{4.10}$$

where $< ... >$ indicates the thermal average taken over several millions of microscopic states at T.

We define the order parameter Q by

$$Q = [q \max(Q_1, Q_2, Q_3) - 1]/(q - 1) \tag{4.11}$$

where Q_n is the spatial average defined by

$$Q_n = \sum_j \delta(\sigma_{ij} - n)/(L \times L \times L_z) \tag{4.12}$$

$n (n = 1, 2, 3)$ being the value attributed to denote the axis of the dimer σ_{ij} at the link (ij). The susceptibility is defined by

$$\chi = \frac{\langle Q^2 \rangle - \langle Q \rangle^2}{k_B T} \tag{4.13}$$

We run our program for a given lattice size at a temperature T. For each lattice size we choose the dimer concentration $p = n_d/N_d(\max)$ small enough to allow

the dimers to move on free links with increasing T. In the following, except when otherwise stated, we shall use $p = 5/6$.

A. Without dipolar interaction $D = 0$

We first show in Fig. 4.6 the energy per dimer $E \equiv < U > /n_d$ and the order parameter $M = < Q >$ versus T, for $(J = 1, D = 0)$. Several remarks are in order:
(i) At very low temperature ($T < 0.4$), the dimers are frozen in the GS configuration except for a few excited dimers.
(ii) For $0.45 < T < 0.95$, dimers are unfrozen (cf. peak of χ at $T \simeq 0.45$), they move to occupy free links in the empty lattice space but they remain orientationally ordered.
(iii) For $T > 0.95$, they are disordered both in their orientations and spatial positions. We find the feature of a second-order transition at $T = T_C \simeq 0.95$.

The above three phases can be called "frozen phase", "smectic phase" and "isotropic phase", as they are defined in section 4.1. We show the snapshots of these phases in Fig. 4.7. The upper part of the frozen phase is empty (not fully shown) and the lower part is compact, while the smectic phase is extended to all the lattice space with vacancies uniformly distributed. Note that the ordering is still that of the GS because the temperature shown ($T = 0.508$) is too close to the unfreezing point ($T = 0.45$).

In order to check the order of the transition, we have calculated the histogram shown in Fig. 4.8 for $D = 0$. One observes a Gaussian distribution in the this case which confirms the smooth second-order transition shown in Fig. 4.6.

B. With dipolar interaction $D \neq 0$

The energy and the order parameter in the case of $D = 0.6$ are shown in Fig. 4.9. The transition is discontinuous at $T \simeq 0.33$ to the disordered phase. Note that the system is unfrozen at $T > 0.12$. We show in Fig. 4.10 the snapshots of the frozen phase, smectic phase and the isotropic phase, similarly to the $D = 0$ case shown above. Note the shape of the empty space in the frozen phase. The "surface" separating occupied

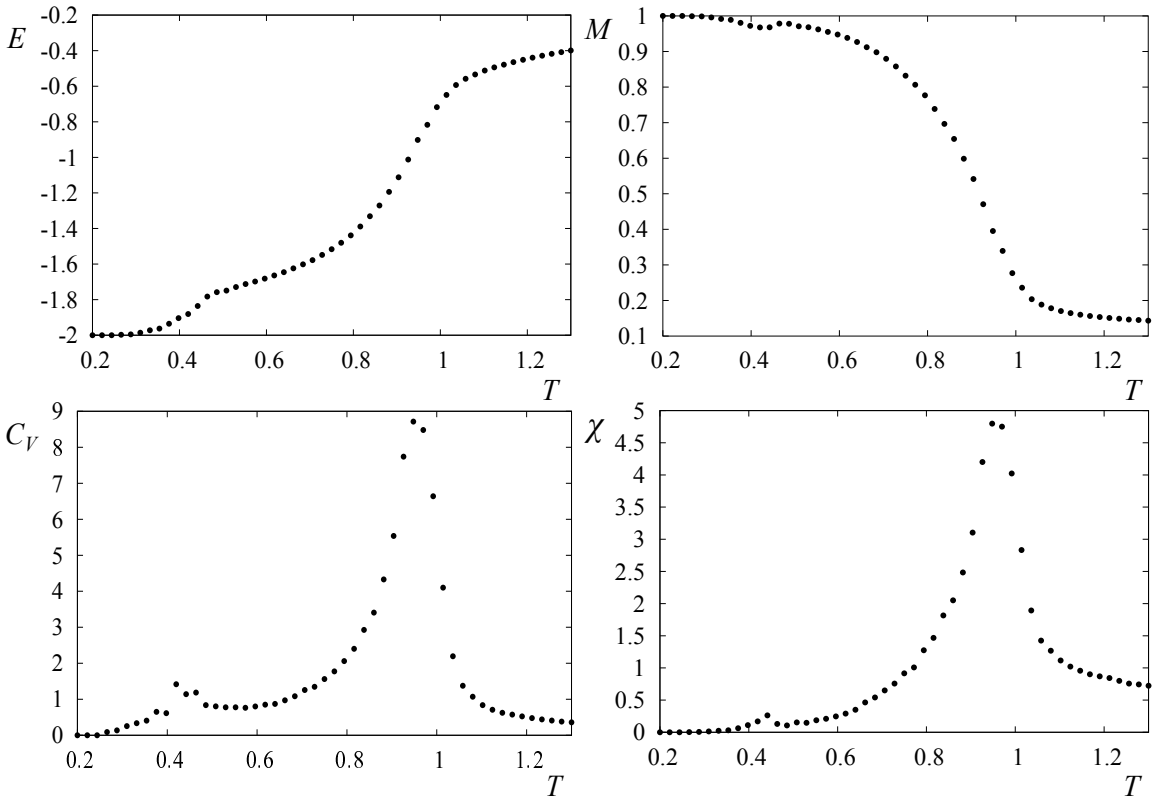

Figure 4.6: Energy per dimer E, order parameter $M =< Q >$, specific heat C_V and susceptibility χ versus temperature T in the case $D = 0$ ($J = 1$).

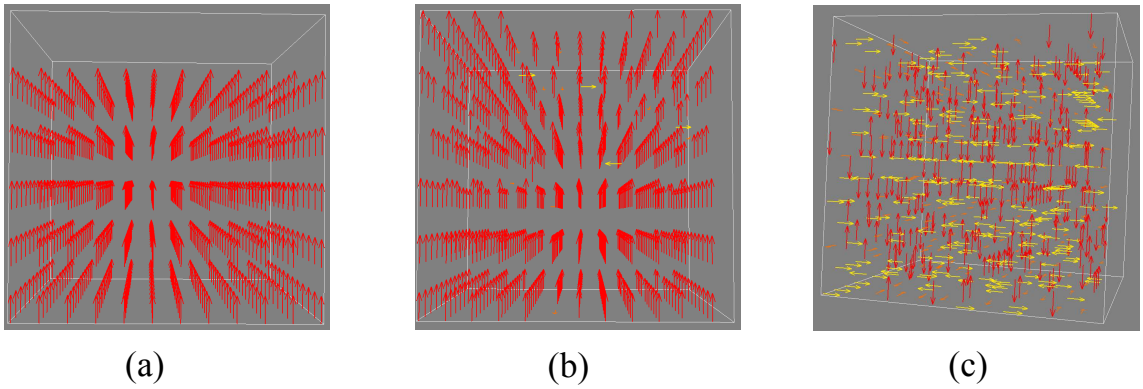

Figure 4.7: (Color on line) Snapshots of the dimer configuration for $D = 0$ at several temperatures (a) $T = 0$, ground state (b) $T = 0.508$, smectic phase (c) $T = 1.19$, disordered (isotropic) phase. See text for comments.

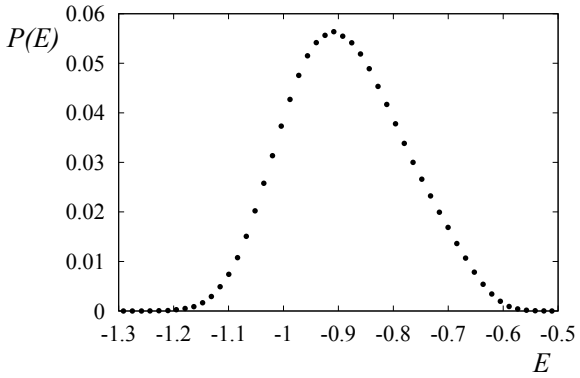

Figure 4.8: Energy histogram at the transition temperature in the case $D = 0$ ($J = 1$).

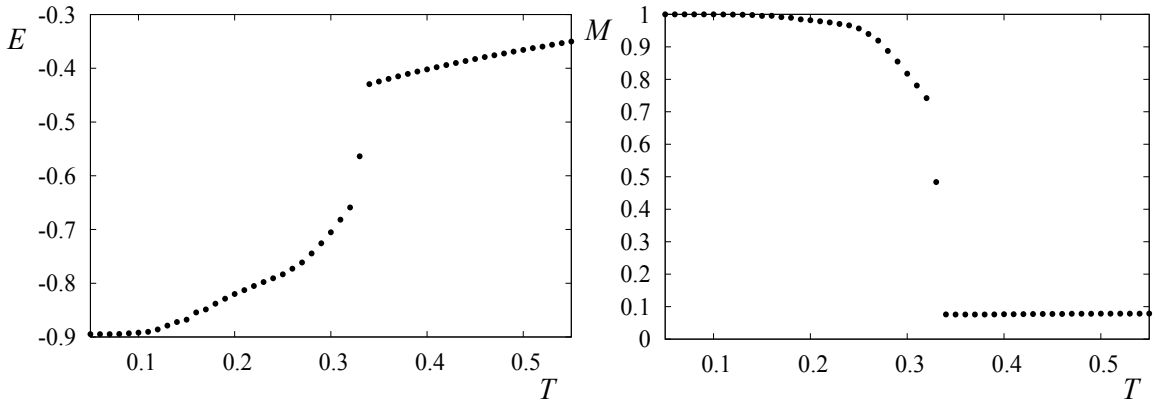

Figure 4.9: Energy per dimer E and order parameter $M =< Q >$ versus T are shown in the case $D = 0.6$ with $r_c = 2.3$ ($J = 1$).

and unoccupied parts is not flat as in the $D = 0$ case shown above. In the smectic phase, dimers move to this empty space: the dimers are uniformly distributed over the whole lattice. The empty space is thus broken into small vacancies.

The energy versus T for $D = 0.6$ and the energy histogram are shown in Fig. 4.11 for several values of r_c. One observes a discontinuous transition and a double-peak structure which is a signature of a first-order transition, for all r_c.

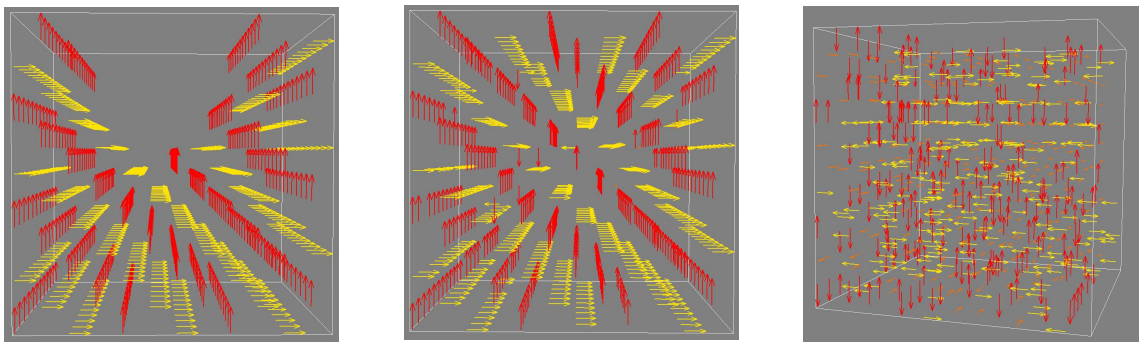

Figure 4.10: (Color on line) Snapshots of the dimer configuration for $D = 0.6$ at several temperatures (a) $T = 0$, ground state (b) $T = 0.17$, smectic phase (c) $T = 0.45$, disordered (isotropic) phase. $r_c = 2.3$, $J = 1$. See text for comments.

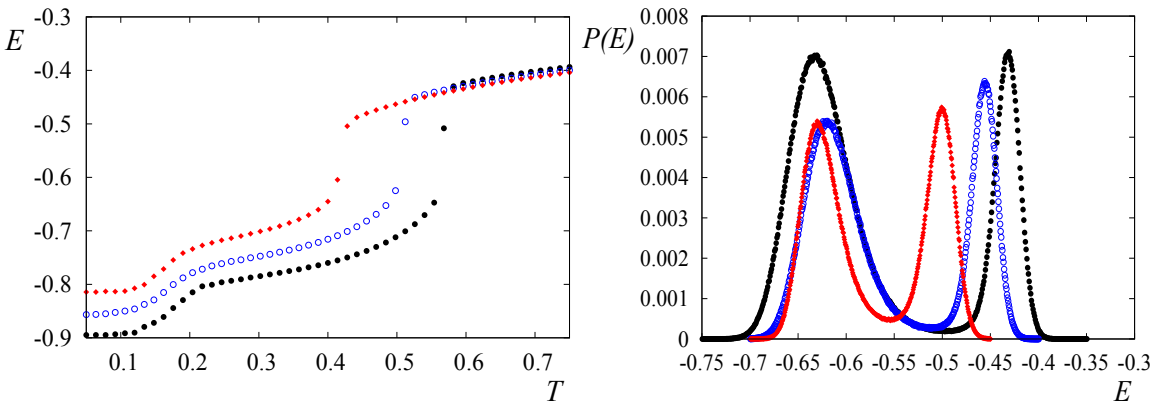

Figure 4.11: (Color on line) Energy versus T and energy histogram at the transition temperature for $D = 0.6$ with $r_c = 2.3$ (black circles), $r_c = 2.5$ (void blue circles) and $r_c = 3.2$ (red diamonds).

4.4 Non Polarized Dimers: Ground State and Phase Transition

The main difference between polarized and non polarized dimers resides in the fact that a polarized dimer has an additional internal degree of freedom which makes more abundantly the number of the GS and more excited states at finite temperature. As a consequence, the number of GS in the non polarized case is smaller, the GS configurations are simpler and the transition temperature is higher than in the polarized case.

4.4.1 Ground state

For non zero D, the results obtained from the steepest descent method are shown in table 4.2. The configurations 1 to 4 are shown in Fig. 4.12. Note that for $D = 0$, the GS is the uniform configuration of type 1, similar to that in the polarized case. We note the diagonal ordering of types 3 and 4.

4.4.2 Phase transition

For small D, the phase transition is of second order as shown in Fig. 4.13 for $D = 0.4$. Again here, we observe three successive phases with increasing temperature: the frozen phase ($T < 0.25$), smectic phase ($0.25 < T < 0.7$) and isotropic phase ($T > 0.7$).

For larger D, the transition becomes of first order. We show in Fig. 4.14 the energy and the order parameter versus temperature for several values of r_c. The transition is discontinuous.

Snapshots of these phases are shown in Fig. 4.15. Note that the unfreezing is not a phase transition, it is a gradual process in which the maximum of the specific

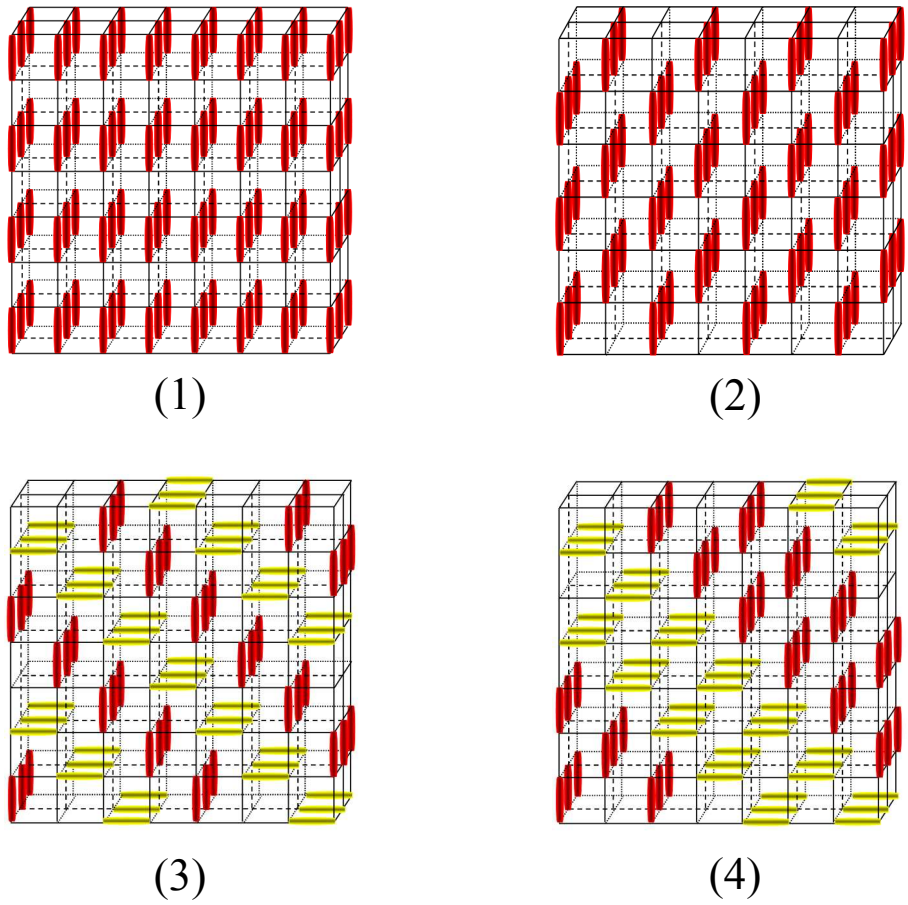

Figure 4.12: (Color on line) Non polarized dimers: Ground-state dimer configurations of the type 1, 2, 3 and 4 indicated in table 4.2 are shown ($J = 1$).

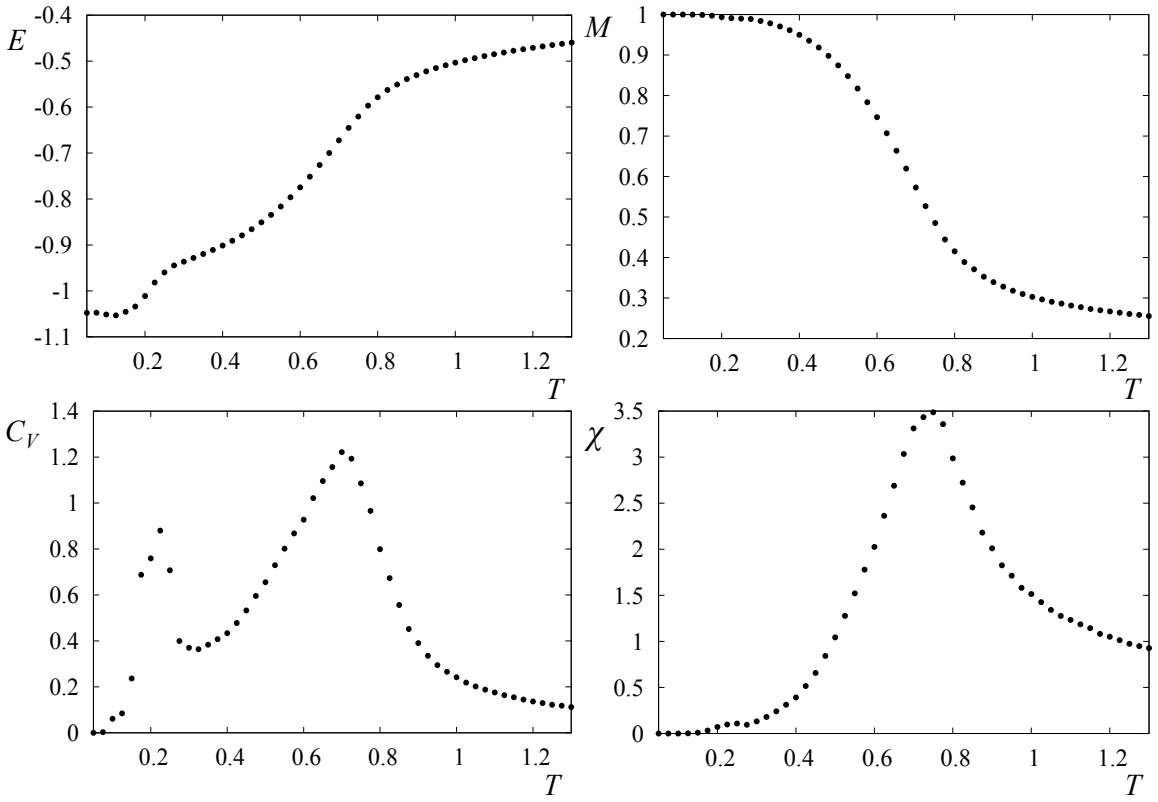

Figure 4.13: Non polarized dimers: Energy per dimer E, order parameter $M =< Q >$, specific heat C_V and susceptibility χ versus temperature T in the case $D = 0.4$ with $r_c = 2.5$ ($J = 1$).

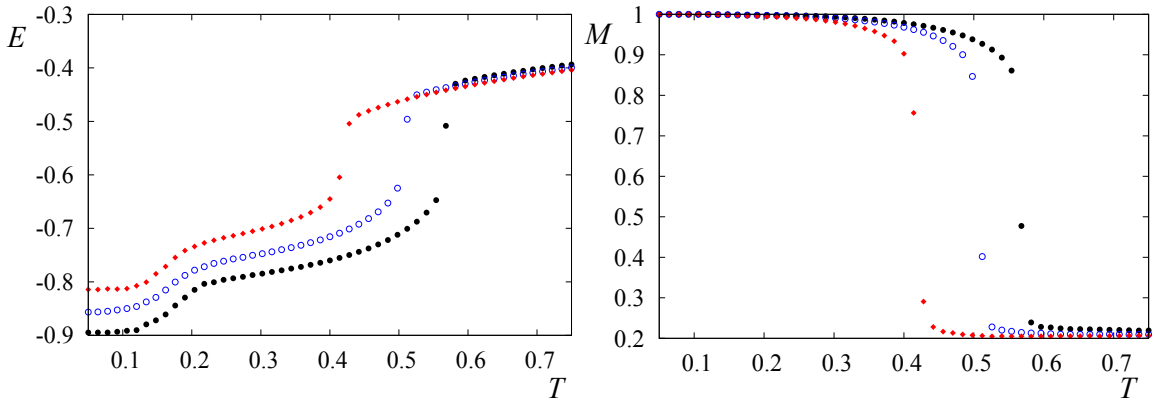

Figure 4.14: (Color on line) Non polarized dimers: Energy per dimer E and order parameter $M =< Q >$ versus T in the case $D = 0.6$ with several r_c: 2.3 (black solid circles), 2.5 (blue void circles), 2.8 (red diamonds), $J = 1$.

r_C \ D	0.30	0.40	0.45	0.48	0.50	0.60
1.5	1	1	1	1	3	3
1.8	1	1	1	2	2	2
2.3	1	1	1	2	2	2
2.5	1	1	1	2	2	2
2.8	1	1	1	2	2	2
3.2	1	1	2	2	2	2
3.6	1	1	4	4	4	4

Table 4.2: Non polarized dimers: Ground state configurations numbered from 1 to 4 obtained by the steepest-descent method in the space (D, r_c). These configurations are displayed in Fig. 4.12.

heat and the susceptibility as well as its unfreezing temperature do not depend on the lattice size, unlike in a true phase transition where these quantities depend on L.

Finally, we show the energy histograms at the respective transition temperatures in Fig. 4.16. The Gaussian energy histogram for $D = 0.4$ confirms the second-order transition while the double-peak structure for $D = 0.6$ clearly indicates the first-order nature.

4.5 Conclusion

We have studied in this chapter a model of dimers moving on the simple cubic lattice. The dimers interact with each other via the nearest-neighbor 3-state Potts model of strength J and a truncated long-range dipolar interaction with amplitude D and cutoff distance r_c. The numerical steepest descent method has been used to determine the GS dimer configuration and MC simulations have been carried out to determine

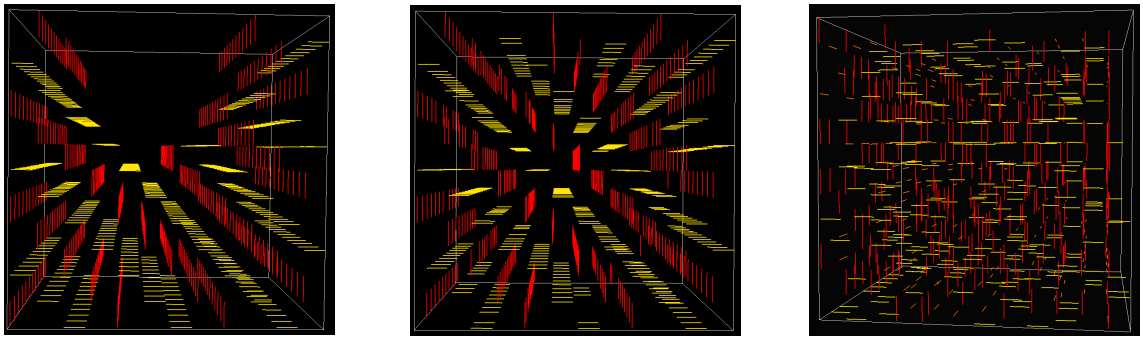

Figure 4.15: (Color on line) Non polarized dimers: Snapshots of the dimer configuration for $D = 0.6$ at several temperatures (a) $T = 0.05$, frozen phase (b) $T = 0.22$, liquid phase (c) $T = 0.70$, disordered phase. $r_c = 2.3$, $J = 1$. See text for comments.

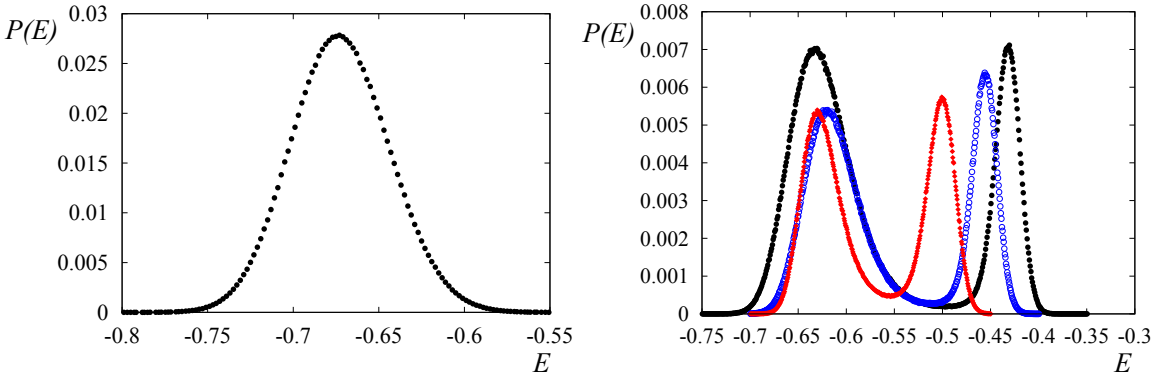

Figure 4.16: (Color on line) Non polarized dimers: Energy histogram for $D = 0.4$ (upper) and $D = 0.6$ (lower), at their respective transition temperatures, with ($J = 1$). For $D = 0.6$, several r_c have been used: 2.3 (black solid circles), 2.5 (blue void circles), 2.8 (red diamonds).

the ordered phase at finite temperature and the nature of the phase transition. We have found for both polarized and non polarized dimers complex GS configurations as functions of (D, r_c) (we took $J = 1$ as unit of energy). There exist three phases with increasing temperature: the frozen compact phase, the smectic phase and the isotropic phase. In the frozen phase, dimers occupy a portion of the lattice in the most compact manner. For small D, the GS is uniform and the surface separating the empty part is flat. For large D, the GS is non uniform, the surface separating the compact part from the empty one is a "parabolic hole". The passage from the frozen phase to the smectic phase is gradual (not a phase transition), however the change from the smectic phase to the isotropic phase is a true phase transition: it is of second order for small D and of first order for large D. What is important in the present study is the possibility to have a first-order transition with a dipolar interaction strong enough to yield a non uniform dimer configuration. Non uniform configurations result from the competition of the two terms in Eq. (4.2). We believe that other interactions which give rise to some frustration, or instability, of the dimer axes would cause a first-order smectic-isotropic transition.

General Conclusion

This thesis is devoted to the investigation of the phase transition and the spin transport in complex systems by stochastic numerical methods including the steepest-descent method, the standard MC method, and histogram MC techniques.

The three following questions have motivated the present work:
(i) the nature of the phase transition in frustrated spin systems,
(ii) the spin transport in spin systems, in particular in frustrated systems,
(iii) the effect of the long-range dipolar interaction in Potts model of molecular crystals and dimer liquids.

The first question comes naturally after a series of recent papers finding that several particular frustrated spin systems undergo a phase transition of first order. These important results put an end to controversial subjects which were lasting for more than 20 years. Among these systems we can mention the fully frustrated simple cubic lattice with Ising, XY and Heisenberg spins [90, 91, 92], the stacked triangular antiferromagnets with XY and Heisenberg spins [131, 18, 19]. At the beginning of this thesis we asked ourselves the question "do frustrated spin systems all undergo a transition of first order?". The answer was not obvious because of the lack of a general theory allowing to conclude. All systems studied so far were particular cases with several different methods. So we started to study several other frustrated systems with large-scale MC simulations as shown in this thesis: the $J_1 - J_2$ model and the HCP lattice. We found indeed a first-order transition in these systems. Although a definite general conclusion cannot be made for all frustrated systems, we believe that all of them have a first-order transition. Our contribution to this question is thus important for the construction of a future general theory.

The second subject concerns the spin transport in magnetic materials. It was amazing that there was very few theories on this question such as the first work by de Gennes and Friedel in 1958 [56] and a few subsequent works by Fisher-Langer [45] and Kataoka [46], among some others. There was surprisingly an absence of Monte Carlo

works on the literature when our group began to study this subject in 2008. From that time, there has been a great and increasing number of experiments on spin resistivity as mentioned in chapter 2, due to numerous applications of magnetic materials in spintronics. Needless to say, there was an urgent matter to carry out Monte Carlo investigations on this subject. Our work in this thesis improves the first results of the group by improving the averaging method and taking into account the effect of temperature-dependence of the relaxation time. A "tour de force" was achieved with the calculation of the spin resistivity in MnTe where an excellent agreement with experiments was obtained [132]. The method we have elaborated for the spin transport can be applied to other dynamic systems.

The third subject we have studied in this thesis stems from the question of the nature of phase transition in molecular crystals and liquid crystals. In these systems, interactions between molecules are weak but may be of long-range character. Many theoretical and numerical works have been done in this area. Our purpose here was to try to search for the origin of layered structures observed in experiments and the nature of the ordering at low temperatures as well as of the phase transition. To model these systems, we used the Potts model with a short-range exchange interaction and a long-range dipolar interaction. The dipolar interaction has been used since a long time ago in theories and in simulations. Often, the long-range sum was treated by using the Ewald's sum [133] which consists in writing the sum in two sums: the short-range real-space sum and the long-range sum in reciprocal space. The necessity to perform the second sum is to choose a central unit and make its translation in the whole space. In spin systems, this choice is not obvious because close to the phase transition, magnetic ordering is no more periodic. A choice of a periodic unit can alter the nature of the phase transition. We have chosen a truncated cutoff distance for the dipolar interaction in real space, and we looked for the effect of this cutoff on physical quantities. This is certainly far from a perfect treatment but we are convinced that many aspects found here remain in a better method. Anyway, results of short-range interaction in models of statistical physics allow to understand experimental systems which are not always of short-range interaction. Results of our study show indeed

layered structures and regions of first-order transition in the phase space. One of the striking results is the re-orientation transition observed in thin films.

To close the present dissertation, let us emphasize that what has been done in this work paves a way for future studies not only for elaborating better simulation methods but also for better modeling physical systems studied here.

Abstract

In this thesis, we have used Monte Carlo simulations combined with different efficient techniques such as histogram methods to study the phase transitions and spin transport in various systems. The first part is devoted to the investigation of phase transition in frustrated spin systems:
(i) the $J_1 - J_2$ model with Ising spin in the full antiferromagnetic regime.
(ii) the HCP lattice with both Ising and XY spin in the full antiferromagnetic regime. The results obtained show indeed a first-order transition as found earlier in other frustrated systems. The second part shows the ground state and phase transitions in molecular crystals and in dimer liquids. To deal with these systems, we have used the Potts model taking into the account the dipolar interaction to explain long-period layered structures experimentally observed. The results show amazing effects of this long-range interaction. The effect of surface exchange interaction has been considered in this work. Finally, we describe the resistivity of itinerant spins. We focused in particular on the effects of spin fluctuations in the phase transition region. Interesting results have been obtained showing a strong correlation between spin fluctuations and the behavior of the resistivity.

Résumé

Dans la thèse, nous avons utilisé des simulations de Monte Carlo combinées avec différentes techniques efficaces tels que les méthodes d'histogramme pour étudier les transitions de phase et transport des spins dans différents systèmes. La première partie est consacrée à l'étude des transition de phase dans les systèmes de spins frustrés:
(i) le modèle $J_1 - J_2$ avec des spins Ising dans le régime antiferromagnétique complet.
(ii) le modèle HCP avec des spins Ising et des spins XY dans le régime antiferromagnétique complet.
Les résultats obtenus montrent en effet une transition du premier ordre que l'on

trouve plus tôt dans d'autres systèmes frustrés. La deuxième partie montre les état fondamental et transitions de phase dans les cristaux moléculaires et dans les liquides de dimères. Pour faire face à ces systèmes, nous avons utilisé le modèle de Potts en tenant compte de l'interaction dipolaire pour expliquer structures périoques en couches observées expérimentalement. Les résultats montrent des effets étonnants de cette interaction à longue portée. L'effet de l'interaction d'échange de surface a été pris en compte dans ce travail. Finalement, nous avons calculé la résistivité des spins itinérants. Nous nous sommes concentrés en particulier sur les effets des fluctuations de spin dans la région de transition de phase. Des résultats intéressants ont été obtenus montrant une forte corrélation entre les fluctuations de spin et le comportement de la résistivité.

List of Publications

The results obtained in this thesis have been partially published or submitted for publication in the following journals:

1. Danh-Tai Hoang and H. T. Diep,
   Hexagonal-Close-Packed Lattice: Ground State and Phase Transition,
   Phys. Rev. E. **85**, 041107, 2012.

2. Danh-Tai Hoang, Yann Magnin and H. T. Diep,
   Spin Resistivity in the Frustrated $J_1 - J_2$ Model,
   Mod. Phys. Lett. B. **25**, 937-945, 2011.

3. Yann Magnin, Danh-Tai Hoang and H. T. Diep,
   Spin Transport in Magnetically Ordered Systems: Effect of the Lattice Relaxation Time,
   Mod. Phys. Lett. B. **25**, 1029-1040, 2011.

4. H. T. Diep, Yann Magnin and Danh-Tai Hoang,
   Spin Resistivity in Magnetic Materials,
   Acta Physica Polonica A, **121**, 985-991, 2012.

5. Danh-Tai Hoang and H. T. Diep,
   Effect of Dipolar Interaction in Molecular Crystals,
   J. Phys.: Condens. Matter., **24**, 415402, 2012.

6. Danh-Tai Hoang, Maciej Kasperski, Henryk Puszkarski and H. T. Diep,
   Re-orientation Transition in Molecular Thin Films: Potts Model with Dipolar Interaction,
   J. Phys.: Condens. Matter., Accepted for publication, 2012. arXiv:1209.0114v1

7. Danh-Tai Hoang and H. T. Diep,
   Phase Transition in Dimer Liquids,
   In preparation.

Bibliography

[1] C. L. Lu, X. Chen, S. Dong, K. F. Wang, H. L. Cai, J.-M. Liu, D. Li, and Z. D. Zhang. Ru-doping-induced ferromagnetism in charge-ordered La0.4Ca0.6MnO3. *Phys. Rev. B*, 79:245105, Jun 2009.

[2] Juan Du, Da Li, Yao Biao Li, Nai Kun Sun, Ji Li, and Zhi Dong Zhang. Abnormal magnetoresistance in ϵ-(Mn1-xFex)3.25Ge antiferromagnets. *Phys. Rev. B*, 76:094401–094405, Sep 2007.

[3] Michael McGuire, Andrew Christianson, Athena Sefat, Brian Sales, Mark Lumsden, Rongying Jin, E. Payzant, David Mandrus, Yanbing Luan, Veerle Keppens, Vijayalaksmi Varadarajan, Joseph Brill, Raphaël Hermann, Moulay Sougrati, Fernande Grandjean, and Gary Long. Phase transitions in LaFeAsO: Structural, magnetic, elastic, and transport properties, heat capacity and Mössbauer spectra. *Physical Review B*, 78(9):1–10, September 2008.

[4] S Chandra, Lk Malhotra, S Dhara, and Ac Rastogi. Low-temperature dynamic susceptibility of thin Cd1-xMnxTe films. *Physical review. B, Condensed matter*, 54(19):13694–13704, November 1996.

[5] Tiffany S. Santos, Steven J. May, J. L. Robertson, and Anand Bhattacharya. Tuning between the metallic antiferromagnetic and ferromagnetic phases of La1-xSrxMnO3 near x=0.5 by digital synthesis. *Phys. Rev. B*, 80:155114–155120, Oct 2009.

[6] Shun Wang, LiDong Pan, R. Pindak, Z. Q. Liu, H. T. Nguyen, and C. C.

Huang. Discovery of a Novel Smectic-C^* Liquid-Crystal Phase with Six-Layer Periodicity. *Phys. Rev. Lett.*, 104:027801, Jan 2010.

[7] P. M. Johnson, D. A. Olson, S. Pankratz, T. Nguyen, J. Goodby, M. Hird, and C. C. Huang. Structure of the Liquid-Crystal Ferrielectric Phases as Determined by Ellipsometry. *Phys. Rev. Lett.*, 84:4870–4873, May 2000.

[8] P. Mach, R. Pindak, A.-M. Levelut, P. Barois, H. T. Nguyen, C. C. Huang, and L. Furenlid. Structural Characterization of Various Chiral Smectic- C Phases by Resonant X-Ray Scattering. *Phys. Rev. Lett.*, 81:1015–1018, Aug 1998.

[9] J. Leblond P. Papon and P. Meijer. *Physique des transitions de phases*. Academic Press, London, 1972.

[10] J. M. Yeomans. *Statistical Mechanics of Phase Transitions*. Clarendon Press, Oxford, 1992.

[11] C. Domb and M. S. Green. *Phase Transitions and Critical Phenomena*. Dunod, Paris, 1999.

[12] Kenneth G. Wilson. Renormalization Group and Critical Phenomena. I. Renormalization Group and the Kadanoff Scaling Picture. *Phys. Rev. B*, 4:3174–3183, Nov 1971.

[13] J. Zinn-Justin. *Quantum field theory and critical phenomena*. International series of monographs on physics. Clarendon Press, 2002.

[14] M. E. J. Newman and G. T. Barkema. *Monte Carlo Methods in Statistical Physics*. OXFORD University press, 2001.

[15] D.P. Landau and K. Binder. *A guide to Monte Carlo in Statistical Physics*. Cambridge University press, 2009.

[16] M. Ferrario, G. Ciccotti and K. Binder (Eds). *Computer Simulations in Condensed Matter Systems: From Materials to Chemical Biology*. Springer, Berlin Heidelberg, 2006.

[17] H. T. Diep. *Frustrated spin systems*. World Scientific Pub Co Inc, 2005.

[18] V. Thanh Ngo and H. T. Diep. Stacked triangular XY antiferromagnets: End of a controversial issue on the phase transition. *J. Appl. Phys*, 103:07C712, 2008.

[19] V. Thanh Ngo and H. T. Diep. Phase transition in Heisenberg stacked triangular antiferromagnets: End of a controversy. *Phys. Rev. E*, 78:031119, Sep 2008.

[20] A. Zangwill. *Physics at Surfaces*. Cambridge University Press, 1988.

[21] J.A.C. Bland and B. Heinrich. *Ultrathin Magnetic Structures*, volume I and II. Springer, London, 1994.

[22] Martin J. Klein and Robert S. Smith. Thin Ferromagnetic Films. *Phys. Rev.*, 81:378–380, Feb 1951.

[23] E. C. Crittenden and R. W. Hoffman. Thin Films of Ferromagnetic Materials. *Rev. Mod. Phys.*, 25:310–315, Jan 1953.

[24] J. C. S. Levy and Diep-The-Hung. Magnetic structures in thin films. *Phys. Rev. B*, 18:3593–3599, Oct 1978.

[25] X.T. Pham Phu, V. Thanh Ngo, and H.T. Diep. Critical behavior of magnetic thin films. *Surface Science*, 603(1):109–116, 2009.

[26] V. Thanh Ngo and H. T. Diep. Effects of frustrated surface in heisenberg thin films. *Phys. Rev. B*, 75:035412, Jan 2007.

[27] Alan M. Ferrenberg and Robert H. Swendsen. New Monte Carlo technique for studying phase transitions. *Phys. Rev. Lett.*, 61:2635–2638, Dec 1988.

[28] Alan M. Ferrenberg and Robert H. Swendsen. Optimized Monte Carlo data analysis. *Phys. Rev. Lett.*, 63:1195–1198, Sep 1989.

[29] Alan M. Ferrenberg and D. P. Landau. Critical behavior of the three-dimensional Ising model: A high-resolution Monte Carlo study. *Phys. Rev. B*, 44:5081–5091, Sep 1991.

[30] P. Grünberg, R. Schreiber, Y. Pang, M. B. Brodsky, and H. Sowers. Layered Magnetic Structures: Evidence for Antiferromagnetic Coupling of Fe Layers across Cr Interlayers. *Phys. Rev. Lett.*, 57(19):2442–2445, Nov 1986.

[31] MN Baibich, JM Broto, A Fert, and FN Van Dau. Giant magnetoresistance of (001) Fe/(001) Cr magnetic superlattices. *Physical Review Letters*, 61(001):2472–2475, 1988.

[32] H. Ehrenreich and F. Spaepen. *Solid state physics*, volume 56. Academic Pr, 2001.

[33] A. Barthélémy, A. Fert, J-P. Contour, M. Bowen, V. Cros, J. M. De Teresa, A. Hamzic, J. C. Faini, J. M. George, J. Grollier, F. Montaigne, F. Pailloux, F. Petroff, and C. Vouille. Magnetoresistance and spin electronics. *Journal of Magnetism and Magnetic Materials*, 242-245(Part 1):68–76, 2002.

[34] A. Fert and I. A. Campbell. Two-Current Conduction in Nickel. *Phys. Rev. Lett.*, 21(16):1190–1192, Oct 1968.

[35] I. A. Campbell. Hall Effect and Resistivity Anisotropy in Ni Alloys. *Phys. Rev. Lett.*, 24(6):269–271, Feb 1970.

[36] F. C. Schwerer and L. J. Cuddy. Spin-Disorder Scattering in Iron- and Nickel-Base Alloys. *Phys. Rev. B*, 2:1575–1587, Sep 1970.

[37] Alla E. Petrova, E. D. Bauer, Vladimir Krasnorussky, and Sergei M. Stishov. Behavior of the electrical resistivity of MnSi at the ferromagnetic phase transition. *Phys. Rev. B*, 74:092401–092404, Sep 2006.

[38] S. Stishov, a. Petrova, S. Khasanov, G. Panova, a. Shikov, J. Lashley, D. Wu, and T. Lograsso. Magnetic phase transition in the itinerant helimagnet MnSi: Thermodynamic and transport properties. *Physical Review B*, 76(5):4–7, August 2007.

[39] F. Matsukura, H. Ohno, A. Shen, and Y. Sugawara. Transport properties and origin of ferromagnetism in (Ga,Mn)As. *Phys. Rev. B*, 57:R2037–R2040, Jan 1998.

[40] T. Kasuya. Electrical resistance of ferromagnetic metals. *Progress of Theoretical Physics*, 16:58–63, 1956.

[41] Y. B. Li, Y. Q. Zhang, N. K. Sun, Q. Zhang, D. Li, J. Li, and Z. D. Zhang. Ferromagnetic semiconducting behavior of Mn(1-x)CrxTe compounds. *Phys. Rev. B*, 72:193308, Nov 2005.

[42] Jing Xia, W. Siemons, G. Koster, M. R. Beasley, and A. Kapitulnik. Critical thickness for itinerant ferromagnetism in ultrathin films of of SrRuO3. *Phys. Rev. B*, 79:140407–140410, Apr 2009.

[43] X. F. Wang, T. Wu, G. Wu, H. Chen, Y. L. Xie, J. J. Ying, Y. J. Yan, R. H. Liu, and X. H. Chen. Superconductivity at 41 K and Its Competition with Spin-Density-Wave Instability in Layered CeO(1-x)FxFeAs. *Phys. Rev. Lett.*, 102:117005–117008, Mar 2009.

[44] Y. Q. Zhang, Z. D. Zhang, and J. Aarts. Charge-order melting and magnetic phase separation in thin films of Pr0.7Ca0.3MnO3. *Phys. Rev. B*, 79:224422–224426, Jun 2009.

[45] Michael E. Fisher and J. S. Langer. Resistive Anomalies at Magnetic Critical Points. *Phys. Rev. Lett.*, 20:665–668, Mar 1968.

[46] Mitsuo Kataoka. Resistivity and magnetoresistance of ferromagnetic metals with localized spins. *Phys. Rev. B*, 63:134435, Mar 2001.

[47] C. Haas. Spin-Disorder Scattering and Magnetoresistance of Magnetic Semiconductors. *Phys. Rev.*, 168:531–538, Apr 1968.

[48] Nicholas Metropolis and S. Ulam. The Monte Carlo Method. *Journal of the American Statistical Association*, 44:335–341, Sep 1949.

[49] Nicholas Metropolis, Arianna W. Rosenbluth, Marshall N. Rosenbluth, Augusta H. Teller, and Edward Teller. Equation of State Calculations by Fast Computing Machines. *Journal of Chemical Physics*, 21:1087–1092, 1953.

[50] M. E. Fisher. *Critical Phenomena (edited by M. S. Green)*, chapter Theory of critical point singularities. Academic Press, New York, 1971.

[51] Michael E. Fisher and Michael N. Barber. Scaling Theory for Finite-Size Effects in the Critical Region. *Phys. Rev. Lett.*, 28:1516–1519, Jun 1972.

[52] V. Privman. *Finite Size Scaling and Numerical Simulation of Statistical Systems*. World Scientific, 1990.

[53] H. T. Diep. *Physique de la matière condensée*. Dunod, paris edition, 2003.

[54] T. Kasuya. Effects of sd interaction on transport phenomena. *Progress of theoretical physics*, 22(2):227–246, 1959.

[55] C. Kittel and P. McEuen. *Introduction to solid state physics*, volume 119. Wiley New York, 1996.

[56] P. G. De Gennes and J. Friedel. Anomalies de résistivité dans certains métaux magniques. *Journal of Physics and Chemistry of Solids*, 4(1-2):71–77, 1958.

[57] C. P. Moca G. Zarand and B. Janko. Scaling Theory of Magnetoresistance in Disordered Local Moment Ferromagnets. *Phys. Rev. Lett.*, 94:247202, Jun 2005.

[58] G. Alvarez and E. Dagotto. Single-band model for diluted magnetic semiconductors: Dynamical and transport properties and relevance of clustered states. *Phys. Rev. B*, 68:045202, Jul 2003.

[59] Şen, Cengiz and Alvarez, Gonzalo and Aliaga, Horacio and Dagotto, Elbio. Colossal magnetoresistance observed in Monte Carlo simulations of the one- and two-orbital models for manganites. *Phys. Rev. B*, 73:224441, Jun 2006.

[60] K. Akabli and H. T. Diep and S. Reynal. Spin transport in magnetic multilayers. *Journal of Physics: Condensed Matter*, 19(35):356204, 2007.

[61] K. Akabli and H. T. Diep. Effects of ferromagnetic ordering and phase transition on the resistivity of spin current. *J. Appl. Phys.*, 103(07F307), 2008.

[62] K. Akabli and H. T. Diep. Temperature dependence of the spin resistivity in ferromagnetic thin films: Monte Carlo simulations. *Phys. Rev. B*, 77:165433, Apr 2008.

[63] P. C. Hohenberg and B. I. Halperin. Theory of dynamic critical phenomena. *Rev. Mod. Phys.*, 49:435–479, Jul 1977.

[64] Yann Magnin, Danh-Tai Hoang, and H. T. Diep. Spin Transport in Magnetically Ordered Systems: Effect of the Lattice Relaxation Time. *Modern Physics Letters B*, 25(12n13):1029, 2011.

[65] Y. Magnin and H. T. Diep. Monte Carlo Study of Magnetic Resistivity in Semiconducting MnTe. *arXiv:1111.1507v1 [cond-mat.mtrl-sci]*, 2011.

[66] K. Akabli, Y. Magnin, Masataka Oko, Isao Harada, and H. T. Diep. Theory and simulation of spin transport in antiferromagnetic semiconductors: Application to MnTe. *Phys. Rev. B*, 84:024428, Jul 2011.

[67] Y. Magnin, K. Akabli, H.T. Diep, and I. Harada. Monte Carlo study of the spin transport in magnetic materials. *Computational Materials Science*, 49(4):S204–S209, October 2010.

[68] Y. Magnin, K. Akabli, and H. Diep. Spin resistivity in frustrated antiferromagnets. *Physical Review B*, 83(14):1–9, April 2011.

[69] Danh-Tai Hoang, Yann Magnin, and H. T. Diep. Spin Resistivity in the Frustrated J1 - J2 Model. *Modern Physics Letters B*, 25(12n13):937, 2011.

[70] Vladimir V. Prudnikov, Pavel V. Prudnikov, Aleksandr S. Krinitsyn, Andrei N. Vakilov, Evgenii A. Pospelov, and Mikhail V. Rychkov. Short-time dynamics and critical behavior of the three-dimensional site-diluted Ising model. *Phys. Rev. E*, 81:011130, Jan 2010.

[71] G. H. Wannier. Antiferromagnetism. The Triangular Ising Net. *Phys. Rev.*, 79:357–364, Jul 1950.

[72] T. A. Kaplan. Classical Spin-Configuration Stability in the Presence of Competing Exchange Forces. *Phys. Rev.*, 116:888–889, Nov 1959.

[73] Akio Yoshimori. A New Type of Antiferromagnetic Structure in the Rutile Type Crystal. *Journal of the Physical Society of Japan*, 14(6):807–821, 1959.

[74] J. Villain. La structure des substances magnetiques. *Journal of Physics and Chemistry of Solids*, 11(3–4):303–309, 1959.

[75] R. J. Elliott. Phenomenological Discussion of Magnetic Ordering in the Heavy Rare-Earth Metals. *Phys. Rev.*, 124:346–353, Oct 1961.

[76] G. Toulouse. Theory of the frustration effect in spin glasses. *Commun. Phys*, 2:115–119, 1977.

[77] H. T. Diep and H. Giacomini. *Fustrated spin systems (edited by H. T. Diep)*, chapter Frustration - Exactly solved frustrated models. World Scientific Pub Co Inc, 2005.

[78] R. Liebmann. *Statistical mechanics of periodic frustrated Ising systems*. Lecture notes in physics. Springer-Verlag, 1986.

[79] H. T. Diep, M. Debauche, and H. Giacomini. Exact solution of an anisotropic centered honeycomb Ising lattice: Reentrance and partial disorder. *Phys. Rev. B*, 43:8759–8762, Apr 1991.

[80] R. J. Baxter. *Exactly Solved Models in Statistical Mechanics*. Dover Books on Physics Series. Dover Publications, 2008.

[81] D. J. Amit. *Field theory, the renormalization group, and critical phenomena*. World Scientific, 1984.

[82] D. Mouhanna B. Delamotte and M. Tissier. *Fustrated spin systems (edited by H. T. Diep)*, chapter Renormalization Group Approaches to Frustrated Magnets in D=3. World Scientific Pub Co Inc, 2005.

[83] Mitsuhiro Itakura. Monte Carlo Renormalization Group Study of the Heisenberg and the XY Antiferromagnet on the Stacked Triangular Lattice and the Chiral ϕ^4 Model. *Journal of the Physical Society of Japan*, 72(1):74–82, 2003.

[84] S. Bekhechi, B. W. Southern, A. Peles, and D. Mouhanna. Short-time dynamics of a family of XY noncollinear magnets. *Phys. Rev. E*, 74:016109, Jul 2006.

[85] Ditza Auerbach, Eytan Domany, and James E. Gubernatis. Anisotropic Ising model on the hexagonal-close-packed lattice. *Phys. Rev. B*, 37:1719–1732, Feb 1988.

[86] H. T. Diep. First-order transition in the hexagonal-close-packed lattice with vector spins. *Phys. Rev. B*, 45:2863–2867, Feb 1992.

[87] B. E. Larson. Ground states of HCP vector antiferromagnets: Zn1xMnxSe. *J. Appl. Phys.*, 67:5240–5242, May 1990.

[88] H. T. Diep and H. Kawamura. First-order phase transition in the FCC Heisenberg antiferromagnet. *Phys. Rev. B*, 40:7019–7022, Oct 1989.

[89] Daniel Blankschtein, M. Ma, and A. Nihat Berker. Fully and partially frustrated simple-cubic Ising models: Landau-Ginzburg-Wilson theory. *Phys. Rev. B*, 30:1362–1365, Aug 1984.

[90] V. Thanh Ngo, D. Tien Hoang, and H. T. Diep. First-order transition in the XY model on a fully frustrated simple cubic lattice. *Phys. Rev. E*, 82:041123, Oct 2010.

[91] V. Thanh Ngo, D. Tien Hoang and H. T. Diep. Phase Transition In The Heisenberg Fully-Frustrated Simple Cubic Lattice. *Modern Physics Letters B*, 25(12n13):929, 2011.

[92] V. Thanh Ngo and D. Tien Hoang and H. T. Diep. Flat energy-histogram simulation of the phase transition in an Ising fully frustrated lattice. *Journal of Physics: Condensed Matter*, 23(22):226002, 2011.

[93] H. T. Diep. Magnetic transitions in helimagnets. *Phys. Rev. B*, 39:397–404, Jan 1989.

[94] S. Chandrasekhar. *Liquid Crystals*. Cambridge University Press, 1992.

[95] L. S. Hirst and S. J. Watson. Interlayer structures of the chiral smectic liquid crystal phases revealed by resonant x-ray scattering. *Phys. Rev. E*, 65:041705, Apr 2002.

[96] M. Cepic and B. Zeks. Flexoelectricity and Piezoelectricity: The Reason for the Rich Variety of Phases in Antiferroelectric Smectic Liquid Crystals. *Phys. Rev. Lett.*, 87:085501, Jul 2001.

[97] D. A. Olson, X. F. Han, A. Cady, and C. C. Huang. Molecular orientation arrangements in the smectic-C^* variant liquid-crystal phases. *Phys. Rev. E*, 66:021702, Aug 2002.

[98] P. V. Dolganov, V. M. Zhilin, V. K. Dolganov, and E. I. Kats. Structures and phase transitions in polar smectic liquid crystals. *Phys. Rev. E*, 67:041716, Apr 2003.

[99] A. V. Emelyanenko and M. A. Osipov. Theoretical model for the discrete flexoelectric effect and a description for the sequence of intermediate smectic phases with increasing periodicity. *Phys. Rev. E*, 68:051703, Nov 2003.

[100] Fernandes, P., Barois, P., Grelet, E., Nallet, F., Goodby, J. W., Hird, M., and Micha, J. -S. Extension of the resonant scattering technique to liquid crystals without resonant element. *Eur. Phys. J. E*, 20(1):81–87, May 2006.

[101] P. V. Dolganov, V. M. Zhilin, V. K. Dolganov, and E. I. Kats. Ferrielectric smectic phase with a layer-by-layer change of the two-component order parameter. *JETP Letters*, 87:253–257, 2008. 10.1134/S0021364008050068.

[102] P. V. Dolganov, V. M. Zhilin, V. K. Dolganov, and E. I. Kats. Commensurate polar smectic structures with a two-component order parameter. *Phys. Rev. E*, 82:040701, Oct 2010.

[103] M. B. Hamaneh and P. L. Taylor. Long-Range Interlayer Interactions in Ferroelectric Liquid Crystals. *Phys. Rev. Lett.*, 93:167801, Oct 2004.

[104] M. B. Hamaneh and P. L. Taylor. Phase sequences and long-range interactions in ferroelectric liquid crystals. *Phys. Rev. E*, 72:021706, Aug 2005.

[105] H. W. DIEHL. The Theory of Boundary Critical Phenomena. *Int. J. Mod. Phys. B*, 11:3503, 1997.

[106] Mermin, N. D. and Wagner, H. Absence of Ferromagnetism or Antiferromagnetism in One- or Two-Dimensional Isotropic Heisenberg Models. *Phys. Rev. Lett.*, 17:1133–1136, Nov 1966.

[107] H. Puszkarski. Quantum Theory of Spin Wave Resonance in Thin Ferromagnetic Films. Part I. *Acta Physica Polonica A*, 38:217–238, 1970.

[108] H. Puszkarski. Quantum Theory of Spin Wave Resonance in Thin Ferromagnetic Films. Part II. *Acta Physica Polonica A*, 38:899–914, 1970.

[109] Diep-The-Hung, J. C. S. LEVY and O. NAGAI. Effect of surface spin-waves and surface anisotropy in magnetic thin films at finite temperature. *Physics Status Solidi (b)*, 93:351, 1979.

[110] Diep-The-Hung. Temperature-dependent surface magnetisation and critical temperature of ferromagnetic thin films. *Physics Status Solidi (b)*, 103:809, 1981.

[111] H. Puszkarski, M. Krawczyk and H. T. Diep. Dipolar Surface Pinning and Spin-Wave Modes vs. Lateral Surface Dimensions in Thin Films. *Surface Science*, 602:2197–2205, 2008.

[112] C. Santamaria and H. T. Diep. Dipolar interaction in magnetic thin films : perpendicular to in-plane ordering transition. *J. Magnetism and Mag. Mater.*, 212:23–28, 2000.

[113] M. Debauche, H. T. Diep, P. Azaria, and H. Giacomini. Exact phase diagram of a generalized Kagomé Ising lattice: Reentrance and disorder lines. *Phys. Rev. B*, 44:2369–2372, Aug 1991.

[114] P. J. Collings. *Liquid crystals: nature's delicate phase of matter*. Princeton University Press, 2002.

[115] Judit Quintans Carou. *Flow of a nematic liquid crystal*. PhD thesis, University of Strathclyde, 2007.

[116] Friedrich Reinitzer. Beiträge zur Kenntniss des Cholesterins. *Monatshefte für Chemie / Chemical Monthly*, 9:421–441, 1888.

[117] G. Friedel. Les états mésomorphes de la matiere. *Ann. Phys.*, 18:273–474, 1922.

[118] P. G. de Gennes and J. Prost. *The Physics of Liquid Crystals*. Clarendon Press, Oxford, 1993.

[119] Yves Galerne and Lionel Liebert. Smectic- O films. *Phys. Rev. Lett.*, 64:906–909, Feb 1990.

[120] P. Mach, R. Pindak, A.-M. Levelut, P. Barois, H. T. Nguyen, H. Baltes, M. Hird, K. Toyne, A. Seed, J. W. Goodby, C. C. Huang, and L. Furenlid. Structures of chiral smectic-C mesophases revealed by polarization-analyzed resonant x-ray scattering. *Phys. Rev. E*, 60:6793–6802, Dec 1999.

[121] Yoichi Takanishi, Megumi Toshimitsu, Michi Nakata, Naoki Takada, Tatsuya Izumi, Ken Ishikawa, Hideo Takezoe, Junji Watanabe, Yumiko Takahashi, and Atsuo Iida. Frustrated smectic layer structures in bent-shaped dimer liquid crystals studied by x-ray microbeam diffraction. *Phys. Rev. E*, 74:051703, Nov 2006.

[122] A. Jákli, G. Liao, I. Shashikala, U. S. Hiremath, and C. V. Yelamaggad. Chirality and polarity transfers between bent-core smectic liquid-crystal substances. *Phys. Rev. E*, 74:041706, Oct 2006.

[123] Chandra Shekhar Pati Tripathi, Patricia Losada-Pérez, Christ Glorieux, Alexandra Kohlmeier, Maria-Gabriela Tamba, Georg H. Mehl, and Jan Leys. Nematic-nematic phase transition in the liquid crystal dimer CBC9CB and its mixtures with 5CB: A high-resolution adiabatic scanning calorimetric study. *Phys. Rev. E*, 84:041707, Oct 2011.

[124] M. Cestari, S. Diez-Berart, D. A. Dunmur, A. Ferrarini, M. R. de la Fuente, D. J. B. Jackson, D. O. Lopez, G. R. Luckhurst, M. A. Perez-Jubindo, R. M. Richardson, J. Salud, B. A. Timimi, and H. Zimmermann. Phase behavior and properties of the liquid-crystal dimer 1″,7″-bis(4-cyanobiphenyl-4′-yl) heptane: A twist-bend nematic liquid crystal. *Phys. Rev. E*, 84:031704, Sep 2011.

[125] Lucia Calucci, Marco Geppi, Alberto Marini, and Carlo Alberto Veracini. Orientational order in liquid crystals by combining ^{2}H and ^{13}C nuclear magnetic resonance spectroscopy and density functional theory calculations. *Phys. Rev. E*, 82:041702, Oct 2010.

[126] George Cordoyiannis, Chandra Shekhar Pati Tripathi, Christ Glorieux, and Jan Thoen. Order of phase transitions and tricriticality in mixtures of octyloxycyanobiphenyl and nonyloxycyanobiphenyl liquid crystals: A high-resolution study by adiabatic scanning calorimetry. *Phys. Rev. E*, 82:031707, Sep 2010.

[127] S. Chakraborty and R. Garcia. Optical-ellipsometric study of the nematic-to-smectic transition in 8cb films adsorbed on silicon. *Phys. Rev. E*, 81:031702, Mar 2010.

[128] Cristian V. Achim, Raphael Wittkowski, and Hartmut Löwen. Stability of liquid crystalline phases in the phase-field-crystal model. *Phys. Rev. E*, 83:061712, Jun 2011.

[129] Stavros D. Peroukidis, Alexandros G. Vanakaras, and Demetri J. Photinos. Molecular simulation of hierarchical structures in bent-core nematic liquid crystals. *Phys. Rev. E*, 84:010702, Jul 2011.

[130] Julio C. Armas-Pérez and Jacqueline Quintana-H. Numerical evidence for nematic and smectic behavior of two-dimensional hard models. *Phys. Rev. E*, 83:051709, May 2011.

[131] M. Tissier, B. Delamotte, and D. Mouhanna. XY frustrated systems: Continuous exponents in discontinuous phase transitions. *Phys. Rev. B*, 67:134422, Apr 2003.

[132] H. T. Diep, Yann Magnin and Danh-Tai Hoang. Spin Resistivity in Magnetic Materials. *Acta Physica Polonica A*, 121:985–991, 2012.

[133] Paul Peter Ewald. Die Berechnung optischer und elektrostatischer Gitterpotentiale. *Ann. Phys.*, 64:253–287, 1921.